MODELING AND STRUCTURAL ANALYSIS OF TOOL WEAR IN VERTICAL MILLING CENTRE

Submitted in the partial fulfillment of requirements for the award of the Degree of

MASTER OF ENGINEERING
IN

CAD/CAM & ROBOTICS

Submitted by
PATEL JIGNESH
Roll No: 80781017

Under guidance of
Mr. V.K SINGLA
Sr. Lecturer, **MED**
Thapar University, Patiala

MECHANICAL ENGINEERING DEPARTMENT
THAPAR UNIVERSITY
PATIALA-147004
JUNE-2009

Certificate

Certified that the thesis Report entitled **"MODELING AND STRUCTURAL ANALYSIS OF TOOL WEAR IN VERTICAL MILLING CENTRE "** submitted by **Patel Jignesh..**, in the partial fulfillment of the requirements, for the award of degree of **MASTER OF ENGINEERING (CAD/CAM & ROBOTICS)**, Degree of **Thapar University, Patiala** is a record of student's own study carried under my supervision.

This report is of desired standard and has not been submitted in any other university or institute for the award of degree.

Mr. V.K SINGLA
Senior Lecturer,
Mechanical Engineering Department,
Thapar University,
Patiala.

COUNTERSIGNED BY

Dr. S.K.MOHAPATRA
Professor& Head
Mechanical Engineering Department
Thapar University,
Patiala.

Dr. R.K.SHARMA 28/7
Dean (Academic Affairs)
Thapar University,
Patiala.

Acknowledgement

Words are often less to revels one's deep regards. With an understanding that work like this can never be the outcome of a single person, I take this opportunity to express my profound sense of gratitude and respect to all those who helped me through the duration of this work.

This work would not have been possible without the encouragement and able guidance of my supervisor **Mr. V.K.SINGLA**. Most of the novel ideas and solutions in this work are the result of our numerous stimulating discussions. Their feedback and editorial comments were also invaluable for the writing of this seminar. I am highly grateful to **Dr. S.K. Mohapatra**, Prof. & Head, MED for providing the all facilities for the completion of the work.

I take pride of myself being son of ideal parents for their everlasting desire, sacrifice, affectionate blessings and help, without which it would not have been possible for me to complete my studies.

At last, I would like to thank to all the members and employees of Mechanical Engineering Department, Thapar University, Patiala for their everlasting support.

Place: TU, Patiala

(PATEL JIGNESH)
Roll No: 80781017

Abstract

The cutting forces exerted by the cutting tool on the work piece during a machining action to be identified in order to control the tool wear and occurrence of vibration, thus to improve tool-life. Modeling of cutting forces in milling is often needed in machining automation. The objective of this study is to predict the effects of cutting parameters on the variations of cutting forces during end milling operation of EN series steel alloy material. The EN 8, EN 44, EN 19 and EN 31 specimens have been machined on vertical milling machine. The cutting forces have been measured using the piezoelectric dynamometer for varying the feed rate, speed and depth of cut. The cutting forces evaluated were used as input for parametric analysis in Ansys 11.0.Software. The transient analysis has been done for a specified duration of time. The maximum stressed area and stress values were calculated using Ansys ls solver. Response surface methodology have been used by designing three factors and the five levels central composite rotatable design matrixes with full replication; for planning, conduction, execution and development of mathematical models. The coefficients of 2nd order quadratic equations were calculated using SYSTAT software. The average cutting forces have been determined at defined value of the parameters (feed, speed, depth of cut) in tangential, radial, and axial direction per tooth period. The immersion and axial depth of cut were maintained constant. A comparison between modeling and experiment also has been presented.

This model and analysis are useful not only for predicting the tool wear but also for selecting optimum process parameters for achieving the stability of the end milling process.

Contents

LIST OF TABLES

LIST OF FIGURES

LIST OF GRAPHS

CHAPTER-1

INTRODUCTION

Milling machines were first invented and developed by Eli Whitney to mass produce interchangeable musket parts. Although crude, these machines assisted man in maintaining accuracy and uniformity while duplicating parts that could not be manufactured with the use of a file. Development and improvements of the milling machine and components continued, which resulted in the manufacturing of heavier arbors and high speed steel and carbide cutters. These components allowed the operator to remove metal faster, and with more accuracy, than previous machines. Variations of milling machines were also developed to perform special milling operations. During this era, computerized machines have been developed to alleviate errors and provide better quality in the finished product.

Milling is the process of removing material from a work piece by moving the work piece (fixed to the table/bed) past a fixed position, rotating multi or single tooth/flute milling cutter (tool bit). The cutting action of teeth around the center axis of the milling cutter provides a fastest and accurate approach to machining. The machined surface may be flat, angular, or a multi dimensional curve or curve surface. The adjoining surfaces or edges (features) may also be milled to produce any combination of shapes and contours. The machine used for these applications is properly referred to as a milling machine tool or a machining center. Today live tooling lathes can now duplicate some of these operations. Eliminating the need for multiple set-ups, the shop has both CNC and manual vertical mills, Precision ±0.0005 or ±0.013mm, these tolerances are operation and operator dependent and under ideal new equipment conditions.

Today milling machines are also used for drilling, reaming, boring, counter boring, counter sinking, tapping, grooving and chamfering holes. Know the difference between the operations above. They are different in their degree of accuracy and function. Learning these terms and uses them in your drawings. It will clarify the requirements of a feature for the machinists working on your job.

CHAPTER – 2

VERTICAL MILLING MACHINE

2.1 Type of milling machine

A wide variety of milling machines are manufactured and may be classified in different ways, such as horizontal and vertical, low, intermediate, and high production and special purpose. Common low production, horizontal and vertical machine will be presented first,

2.1.1 Horizontal milling machine

The horizontal milling machine shown in Fig 2.1 is so called because the milling cutter is held in a horizontal position. It is also called a column and knee machine because they make up the main structure members. Although the machine shown is very versatile, it is limited to low production.

Figure 2.1 Horizontal milling machine

2.1.2 Vertical milling machine

The vertical milling machine as shown in Fig 2.2 has the cutting tool held in a vertical position. This machine can also be classified as a column and knee type since they

represented the main structure member. The CNC control shown makes this machine extremely versatile and of intermediate production,

To again a better understanding of the use of both vertical and horizontal milling machines, study the type of work done by each shown in figure. However each machine has its own advantages.

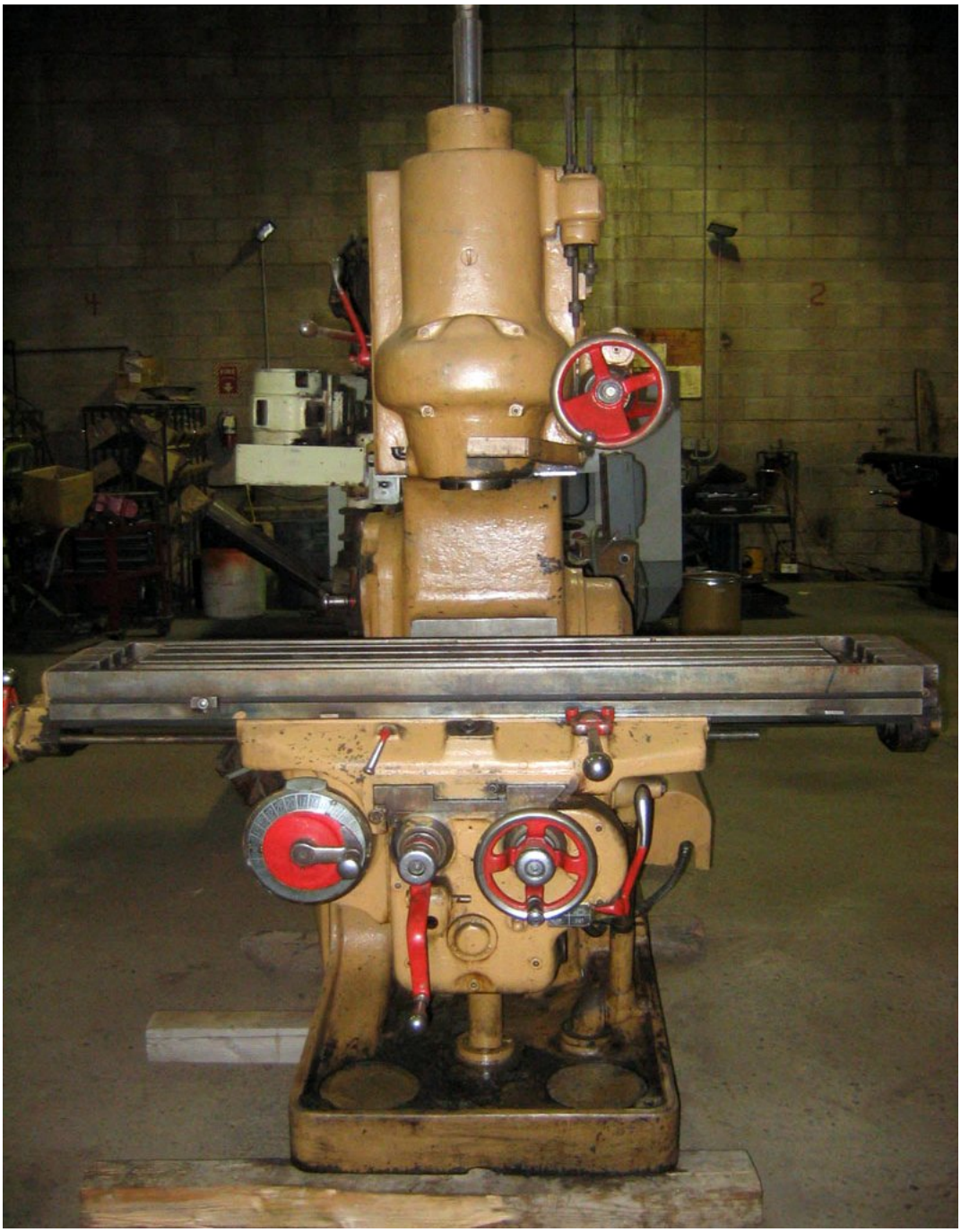

Figure 2.2: Vertical milling machine

2.1.3 Planer milling machine

The larger milling machine is equipped with two cutting heads of 250hp each. The cuts are made by the rotating milling cutters as the table reciprocates back and forth. The cutters can be made to cut either on the top surface or on the edge of the stock.

2.2 Major components

The machinist must know the name and purpose of each of the main parts of a milling machine to understand the operations discussed in this text. Keep in mind that although we are discussing a knee and a column milling machine, this information can be applied to other types.

(1) Column

The column, including the base, is the main casting which supports all other parts of the machine, an oil reservoir and a pump in the column keeps the spindle lubricated. The column rests on a base that contains a coolant reservoir and a pump that can be used when performing any Machining operation that requires a coolant.

(2) Knee

The knee is the casting that supports the table and the saddle. The feed change gearing is enclosed within the knee. It is supported and can be adjusted by the elevating screw. The knee is fastened to the column by dovetail ways. The lever can be raised or lowered either by hand or power feed. The hand feed is usually used to take the depth of cut or to position the work, and the power feed to move the work during the machining operation.

(3) Saddle and Swivel Table

The saddle slides on a horizontal dovetail, parallel to the axis of the spindle, on the knee. The swivel table (on universal machines only) is attached to the saddle and can be swiveled approximately 45° in either direction.

(4) Power Feed Mechanism

The power feed mechanism is contained in the knee and controls the longitudinal, transverse (in and out) and vertical feeds. The desired rate of feed can be obtained on the machine by positioning the feed selection levers as indicated on the feed selection plates. On some universal knee and column milling machines the feed is obtained by turning the speed selection handle until the desired rate of feed is indicated on the feed dial. Most

milling machines have a rapid traverse lever that can be engaged when a temporary increase in speed of the longitudinal, transverse, or vertical feeds are required. For example, this lever would be engaged when positioning or aligning the work.

For safety reasons, extreme caution should be exercised while using the rapid traverse controls.

(5) Table

The table is the rectangular casting located on top of the saddle. It contains several T-slots for fastening the work or work holding devices. The table can be moved by hand or by power. To move the table by hand, engage and turn the longitudinal hand crank. To move it by power, engage the longitudinal directional feed control lever. The longitudinal directional control lever can be positioned to the left, to the right, or in the center. Place the end of the directional feed control lever to the left to feed the table to the left. Place it to the right to feed the table to the right places it in the center position to disengage the power feed, or to feed the table by hand.

(6) Spindle

The spindle holds and drives the various cutting tools. It is a shaft, mounted on bearings supported by the column. The spindle is driven by an electric motor through a train of gears, all mounted within the column. The front end of the spindle, which is near the table, has an internal taper machined on it. The internal taper (3 1/2 inches per foot) permits mounting tapered-shank cutter holders and cutter arbors. Two keys, located on the face of the spindle, provide a positive drive for the cutter holder, or arbor.

(7) Over arm

The over arm is the horizontal beam to which the arbor support is fastened. The over arm, may be a single casting that slides in the dovetail ways on the top of the column. It may consist of one or two cylindrical bars that slide through the holes in the column. On some Machines to position the over arm, first unclamp the locknuts and then extend the over arm by turning a crank. On others, the over arm is moved by merely pushing on it. The over arm should only be extended far enough to so position the arbor support as to make the setup as rigid as possible. To place the arbor supports on an over arm, extend one of the bars approximately 1-inch farther than the other bar, Always tighten the locknuts after the over arm is positioned. On some milling machines, the coolant supply

nozzle is fastened to the over arm. The nozzle can be mounted with a split clamp to the over arm after the arbor support has been placed in position.

(8) Arbor Support

The arbor support is a casting containing a bearing which aligns the outer end of the arbor with the spindle. This helps to keep the arbor from springing during cutting operations. Two types of arbor supports are commonly used. One type has a small diameter bearing hole, usually 1-inch maximum in diameter. The other type has a large diameter bearing hole, usually up to 2 3/4 inches, an oil reservoir in the arbor support keeps the bearing surfaces lubricated. An arbor support can be clamped anywhere on the over arm. Small arbor supports give additional clearance below the arbor supports when small diameter cutters are being used.

(9) Size Designation

All milling machines are identified by four basic factors: size, horsepower, model, and type. The size of a milling machine is based on the longitudinal (from left to right) table travel, in inches. Vertical, cross, and longitudinal travel are all closely related as far as the overall capacity. However, for size designation, only the longitudinal travel is used. There are six sizes of knee-type milling machines, with each number representing the number of mm of travel.

Table 2.1 Standard size longitudinal table travel

Number	(Size)(mm)
1	22
2	28
3	34
4	42
5	50
6	60

If the milling machine in the shop is labeled No. 2HL, it has a table travel of 28 inches; if it is labeled No. 5LD, it has a travel of 50 inches. The horsepower designation refers to the rating of the motor which is used to power the machine. The model designation is determined by the Manufacturer and features vary with different brands. The type of milling machine is designated as plain or universal, horizontal or vertical, and knee and

column, or bed. In addition, machines may have other special type designations and, therefore, may not fit any standard classification.

2.3 Special type of milling machines

Many types of special milling machines are to accomplish specific kind of work more easily than the standard types. In this category are duplicating mills, profiling machines, and pantograph. Most of these machines are vertical mills that have been adapted to reproduce accurately. By means of a tracer, the forms and contours from a master pattern. Automatics machines are made to traverse the pattern either electrically or hydraulically. Once the cycle is started, the tracer will automatically follow the master pattern until it is completed. The pattern may be of easily formed material such as wood plaster. Larger electrically controlled machine of this type, used extensively in making sheet metal dies for aircraft and automotive bodies are better known by their trade name of kellering machines.

Machining center

The most versatile milling machine Is now the machining center, machining centers are designed and built to provide for flexible manufacturing (FM). Therefore, they can be used for wide range from a just few part to production quantities. Programming can be relatively simple and the use of canned cycles provides a great deal of versatility. An NC machining center by definition is able to perform milling, drilling, and boring cuts and has either indexing turret tool holder or provides for automatics tool change.

Machining centers are built in either the horizontal or vertical configuration; the relative merits of each will be discussed briefly.

2.3.1 Horizontal machines

Horizontal machine tend to be advantageous for heavy, box-shaped parts, such as gear housing, they have many feature that need to be machined on the side faces, the horizontal machine easily supports heavy work piece of this type. The chips drop out of the way during machine. Providing an uncluttered view of the cut and preventing chip re' cutting, If a rotary indexing worktable added, four sides of the work piece may be machined without re fixturing, Pallet system used to shuttle pieces in and out of the work

station to be easier to design for a horizontal machine. Where everything in front of the main column is open and accessible,

2.3.1 Vertical machines

Vertical machining centers are often preferred for flat parts that must have through holes. Fixture for these parts are more easily designed and built for a vertical spindle. Also, the thrust of cut developed in drilling or in milling pockets can be absorbed directly by the bed of the machine.

The vertical machine is preferred where three-axis work is done on a single face, as in mold and die work. The operator can easily peer down into the cutting area unobstructed by the column. However, when work piece sizes increase to where the operator can no longer peer into the cut, the vertical machine loses that advantage.

The weight of a vertical machine as it extends away from the column, particularly on larger machines, can be a factor in maintaining accuracy, as there may be some tendency for it to droop and lose accuracy and cause chatter.

Figure 2.3 Vertical milling center (machine tool lab)

2.4 Milling machine operations

Milling operations may be classified under four general headings as follows:

(1) Face Milling - machining flat surfaces which are at right angles to the axis of the cutter.

(2) Plain or Slab Milling - machining flat surfaces which are parallel to the axis of the cutter.

(3) Angular Milling - machining flat surfaces which are at an inclination to the axis of the cutter.

(4) Form Milling - machining surfaces having an irregular outline

2.5 Milling fundamentals

Milling cutting geometry

Three main types of insert-tooth-type milling cutters are now available: double negative, double positive, and shear angle or negative/positive. The names given refer to the radial and axial rake, the negative rake tool is especially good for interrupted cutting or heavy roughing cut and the removal of scale. It tends to more stress on the work piece and is therefore not recommended for parts that may distort during machining. It is also not the type of cutter to use on materials that strains harden readily. The horsepower requirements are more than for a conventional cutter. It has advantage of being able to utilize all edges of indexible insert-type tooling.

A double positive tool requires less horsepower and exerts the minimum of force on the work piece. There is little tendency to chatter. As can be seen from the sketch, it is not possible to reverse the tool, so on a square insert only four cutting edges are available, instead of eight. Also, the clearance angles make the cutting edges weaker.

The shear-angle cutter is a newer design. It combines negative radial rake with a positive axial rake, this design cause the chips to flow away from the cutter so that higher feed rates can be used. It also produces a fine surface finish.

Shear-angle cutter is usually made with high lead angle, whereas the double-positive angle may vary from 2° to 30°. The standard lead angle for the double-negative cutter is 10°. As with single-point tools, the lead angle serves to protect the cutting point and thin out the chip. This allows higher feed rates without overloading the insert. A 2° lead angle permits cutting up to a shoulder.

1 True rake

True rake is the slope of the tooth face with respect to a radial reference plane through the nose of the cutting edge and is the resultant of the axial, radial, and angles, it is measured in the perpendicular to the surface generated by the cutting edge, as shown in fig , the true rake of a given axial and radial combination becomes more positive as the lead angle increases, which offers freer cutting and lower horsepower consumption.

2 Angle of inclination

The same angles used to determine true rake are also used to measure inclination angles, as shown in fig. the plane of measurement differs, however; measurement is made from the plane generated by the cutting edge rather than perpendicular to it. This cutter with a $+6^{\circ}$ true rake, $+13^{\circ}$ inclination angle,and a lead angle has proved to be quite efficient in terms of metal-removal capability.

3 Cutter effect on surface finish

A number of variables affect the surface finish produced by a cutter, such as machine rigidity, work material, fixturing and feed rate. Once methods of improving the surface finish is by using an insert that has a wiper flat, to be effective ,the wiper flat should be approximately 25% longer than the feed per revolution in order to wipe out any high points left by the preceding insert.

2.6 Speeds for milling cutters

(1) general

The speed of a milling cutter is the distance in feet per minute that each tooth travels as it cuts its chips. The number of spindle revolutions per minute necessary to give a desired peripheral speed on the size of the milling cutter. The best speed is determined by the type of material being cut and the size and type of cutter used. The smoothness of the finish desired and the power available are other factors relating to the cutter speed.

(2) Selecting proper cutting speed

1. The approximate values given in table 1 on the following page may be used as a guide for selecting the proper cutting speed. If the operator finds that the machine, the milling cutter, or the work piece cannot be handled suitably at these speeds, immediate readjustment should be made.

2. Table 1 lists speeds for high-speed steel milling cutters. If carbon steel cutters are used, the speed should be about one-half the speed recommended in the table. If carbide-tipped cutters are used, the speed can be doubled.

Table 2.2 Milling machine cutting speeds for high-speed steel milling cutter

Material	Cutting speed(mm/m)			
	Plain milling cutter		End milling cutter	
	Roughing	Finishing	Roughing	Finishing
Aluminum	400 to 1000	400 to 1000	400 to 1000	400 to 1000
Brass	125 to 200	90 to 200	90 to 150	90 to 150
Brass ,yellow	150 to 200	100 to 250	100 to 200	100 to 200
Bronze, phosphor and manganese	30 to 80	25 to 100	30 to 80	30 to 80
Cast iron(hard)	25 to 40	10 to 30	25 to 40	20 to 45
Cast iron(soft and medium)	40 to 75	25 to 80	35 to 65	30 to 80
Monel metal	50 to 75	50 to 75	40 to 60	40 to 60
Steel hard	25 to 50	25 to 70	25 to 50	25 to 70
Steel soft	60 to 120	45 to 110	50 to 85	45 to 100

(c) If a plentiful supply of cutting oil is applied to the milling cutter and the work piece, the speeds can be increased from 50 to 100 percent. (d) For roughing cuts, a moderate speed and coarse feed give best results; for finishing cuts, the best practice is to reverse these conditions, using a higher speed and a lighter cut.

2.7 Speed computation

The formula for calculating spindle speed in revolutions per minute

Is as follows

$$rpm = \frac{C.S \times 4}{D} \qquad \text{..... (1)}$$

Where, rpm = spindle speed (in revolution per minute)

C.S = cutting speed of milling cutter (in surface mm per minute)

D = diameter of milling cutter (in mm)

2.8 Feeds for milling

General

The rate of feed, or the speed at which the work piece passes the cutter, determines the time required for cutting a job. In selecting the feed, there are several factors which should be considered.

These factors are:

1. Forces are exerted against the work piece, the cutter, and their holding devices during the cutting process. The force exerted varies directly with the amount of metal removed and can be regulated by the feed and the depth of cut.

Therefore, the correct amount of feed and depth of cut are interrelated, and in turn are dependent upon the rigidity and power of the machine. Milling machines are limited by the power that they can develop to turn the cutter and the amount of vibration they can resist when using coarse feeds and deep cuts.

2. The feed and depth of cut also depend upon the type of milling cutter being used. For example, deep cuts or coarse feeds should not be attempted when using a small diameter end milling cutter, as such an attempt would spring or break the cutter. Coarse cutters with strong cutting teeth can be fed at a faster rate because the chips may be washed out more easily by the cutting oil.

3. Coarse feeds and deep cuts should not be used on a frail work piece, or on a piece that is mounted in such a way that its holding device is not able to prevent springing or bending.

4. The degree of finish required often determines the amount of feed. Using a coarse feed, the metal is removed more rapidly but the appearance and accuracy of the surface produced may not reach the standard desired for the finished product. Because of this, finer feeds and increased speeds are used for finer, more accurate finishes. Most mistakes are made through over speeding, under speeding, and overfeeding. Over speeding may be detected by the occurrence of a squeaking, scraping sound. If vibration (referred to

As "chattering") occurs in the milling machine during the cutting process, the speed should be reduced and the feed increased. Too much cutter clearance, a poorly supported work piece, or a badly worn machine gear is common causes of "chattering.

2.9 Power computation

The most practical method of estimating the power required for a milling cut is based on the metal-removal rate, Q in mm^3 per minute.

$$Q = w \times d \times f_m \quad \text{.....} \quad (2)$$

Where w= width of cut (mm)

D=depth of cut (mm)

f=table feed rate (mm./ min)

The horsepower at the spindle is

$$HP_s = Q \times P \quad \text{.....} \quad (3)$$

Where Q=cubic mm removal rate per minute ($mm.^3$ / *per min)*

P=unit horsepower factor (hp/ mm^3 /min)

The unit horsepower factor (P) is the approximate power required at the cutter to remove 1 mm^3/min of a given material.

In practice, P is also dependent on the cutting peed, feed per insert, true rake angle, and tool wear land, if these factors are to be considered, a rule of thumb I to increase, the horsepower requirements by 50%from that given by the basic formula.

2.9.1 Horsepower at the motor is

$$HP_m = \frac{Q \times P}{E} \quad \text{.....} \quad (4)$$

Where E is the efficiency of the machine, normally 20% of the motor efficiency is lost through the gear train.

2.9.2 Cutting speed

To determine the proper speed for milling,

$$\text{Rpm}=3.82\times\frac{V_c}{D_c} \quad \text{..... (5)}$$

Where V_c=cutting velocity (mm/m)

D_c=cutter diameter (mm)

2.9.3 Feed rate

The milling cutter rate is

$$f_{m=}f_m\times n\times rpm \quad \text{..... (6)}$$

Where f_t= mm per tooth, at least two or three teeth should be in the cut at one time to reduce vibration, cutter deflection, and insert chipping.

N=number of teeth in the cutter

2.9.4 Cutting time

The time required to make a cut is based on the length of the cut plus the cutter approach and over travel of the cutter divided by the feed rate;

$$Time=\frac{L+\Delta L}{f_m} \quad \text{..... (7)}$$

Where L=length of stroke

ΔL= cutter approach to the work; an approximation for the cutter approach can be taken as one-half the diameter of the cutter

f_m=feed rate (mm/min)

CHAPTER-3

FINITE ELEMENT ANALYSIS

Computer-aided engineering (CAE) is the application of computer software in engineering to evaluate components and assemblies. It encompasses simulation, validation, and optimization of products and manufacturing tools. The primary application of CAE, used in civil, mechanical, aerospace, and electronic engineering, takes the form of FEA alongside computer-aided design (CAD).

3.1 Finite element analysis

In general, there are three phases in any computer-aided engineering task:

- Pre-processing – defining the finite element model and environmental factors to be applied to it
- Analysis solver – solution of finite element model
- Post-processing of results using visualization tools

3.1.1 Pre-processing

The first step in using FEA, pre-processing, is constructing a finite element model of the structure to be analyzed. The input of a topological description of the structure's geometric features is required in most FEA packages. This can be in either 1D, 2D or 3D form, modeled by line, shape, or surface representation, respectively, although nowadays 3D models are predominantly used. The primary objective of the model is to realistically replicate the important parameters and features of the real model. The simplest mechanism to achieve modeling similarity in structural analysis is to utilize pre-existing digital blueprints, design files, CAD models, and/or data by importing that into an FEA environment. Once the finite element geometric model has been created, a meshing procedure is used to define and break up the model into small elements. In general, a finite element model is defined by a mesh network, which is made up of the geometric arrangement of elements and nodes. Nodes represent points at which features such as displacements are calculated. FEA packages use node numbers to serve as an identification tool in viewing solutions in structures such as deflections. Elements are

bounded by sets of nodes, and define localized mass and stiffness properties of the model. Elements are also defined by mesh numbers, which allow references to be made to corresponding deflections or stresses at specific model locations.

3.1.2 Analysis (computation of solution)

The next stage of the FEA process is analysis. The FEM conducts a series of computational procedures involving applied forces, and the properties of the elements which produce a model solution. Such a structural analysis allows the determination of effects such as deformations, strains, and stresses which are caused by applied structural loads such as force, pressure and gravity.

3.1.3 Post-processing (visualization)

These results can then be studied using visualization tools within the FEA environment to view and to fully identify implications of the analysis. Numerical and graphical tools allow the precise location of data such as stresses and deflections to be identified.

3.2 Applications of FEA to the mechanical engineering industry

A variety of specializations under the umbrella of the mechanical engineering discipline such as aeronautical, biomechanical, and automotive industries all commonly use integrated FEA in design and development of their products. Several modern FEA packages include specific components such as thermal, electromagnetic, fluid, and structural working environments. In a structural simulation FEA helps tremendously in producing stiffness and strength visualizations and also in minimizing weight, materials, and costs. FEA allows detailed visualization of where structures bend or twist, and indicates the distribution of stresses and displacements. FEA software provides a wide range of simulation options for controlling the complexity of both the modeling and the analysis of a system. Similarly, the desired level of accuracy required and the associated computational time requirements can be managed simultaneously to address most engineering applications. FEA allows entire designs to be constructed, refined, and optimized before the design is manufactured. This powerful design tool has significantly improved both the standard of engineering designs and the methodology of the design

process in many industrial applications. The introduction of FEA has substantially decreased the time taken to take products from concept to the production line. It is primarily through improved initial prototype designs using FEA that testing and development have been accelerated. In summary, the benefits of FEA include increased accuracy, enhanced design and better insight into critical design parameters, virtual prototyping, fewer hardware prototypes, a faster and less expensive design cycle, increased productivity, and increased revenue.

3.3 Computer-aided design and finite element analysis in industry

The ability to model a structural system in 3D can provide a powerful and accurate analysis of almost any structure. 3D models, in general, can be produced using a range of common computer-aided design packages. Models have the tendency to range largely in both complexity and in file format, depending on 3D model creation software and the complexity of the model's geometry. FEA is a growing industry in product design, analysis, and development in engineering. The trend of utilizing FEA as an engineering tool is growing rapidly. The advancement in computer processing power, FEA, and modeling software has allowed the continued integration of FEA in the engineering fields of product design and development. In the past, there have been many issues restricting the performance and ultimately the acceptance and utilization of FEA in conjunction with CAD in the product design and development stages. The gaps in compatibility between CAD file formats and FEA software limited the extent to which companies could easily design and test their products using the CAD and FEA combination, respectively. Typically, engineers would use specialist CAD and modeling software in the design of the product and then wish to export that design into a FEA package to test. However, those engineers who depended on data exchange through custom translators or exchange standards such as IGES or STEP cite occasional reliability problems causing unsuccessful exchange of geometry. Thus, the creation of many models external to FEA environments was considered to be problematic in the success of FEA.

The current trend in FEA software & industry in engineering has been the increasing demand for integration between solid modeling and FEA analysis. During product design

and development engineers require automatic updating of their latest models between CAD and FEA environments. There is still a need to improve the link between CAD and FEA, making them technically closer together. However, the demand for unitary CAD-FEA integration coupled with the improved computer and software developments has introduced a more robust and collaborative trend where compatibility problems are beginning to be eliminated. Designers are now beginning to introduce computer simulations capable of using pre-existing CAD files, without the need to modify and re-create models to suit FEA environments.

C. Betegon Biempica et al (2007), the aim of this paper is to study the residual stresses in an UIC-60 rail and their reduction by means of roller straightening. Both experimental and numerical investigations have been carried out in the past to reveal the formation of dominant longitudinal residual stresses. However, the agreement between both investigations was not particularly good. The finite element method (FEM) has also been used to simulate one, two and three-dimensional analyses of a rail during roller straightening processes. The present model considers the longitudinal movement of a rail through the straightening machine, contact conditions between rail and rollers and kinematic hardening so as to take into account the plastic behavior of the rail material (steel). These results were compared with the experimental investigations and good agreement was observed. In this respect, this paper presents a novel, more realistic numerical simulation by FEM for the roller straightening process. Finally, an improvement of the straightening process in order to obtain smaller residual stress in the rail section is proposed.

Gupta Amit (2005), the problem of tool wear monitoring in machining operations, has been an active area of research for quite a long time. The accurate prediction of tool wear is important to have a better product quality and dimensional accuracy. In cutting tools the area close to the tool tip is the most important region and conditions at the tool tip must be carefully examined, if improvements in tool performance are to be achieved The present work involves the study of tool wear caused by the change in hardness of single point cutting tool for a turning operation to predict the tool life in orthogonal cutting based on the heat transfer analysis using Finite Element Method (FEM). The Experiments

were performed with EN-24 steel as work piece and Carbide uncoated tool bit as a tool material and the flank wear has been measured experimentally. An empirical relation is used to determine temperature at tool-tip and further Finite Element Method is used to determine the distribution of temperature over the surface of tool and its impact on hardness which is related by an empirical relations. The study shows the effect of Modified temperature due to strain rate on carbide tool to describe the thermal softening of tool material and becomes prone to wear. The results reveal that by increasing process variables in machining the wear and temperature increases causing thermal softening of tool causing it to wear. The results obtained have been verified with the available results from literature for the variation of wear with the temperature and thermal softening of carbide tool. The results prescribed demonstrate the significance of cutting parameters (speed, feed and depth of cut) in thermal analysis for study of the cutting tool wear.

Arsen Narimanyan et al (2007), this study is devoted to the application of the moving-boundary methodology in the modeling of thermal plasma cutting of materials. The aim of the model is to determine the temperature distribution in the work piece and the geometry of the cutting front during the cut. Mathematically, we model the problem as a coupled system of equations; heat conduction equation with Signorini-type boundary conditions and level-set equation as a result of reformulation of Stefan-type boundary condition. The weak formulation of the model is discussed in the framework of variation inequalities and level-set theory. Using the adaptive finite elements method, numerical results are obtained and illustrated in the manuscript. Our formulations provide a conceptually new approach towards the mathematical understanding of physical phenomena involved in the process of thermal plasma cutting

E. Correa et al (2008), the two main problems reducing electrolysis copper anode production are: the excessive warping/bending and the alteration of the flat aspect of the surface of the anodes. Both problems are related to the stress state generated in the anode mould during the manufacturing process of the anodes themselves. In this paper a finite element model is carried out to analyses the thermo-mechanical evolution of the mould during the anode manufacturing process. The responsibility of the stress state in the

origin or aggravation (where they already existed) of the aforementioned problems is investigated. Experimental data are used to validate the numerical model, its utility as a design tool being proved.

Z. Barsoum et al (2008), this was paper presented on welding simulation procedure is developed using the FE software ANSYS in order to predict residual stresses. The procedure was verified with temperature and residual stress measurements found in the literature on multi-pass butt welded plates and T-fillet welds. The predictions show qualitative good agreement with experiments. The welding simulation procedure was then employed on a welded ship engine frame box at MAN B&W. A subroutine for LEFM analysis was developed in 2D in order to predict the crack path of propagating fatigue cracks. The objective was to investigate fatigue test results from special designed test bars from the frame box where all test failed from the no penetrated weld root. A subroutine was developed in order to incorporate the predicted residual stresses and their relaxation during crack propagation by isoperimetric stress mapping between meshes without and with cracks, respectively. The LEFM fatigue life predictions shows good agreement with the fatigue test result when the residual stresses are taken into account in the crack growth analysis.

W.L. Chan et al (2008), In the traditional metal-formed product development paradigm, the design of metal-formed product and tooling is usually based on heuristic know-how and experiences, which are generally obtained through long years of apprenticeship and skilled craftsmanship. The uncertainties in product and tooling design often lead to late design changes. The emergence of finite element method (FEM) provides a solution to verify the designs before they are physically implemented. Since the design of product and tooling is affected by many factors and there are many design variables to be considered, the combination of those variables comes out with various design alternatives. It is thus not pragmatic to simulate all the designs to find out the best solution as the coupled simulation of non-linear plastic flow of billet material and tooling deformation is very time-consuming. This research is aimed to develop an integrated methodology based on FEM simulation and artificial neural network (ANN) to

approximate the functions of design parameters and evaluate the performance of designs in such a way that the optimal design can be identified. To realize this objective, an integrated FEM and ANN methodology is developed. In this methodology, the FEM simulation is first used to create training cases for the ANN(s), and the well-trained ANN(s) is used to predict the performance of the design. In addition, the methodology framework and implementation procedure are presented. To validate the developed technique, a case study is employed. The results show that the developed methodology performs well in estimation and evaluation of the design

Sharma parveen (2008), in present highly competitive environment need for better design features along with reduced costing has become very important. Rapid Prototyping also referred to as solid free-form manufacturing, computer automated manufacturing, and layered manufacturing has obvious use as a vehicle for visualization. In addition, RP models can be used for testing, such as when an airfoil shape is put into a wind tunnel. Rapid tooling arises from rapid prototyping, such as silicone rubber molds and investment casts. Rapid manufacturing arises from rapid prototyping to use rapid prototyping systems to directly produce parts which are functional end-use item with the advantage that there is no need for tooling. The rapid prototyping (RP) process is the fastest and most feasible method for prototype construction. However, with the use of any material or build method the phenomenon of volume shrinkage is unavoidable. It is known that volume shrinkage and curl distortion are the major causes that lead to poor accuracy of the built prototype. Subsequently, in order to improve the precision of dimension and volume shrinkage, more expensive equipment is used on the market. Also, it is expensive and inefficient to obtain better process parameters through trial and error in the RP process. In order to improve the precision of dimension, reduce the processing cost and the frequency of trial and error, this study first induces the concept of computer aided engineering (CAE) into the processing of RP, which uses a finite element simulation code to simulate the photo polymerization process, so as to obtain the distortion data. Besides, it is believed that this research method can be promoted to other materials or build methods in RP fabrication.

Zhichao li (2006), Grinding is one of the important operations employed in modern manufacturing industry to remove materials and achieve desired geometry and surface finish. Simultaneous double side grinding (SDSG) and ultrasonic vibration assisted grinding (UVAG) are two typical cost effective grinding processes which are utilized to grind semiconductor materials and high performance ceramic materials, respectively. The objectives of this research are to investigate several technical issues in modern grinding processes by using theoretical, numerical, and experimental research approaches. Those technical issues are related to SDSG and UVAG, which have been chosen as two typical grinding processes for this research. This thesis reviews the literature on SDSG (covering process applications, modeling of grinding marks, and modeling of wafer shapes) and UVAG (covering process applications, edge chipping, and coolant effects, etc). The theoretical research work of this thesis is conducted by developing mathematical models for grinding marks and wafers shapes in SDSG of silicon wafers. These developed models are then used to study the effects of SDSG parameters on the curvature of the grinding marks, the distance between adjacent grinding marks, and the wafer shapes. The numerical research work of this thesis is done by conducting a three dimensional (3- D) finite element analysis (FEA) of UVAG process. A 3-D FEA model is developed to study the edge chipping commonly observed in UVAG of ceramics. Edge chippings not only compromises geometric accuracy but also possibly causes an increase in machining cost. A solution to reduce the edge chipping is proposed based upon the FEA simulations and validated by pilot experiments. Several experimental studies are conducted to provide new knowledge for the UVAG process. Firstly, a novel coolant delivery system is explored for UVAG machine system. Secondly, UVAG is introduced into machining of fiber-reinforced ceramic matrix composites (CMC). Results of a feasibility study and a designed experimental investigation show that UVAG is a promising process for CMC machining. Finally, an experimental study on cutting forces during UVAG of zirconia/alumina composites is conducted. The feasibility to machine different zirconium/alumina composites using UVAG is also investigated and discussed. The findings in this thesis will provide theoretical and practical guidance for modern grinding processes especially for SDSG and UVAG.

Singla Vinod (2008), with the rapid advances in the product and process technology, newer materials are being discovered and developed. These materials have the rare combination of properties like light weight, high strength, corrosive resistance and thermal and electrical conductivity and so on. These new materials satisfy the present day product needs of Aerospace and other applications, but at the same time are more difficult to machine and manipulate. Electro Discharge Machining (EDM) is one such process which is widely employed to process these materials. EDM has been recently employed to alter the properties of the raw materials by using appropriate electrodes and various types of powders and additives in the dielectric fluid. In this thesis work the literature available in the area of MRR and TWR in EDM. It is found that the process has been successfully tried on materials like Nickel, Tungsten, Cobalt, Silicon by proper control of the parameters, electrode materials, electrolyte and powers. The objective of this work will be, modeling of a cutting tool considering the effects of the temperature and using the modified temperature concept to see the effects of temperature on the mechanical properties of the cutting tool. Once a model is developed for machining operation, it can be implemented for other processes like Die sinking and Wire cut EDM etc. An attempt is made to correlate the temperature and stress distribution patterns with the failure of the tool. The methodology will be used to develop a Finite Element Analysis program for thermal modeling to predict tool wear rate using ANSYS and also compare the results with experimental data. Considering the importance of copper for tooling applications it is chosen to investigate the TWR. Using high carbon high cromium steel as the work piece, Copper as the tool, kerosene as dielectric, experimentation was performed. At the end theoretical tool wear rate calculated using the ANSYS software is compared with the experimental results to validate the results.

Harminder Singh (2008), A thermal–electrical model was developed for sparks generated by electrical discharge in a liquid media (kerosene). A single spark has been used for the discharge channel created between the electrodes. The discharge channel being an electrical conductor will dissipate heat, which is taken as Gaussian heat source. The amount of heat dissipated varies with the thermal–physical properties of the conductor, as a result the maximum temperature reached is different. In the present model, the heat flux

is taken as a function of radii value of the conductor and directly proportional to the current, breakdown voltage and fraction of heat input to work piece. In this work, the study of mechanism of material removal in die steel with emphasis on AISI D2 die steel, with copper tool is carried out using Finite Element Method. Temperature distribution within zone of influence of single spark is obtained with the application of finite element method (FEM). The nodal temperatures obtained by FEM are further post processed for estimating MRR. The ANSYS 11.0 software has been employed to model the problem and the same is used to evaluate the temperature distribution. An attempt has been made to find the material removal rate from the FEM model. Further experiments have been carried out to validate the results obtained by the developed FEM model for different values of current, pulse on time and pulse off time.

Muammer Koc et al (2003), This paper was presented on the use of stress pins as an innovative pre-stressing element, and presents the results of a design methodology investigation through combined finite element analysis (FEA) and design of experiment (DOE) studies for large and non-ax symmetric precision forming tooling (i.e. as in hydro forming and precision forging of connecting rod) where conventional shrink-fit solutions cannot be applied effectively and economically. In summary, smart pre-stressing elements (i.e. stress pins) are implemented to overcome very fundamental and practical problem of prolonging the die life, preventing die failures and improving dimensional part tolerances by applying local and controlled pre-stressing effects.

Cristian Simion et al (2006), the paper was presented on both a methodology of detailed ax symmetric simulation of a small scale welding test using the ANSYS general purpose finite element computer code and a comparison with test data. To simulate this manufacturing process, an APDL (ANSYS Parametric Design Language) macro was developed and implemented. The methodology implemented deals with the major phenomena of the welding process from transient heat analysis to structural thermal-plastic analysis. The methodology is based on an ax symmetric approach and accounts for nonlinearities due to temperature-dependent thermal and mechanical material properties as well as surface contacts. It predicts, with reasonable accuracy, the real test

measurements. CANDU nuclear reactors use horizontal fuel channels housed in a large fabricated horizontal vessel called the calandria vessel. This calandria vessel has two end shields (each consists of double endplates), which provide support for the fuel channels as well as defining the basic reactor geometry. Each pair of double endplates is joined by tubes called lattice tubes. The lattice tubes, which are welded to the endplates, provide passages for the fuel channels and stiffness to the calandria vessel. To ensure that the distortions of the endplates due to welding satisfy the design requirements, small scale and large scale welding tests are performed. The initial small scale welding test consisted of welding a lattice tube to the associated section of an endplate. A larger scale welding test consists of welding a 2x6 array of lattice tubes to assess the accumulated distortion on the end plate. In order to develop a deep understanding of the distortions generated by welding, these welding tests are simulated using detailed finite element analyses. The detailed simulations include heat flow and elastic plastic analysis. Numerical simulations of the complete assembly, using coarse finite element models and elastic-only analyses of the endplate assembly, are also included as part of the design qualification effort.

Madnaik S.D. et al (1987), Metal forming problems generally involve large plastic deformations. In cold forming most materials have a nonlinear strain hardening behavior. F.E.M. solutions of such problems require elastic plastic analysis and an incremental approach. While a number of such approaches exist they require fairly small step size and hence a large computational effort. Madnaik, Maiti and Chaturvedi (I) had proposed a modification to the tangent modulus method of Yamada et al (2) and showed that this method is able to solve the problem of plane strain compression with considerably less computational effort and reasonable accuracy; and presented results to show the stress distributions at various levels of reductions and for different aspect ratios (3). This paper uses the same procedure termed the Modified Elastic Plastic Incremental Analysis Procedure (MEPIAP) for obtaining solution to another problem i.e. plane Strain Compression of Preshaped Material between Inclined Tools.

K Choil et al (2006), Three-dimensional finite element analysis of arc-welding processes is presented with emphasis on practical applications for numerical simulation. We use an

implicit numerical implementation for Leblond's transformation plasticity constitutive equations, which are widely used in steel-structure welding. Several numerical examples, particularly including a large structure undergoing significant elastic–plastic deformations before welding, are presented to demonstrate the effectiveness of the three-dimensional analysis of welding processes.

J.C. Outeiro et al (2008), Critical issues in machining of difficult-to-cut materials are often associated with short tool-life and poor surface integrity, where the resulting tensile residual stresses on the machined surface significantly affect the component's fatigue life. This study presents the influence of cutting process parameters on machining performance and surface integrity generated during dry turning of Inconel 718 and austenitic stainless steel AISI 316L with coated and uncoated carbide tools. A three-dimensional Finite Element Model was also developed and the predicted results were compared with those measured.

Xinmin Lai et al(2007), This paper was presented on mechanisms studies of micro scale milling operation focusing on its characteristics, size effect, micro cutter edge radius and minimum chip thickness. Firstly, a modified Johnson–Cook constitutive equation is formulated to model the material strengthening behaviors at micron level using strain gradient plasticity. A finite element model for micro scale orthogonal machining process is developed considering the material strengthening behaviors', micro cutter edge radius and fracture behavior of the work material. Then, an analytical micro scale milling force model is developed based on the FE simulations using the cutting principles and the slip-line theory. Extensive experiments of OFHC copper micro scale milling using 0.1mm diameter micro tool were performed with miniaturized machine tool, and good agreements were achieved between the predicted and the experimental results. Finally, chip formation and size effect of micro scale milling are investigated using the proposed model, and the effects of material strengthening behaviors and minimum chip thickness are discussed as well. Some research findings can be drawn: (1) from the chip formation studies, minimum chip thickness is proposed to be 0.25 times of cutter edge radius for OFHC copper when rake angle is 101 and the cutting edge radius is 2 mm; (2) material

strengthening behaviors are found to be the main cause of the size effect of micro scale machining, and the proposed constitutive equation can be used to explain it accurately. (3) That the specific shear energy increases greatly when the uncut chip thickness is smaller than minimum chip thickness is due to the ploughing phenomenon and the accumulation of the actual chip thickness.

B. Ganesh babu et al (2008), the cutting forces exerted by the cutting tool on the work piece during a machining action to be identified in order to control the tool wear and occurrence of vibration, thus to improve tool-life. Modeling of cutting force in milling is often needed in machining automation. The objective of this study is to predict the effects of cutting parameters on the variations of cutting forces during end milling operation of Al SiC metal matrix composite material. Cutting forces are measured for varies feed rates. In this study Response Surface Methodology is used by designing four factors, five level central composite rotatable design matrixes with full replication; for planning, conduction, execution and development of mathematical models. The average cutting forces are determined at different feed rates in tangential, radial, and axial directions per tooth period by keeping immersion and axial depth of cut as constant. A comparison between modeling and experiment is presented. This model and analysis are useful not only for predicting the tool wear but also for selecting optimum process parameters for achieving the stability of the end milling process.

W .Hsiang Lai (2000), According to previous research of dynamic end milling models, the instantaneous dynamic radii on every cutting position affects the cutting forces directly since the simulated forces are proportional to the chip thickness, and the chip thickness is a function of dynamic radii and federates. With the concept of flute engagement introduced, it is important to discuss it with respect to radial and axial depths of cut because the length of the engaged flutes is affected by factors in the axial feed and rotational directions. Radial and axial depths of cut affect the “contact area”, which is the area that a cutter contacts with the work piece. When radial and axial depths of cut increase, the cutting forces also increase since the engaged flute lengths are increased.

Therefore, in order to have a clearer idea of the milling forces, the influences of dynamic radii, cutting federate, and radial and axial depths of cut are discussed in this paper.

Y. Li et al (1999), this paper proposed a method for predicting transient state forces in milling processes as the cutter engages with and disengages from a work piece. Analysis of this nature can contribute to the fundamental understanding of forced vibrations, deflections, and dynamic stability of multi-flute milling systems at the start and end of a cutting pass, thereby facilitating process planning, tool geometry optimization, and on-line diagnostics. The calculation of transient cutting forces is commonly performed with the determination of local forces and numerical integration along cutting edges. In an effort to provide an estimation of transient cutting forces without resorting to numerical integration, this paper uses the result of a frequency domain model obtained from convolution integration as a basis for examining the temporal discretisation of a transient state cutting into steady-state conditions with various engagement and disengagement positions. The resulting milling forces in axial, feed, and cross-feed directions are expressed explicitly in terms of work piece material properties, tool geometry, cutting parameters and process configuration. The process of end milling is presented to illustrate the applicability of the proposed method. End-milling experiments were performed and results compared to the force predictions for the verification of the analytical models.

K. Hua Fuh et al (1998), in this study, a predicted milling force model for the end milling operation is proposed. The speed of spindle rotation, feed per tooth, and axial and radial depth of cut are considered as the affecting factors. An orthogonal rotatable central composite design and the response surface methodology are used to construct this model. The milling force per spindle revolution period obtained from each treatment is equally divided into suitable sections. The extreme value of the milling force in each section is selected to build the predicted model so as to predict the extreme force in each section for any cutting conditions within the specified range of the design database, including the speed of spindle rotation, feed per tooth, and axial and radial depth of cut. Moreover, the predicted extreme force in each section is applied to reconstruct the milling force waveform by means of the expansion of the Fourier series. The predicted model

presented in this paper is adequate for a 95% confidence interval, and shows good correlation between experimental and predicted results.

S. G. Kapoor et al (1997), the paper was presented on a summary of work performed in the area of modeling of the dynamic metal cutting process is presented. A general view of evolution of the dynamic cutting process models is depicted. Specifically four modeling approaches including analytical, experimental, mechanistic and numerical methods are critically reviewed. A brief assessment of future research needs is also given.

B. Li et al (2000), this paper was presented on a model for analyzing the reaction forces and moments for machining fixtures with large contact areas, e.g. a mechanical vice. Such fixtures transmit torsional loads in addition to normal and tangential loads and thus differ from fixtures using point or line contacts. The model is developed using a contact mechanics approach where the work piece is assumed to be elastic in the contact region and the fixture element is treated as rigid. Closed-form contact compliance solutions for normal, tangential, and torsional loads are used to derive the elastic deformation model for each contact. A minimum energy principle is used to solve the multiple contact problem yielding unique predictions of the fixture–work piece contact forces and moments due to clamping and machining forces. This model is then used to determine the minimum clamping force necessary to keep the work piece in static equilibrium during machining. An example is given to demonstrate its effectiveness in analyzing the clamping performance of a mechanical vice during machining.

K. Kadirgama et al (2008), corrosion-resistant high alloy casting is often subject of major concern because failures of cast components have led to significant downtime costs and operating problems. With its considerable industrial benefit as an effluent coolant, seawater remains a corrosive environment to many structural materials such as in marine and power generation sector. Hastelloy C-22HS is one of the best alloys for seawater resistance. Finite element (FEA) method and response surface method (RSM) are used to find the effect of milling parameters (cutting speed, feed rate and axial depth) on cutting force when milling Hastelloy C-22HS. Based on variance analysis of First- and second order RSM models, most influential design variable is feed rate. Optimized cutting force

values are subsequently obtained from model equations.FEA model shows distribution of cutting force.

David Burton et al (2000), This paper was presented on a concept for a dynamometer designed to operate within a frequency range of 10 kHz to 16 kHz while measuring cutting forces less than 1 N. The design is based on two coupled, single degree-of-freedom (SDOF) flexures that interact to produce vibration modes at the edge of the bandwidth of interest. These modes produce a FRF within the desired frequency band that has a magnified response and nearly constant value between modes. The work piece is mounted to the first of the two flexures while a precision accelerometer with a frequency range up to 20 kHz is mounted to the second flexure. To limit the effect of additional structural modes, finite element analysis (FEA) is used to optimize the flexure design by forcing the natural frequencies of additional modes above the bandwidth of interest. To validate the dynamometer design prior to manufacture, an uncertainty analysis is performed.

Turnad L. Ginta et al (2009), this paper was presented on the investigation of tool life improvement in end-milling of Titanium Alloy Ti-6Al-4V through work piece reheating. End milling tests were conducted on Vertical Machining Centre with full immersion cutting. Induction heating was utilized during end milling for preheating. The titanium alloy Ti-6Al-4V bar was used as the work piece. Machining was performed with a 20 mm diameter end-mill tool holder fitted with one PCD inserts. All of the experiments were run under room temperature and preheating condition at 315, 450, and 650ºC. Flank wear has been considered as the criterion for tool failure and the wear was measured using a Hisomet II Toolmaker's microscope. Tests were conducted until an insert was rejected when an average flank wear greater than 0.30 mm was recorded. Cutting force and torque measurements were conducted using the Kistler Rotating Cutting Force Dynamometer. Vibration during cutting was captured using an online vibration monitoring system. Scanning electron microscope (SEM) was also used to investigate the wear morphology. The results led to conclusions that work piece preheating significantly increases the tool life of PCD inserts in end-milling of Titanium Alloy Ti-6Al-4V.

M. Bouaziz et al (2000), the article presented on a method of a cutting force prediction in the case of a ball-end milling. We have proposed a geometrical description of generic tool so as to simulate the 3 axis milling operation with s hemispherical ball-end cutter. The tool is decomposed into elementary discs. a mechanical approach of the cut is applied onto each disc to obtain the cutting force from th machined material behavior and from the cutting conditions. The model thus obtained will be afterward generalized in the case of an inclined or circular surface. This generalization is carried out by adopting, at each time, an adequate reference change, dependent on trajectory inclination angle. For application we will consider the milling of a complex part. In fact the synthesized cut model will be applied to the different types of surfaces which constitute this work piece. And this will be executed according to the two machining senses, longitudinal and transversal.

J.P. Wulfsberg et al (2001), the measurement of cutting forces is however problematic during micro machining operations, because the today's cutting force measuring devices have too low natural frequencies and is not qualified consequently for that. Therefore new force measurement systems with higher natural frequencies must be developed and assayed for their suitability. A solution of a piezoelectric force measurement system for the micro machining operations like micro milling is detailed presented and examined here. Results of first experiments show that with this new system more accurate force measurements are possible.

A. Chukwujekwu Okafor et al (2006), Cutting forces are essential determinants in machining processes, and designing tools and fixtures necessary for production. Excessive cutting forces cause unacceptable large deformation of cutting tool, work piece, and quality of the machined surface. They also have a major influence on the life of the machine tool. Therefore a sound knowledge of cutting forces and the effect of cutting parameter s on them is vital. This paper presents the results of 3-D finite element modeling and simulation of cutting forces in end-milling of titanium (Ti-6Al-4V) alloy work piece used in aerospace industry. Simulations are done using carbide end-mills with varying corner radius, coated with TiAlN. Finite element modeling and simulations were

performed using Thirdwave AdvantEdge software. The effects of spindle speed, feed per tooth, axial depth of cut, radial depth of cut, and corner radius were investigated using Taguchi L16 design of experiment. Mechanistic model of cutting forces for the same tool was developed and cutting forces predicted from this model were compare with the results obtained from finite element analysis. End-milling experiments were conducted on Cincinati Milacron Sabre 750 Vertical Machining Center for validating the results obtained by the above two methods. Cutting forces were acquired using Kistler 4-component dynamometer. The results and optimum machining parameters for machining titanium are presented

F. Cus et al (2001), this paper was presented on an approach, for the systematic design of condition monitoring system for machine tool and machining operations. The research is based on utilizing the genetic optimization method for the on-line optimization of the cutting parameters and to design a programme for the signal processing and for the detection of fault conditions for milling processes. Cutting parameters and the measured cutting forces are selected in this work as an application of the proposed approach.

Andrew Otieno et al (2008), Micromachining is increasingly continuing to have very significant impacts on national security, defense, energy, healthcare and domestic manufacturing base. Micro-parts are being utilized in the electronic and drive systems for small unmanned reconnaissance planes, for high precision parts used in missile guided systems, for medical devices to deliver medicines in tumors located in fragile internal organs, and many other significant applications. Tooling in micromachining involves end mills and drills with dimensions that make them usually invisible to the human eye. It is therefore difficult to detect tool wear, let alone tool failure or breakage. This problem is also compounded by the lack of mach inability data that could be used to select optimum cutting conditions that minimize possibility of failure in addition to lowering the amount of wear on the tool. This paper presents a finite element analysis of the machining of aluminum T6061 alloys. The cutting forces and temperatures are predicted using advantaged software. The results are used to guide machining operators to select

machining conditions that produce favorable stresses on the tools, thus avoiding tool breakage.

Süleyman Yaldız et al (1999), In this study, a turning dynamometer that can measure static and dynamic cutting forces by using strain gauge and piezo-electric accelerometer respectively has been designed and developed. The orientation of octagonal rings and strain gauge locations has been determined to maximize sensitivity and to minimize cross-sensitivity. The developed dynamometer is connected to a data acquisition system. Cutting force signals were captured and transformed into numerical form and processed using a data acquisition system consisting of necessary hardware and software running on MS-Windows based personal computer. The obtained results of machining tests performed at different cutting parameters showed that the dynamometer could be used reliably to measure cutting forces.

CHAPTER-4

DESIGN OF EXPERIMENT

4.1 OUTLINE OF THESIS WORK

The recent study consists of experimentations, parametric analysis using ANSYS v11.0 software and finally theoretical modeling using SYSTAT software.

Experimentation generally specifies the machining of EN series specimen on vertical milling machine. A piezoelectric dynamometer has been installed on milling machine for calculating forces on work piece while machining. Once forces are known in 3-D space, these are fed into ANSYS input table and we can get maximum stress region and stress values over the volume of specimen. For validation of experiment results we need theoretical method, for that purpose 2^{nd} order mathematical equation is used and its coefficients are calculated using SYSTAT.

Once we have a valid mathematical model compatible with the experimentation we don`t need to repeat experiments for large number of time. Here we can feed parameters and we will get the desirable forces thus saving lot of effort and time. The properties of the specimen are given in the Table-4.1.

Table 4.1 Materials and compositions

MATERIAL	C	Si	Mn	S(max)	P(max)	Cr	Ni	Mo
EN8	0.33-0.38	0.05-0.35	0.7-0.9	0.06	0.06			
EN19	0.05-0.35	0.1-0.35	0.5-0.8	0.05	0.05			0.2-0.4
EN31	0.9-1.2	0.1-0.35	0.3-0.7	0.05	0.05	1-1.4		
EN353	0.2(max)	0.35(max)	0.5-1	0.05	0.05	0.75-1.25	1-1.5	0.08-0.15
EN44	0.9-1.05	0.35(max)	0.3-0.7	0.05	0.05			

Test conditions leading to various components of cutting force in EN series material were chosen. The upper limit of a factor is coded as 1 and lower limit as -1.

Table 4.2 Input parameters

SI No.	Parameters	Unit	Notation	Factor Levels		
				-1	0	+1
1	Feed Rate	mm/min	F	20	35	65
2	Cutting Speed	m/min	V	102	204	340
3	Depth of cut	mm	A	0.25	0.50	0.75

4.2 EXPERIMENTAL DATA AND ANALYSIS OF EN SERIES MATERIALS

The above mentioned specimen are machined on vertical milling machine for experimentation a KISTLER DYNO WARE is installed on the machine bed according to the design of experiment input variables are varied while end milling the forces on the work pieces are calculated by dynamometer which was coupled with CPU for each set of reading 40 sec time duration is considered next section gives the detailed study of force reading given by dynamometer for specified duration of time.

Now we will discuss each specimen one by one taking its forces values and thereby analyzing the maximum stress regions with each set of varying variables has been discussed.

Table 4.3 Material composition of EN8

C	Si	Mn	S	P
0.33-0.38	0.05-0.35	0.7-0.9	0.06max	0.06max

Table 4.4 Mechanical properties of EN8

Tensile Strength	100-1068 N/mm²
Yield Stress	61-930 N/mm²
Reduction of Area	45-50%
Elongation	14-17%
Modulus of elasticity	215 000 N/mm²
Density	7.8 Kg/m3
Hardness	56 HRC

Figure 4.1 Specimen Details EN8

4.2.1.1

Table 4.5 Machining Parameters of EN8

SPEED	102	r.p.m
FEED	20	mm/min
DOC	0.25	mm

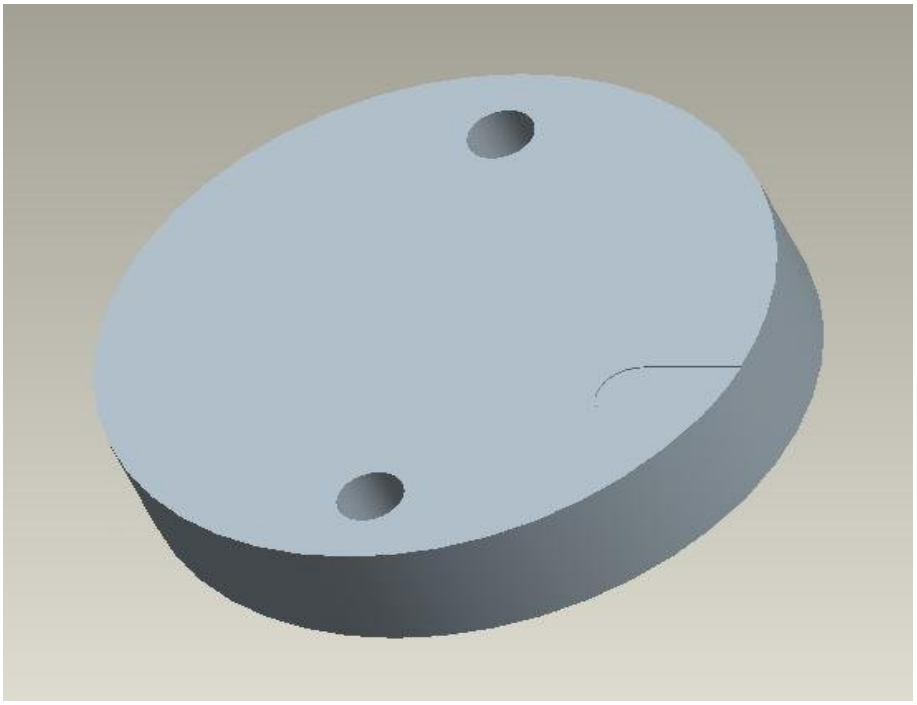

Figure 4.2 Pro-E Model of Specimen of EN8(V=102,F=20,A=0.25)

Table 4.6 Force Values (Kistler\DynoWare)

File Type:			
Path:	C:\Kistler\DynoWare\Data\		
Filename:	millig2.dwd		
Config ID:	millig2.cfg		
Sampling rate [Hz]:	10		
Measuring time [s]:	40		
Delay time [s]:	0		
Cycle time [s]:	0		
Cycles:	1		
Samples per channel:	401		
Channel enabled:	1	1	1
Cycle No:	1		
Time [s]	Fx	Fy	Fz
0	-60.791	14.3066	-67.572

1	-29.3335	17.5171	-57.7087
2	0.146484	-0.12207	1.30005
3	-70.6696	15.0757	-83.6243
4	-50.1343	43.4082	-77.5024
5	-76.7487	30.8472	-116.302
6	-24.2432	31.897	-53.4607
7	-8.04749	13.9038	-25.1465
8	-39.1663	21.46	-34.436
9	-63.0157	15.6372	-85.9863
10	-54.6112	46.4844	-91.8457
11	-42.746	26.7578	-88.208
12	-1.81274	31.5552	-34.1675
13	6.74744	8.94775	-3.16162
14	-57.7148	20.1172	-59.1187
15	-45.813	16.2354	-73.6938
16	-44.0735	44.519	-92.1448
17	-12.4054	22.5464	-54.0222
18	18.5303	30.6519	-12.3962
19	2.74658	3.03955	2.9541
20	-62.796	18.8843	-74.8657
21	-42.5262	25.8179	-75.8667
22	-45.2087	53.1738	-100.745
23	12.5153	25.7446	-28.4241
24	-10.144	16.2964	-31.9519
25	0.357056	10.083	7.62939
26	-51.7273	17.1265	-76.2085
27	-44.1284	39.4531	-92.5354
28	-16.9281	51.0132	-72.9431
29	17.1021	23.3398	-16.571
30	6.63757	16.1255	-16.2659
31	-37.9852	19.6045	-41.7236
32	-51.1139	22.644	-94.9097
33	-34.7992	41.626	-94.6533
34	-24.9298	25.708	-86.2244
35	16.8549	27.9419	-16.2048
36	19.0338	19.9463	13.3423
37	-42.1051	11.8164	-56.0486
38	-33.078	25.7446	-81.6284
39	-32.309	44.4336	-102.606
40	6.80237	14.1724	16.5466

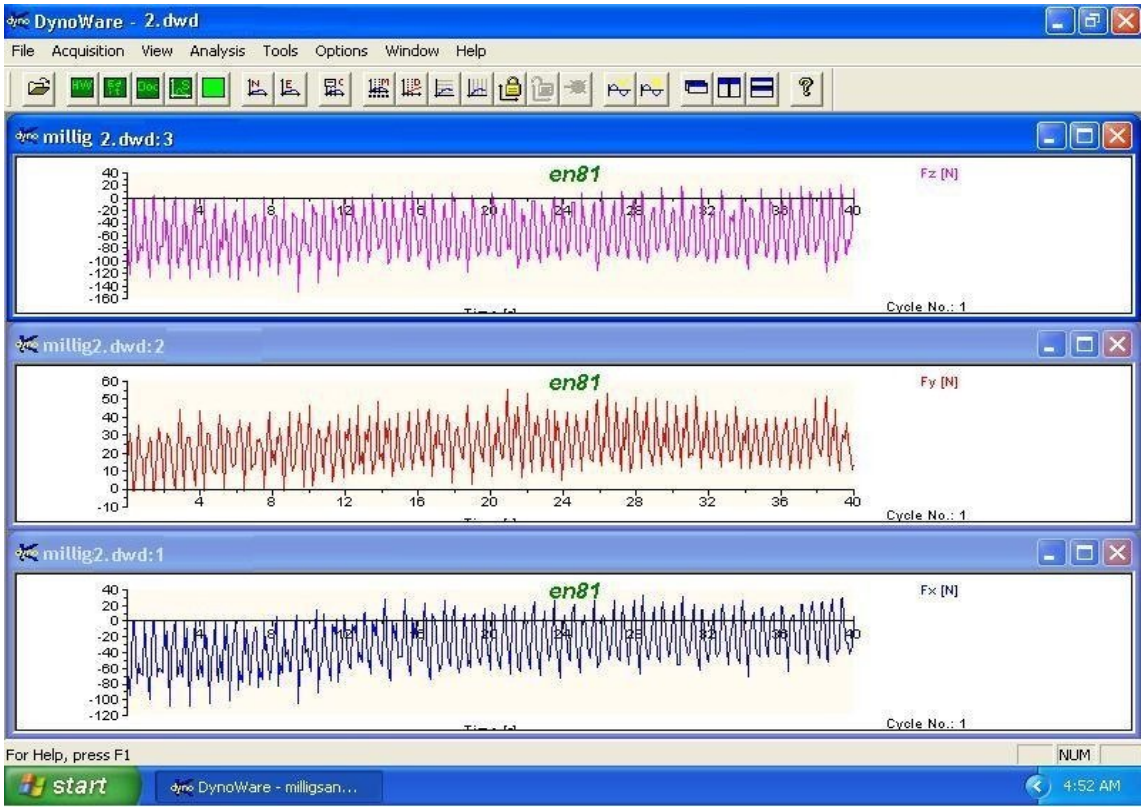

Figure 4.3 Graphical representation of Force Variations of EN8

- **Analysis of EN8**

Analysis software: ANSYS V11.0 (WORKBENCH INTERFACE)

Analysis type : TRANSIENT (40 Sec)

Inputs : IGES (PRO-E), SOLID ELEMENT TETRAHEDRAL 8-NODES

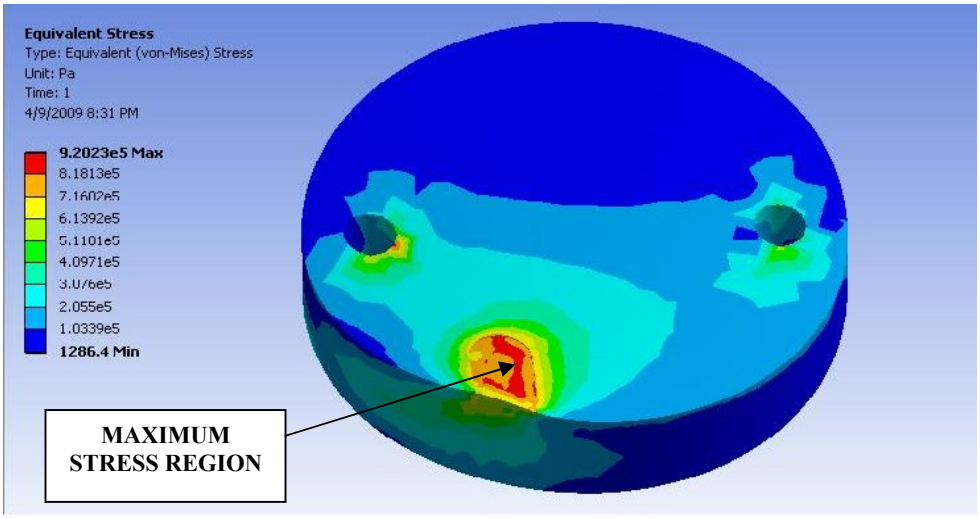

Figure 4.4 Analysis of EN8 (V=102,F=20,A=0.25)

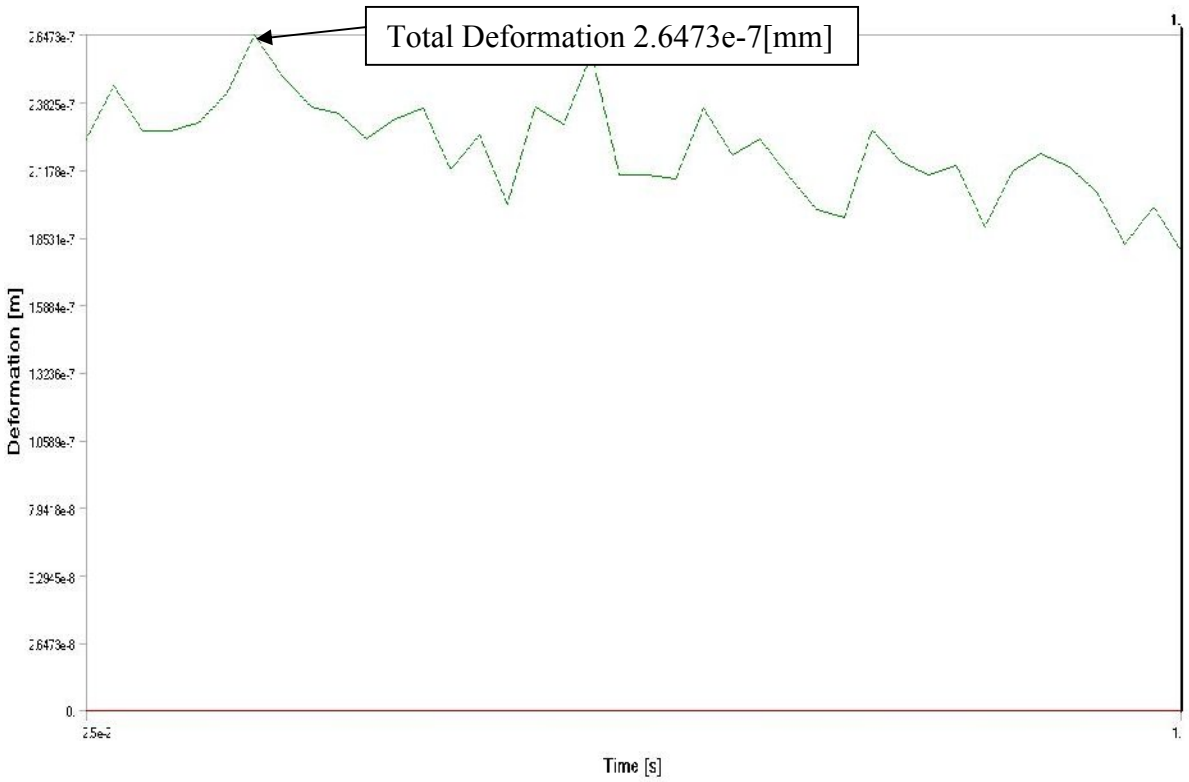

Figure 4.5 Total Deformation of EN8 (V=102,F=20,A=0.25)

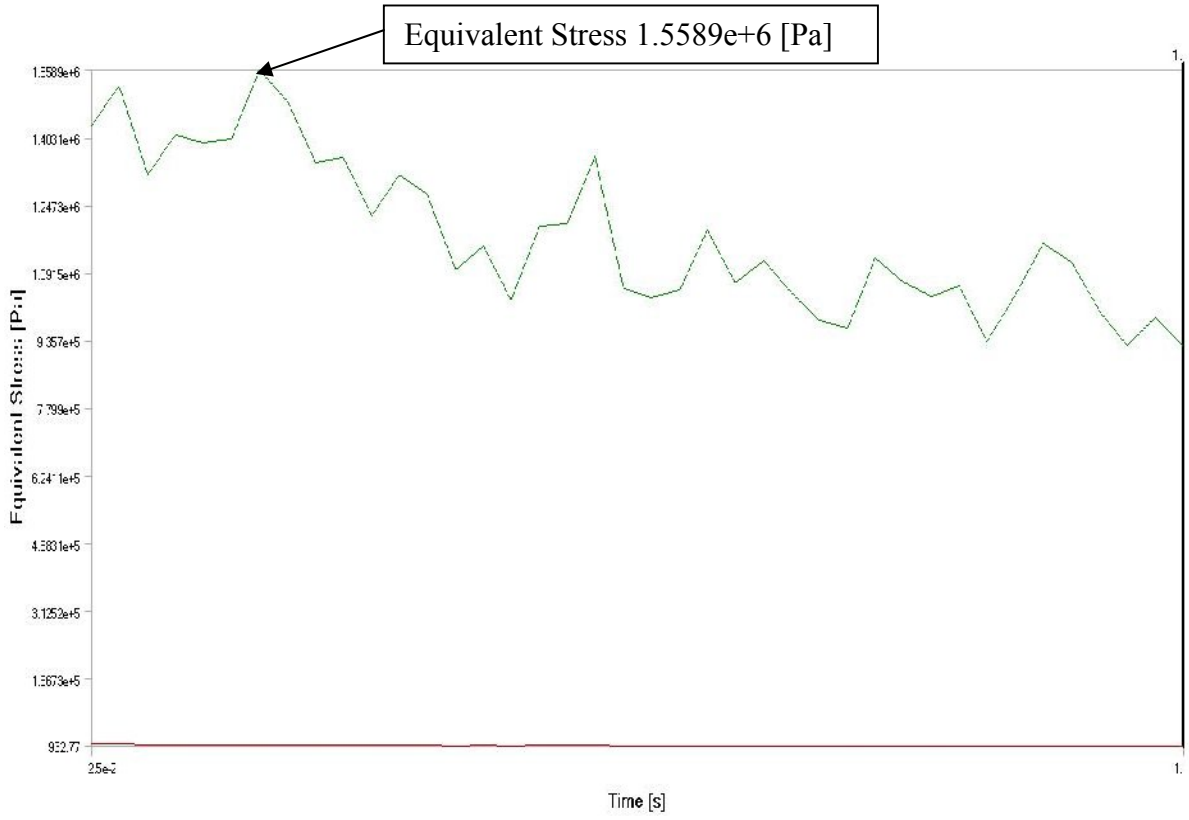

Figure 4.6 Equivalent Stress of EN8 (V=102,F=20,A=0.25)

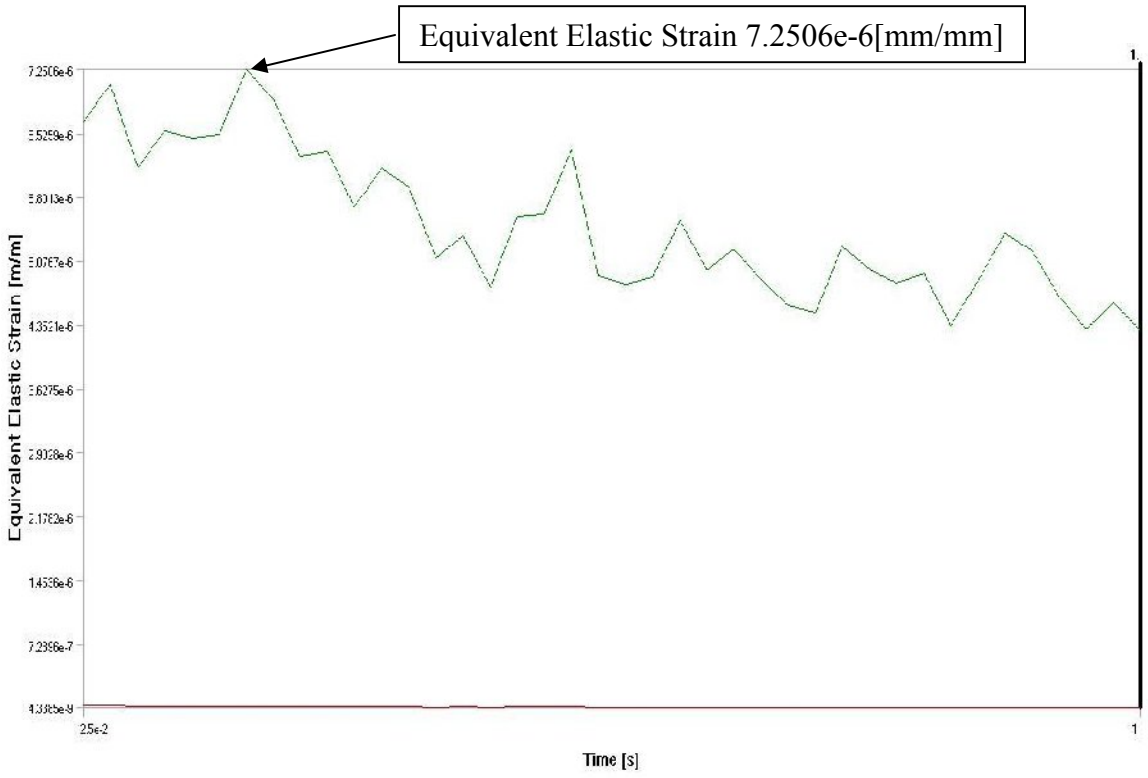

Figure 4.7 Equivalent Elastic Strain of EN8 (V=102,F=20,A=0.25)

4.2.1.2

Table 4.7 Machining parameters of EN8

SPEED	102	r.p.m
FEED	35	mm/min
DOC	0.25	mm

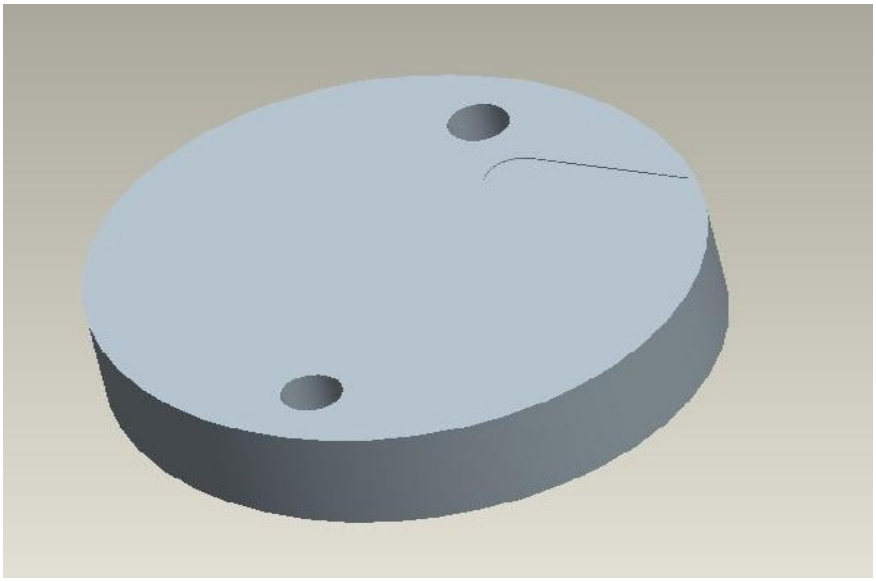

Figure 4.8 Pro-E model of Specimen of EN8(V=102,F=35,A=0.25)

Table 4.8 Force Values (Kistler\DynoWare)

File Type:			
Path:	C:\Kistler\DynoWare\Data\		
Filename:	millig2.dwd		
Config ID:	millig2.cfg		
Sampling rate [Hz]:	10		
Measuring time [s]:	40		
Delay time [s]:	0		
Cycle time [s]:	0		
Cycles:	1		
Samples per channel:	401		
Cycle interval:	0		
Channel enabled:	1	1	1
Cycle No:	1		
Time [s]	Fx	Fy	Fz
0	-76.3184	-111.963	11.2854
1	-82.2784	-161.23	24.8108
2	-84.3475	-132.458	16.2659
3	-1.62964	-81.4941	17.6575
4	-88.9709	-20.813	4.70581
5	-115.796	-25.8789	10.0586
6	-179.306	-114.661	10.8276
7	-74.4781	-151.587	28.7598
8	-63.7299	-102.539	13.7451
9	41.9037	-67.5171	18.1213
10	-186.145	29.2358	8.54492
11	-166.653	-43.6523	15.7104
12	-203.101	-110.315	19.7021
13	-63.5559	-146.216	24.7253
14	-112.427	-101.27	15.7043
15	14.2822	-71.936	17.0227
16	-207.568	30.7251	7.78198
17	-171.167	-36.6577	17.4622
18	-203.174	-82.5684	15.7166
19	-69.0491	-128.04	25.3662
20	-79.4861	-86.1938	14.7766
21	11.3892	-61.0229	14.0442
22	-198.541	26.9287	8.44727
23	-211.111	-30.5054	16.8518
24	-176.321	-90.1001	22.821

25	-49.1364	-111.414	29.9438
26	-59.2072	-79.5044	16.217
27	3.76282	-68.457	14.7217
28	-235.089	11.8774	4.22363
29	-174.646	-5.70068	21.4111
30	-182.227	-70.1782	22.1619
31	-72.1527	-98.6084	25.7141
32	-80.2826	-76.0254	19.6533
33	-29.6173	-69.9097	11.4624
34	-231.665	4.57764	4.66309
35	-204.373	-10.9985	21.7834
36	-209.665	-65.6128	21.0815
37	-76.886	-80.3711	27.4353
38	-64.9384	-67.2241	18.7317
39	-49.6399	-61.8896	11.6821
40	-262.839	13.1104	5.97534

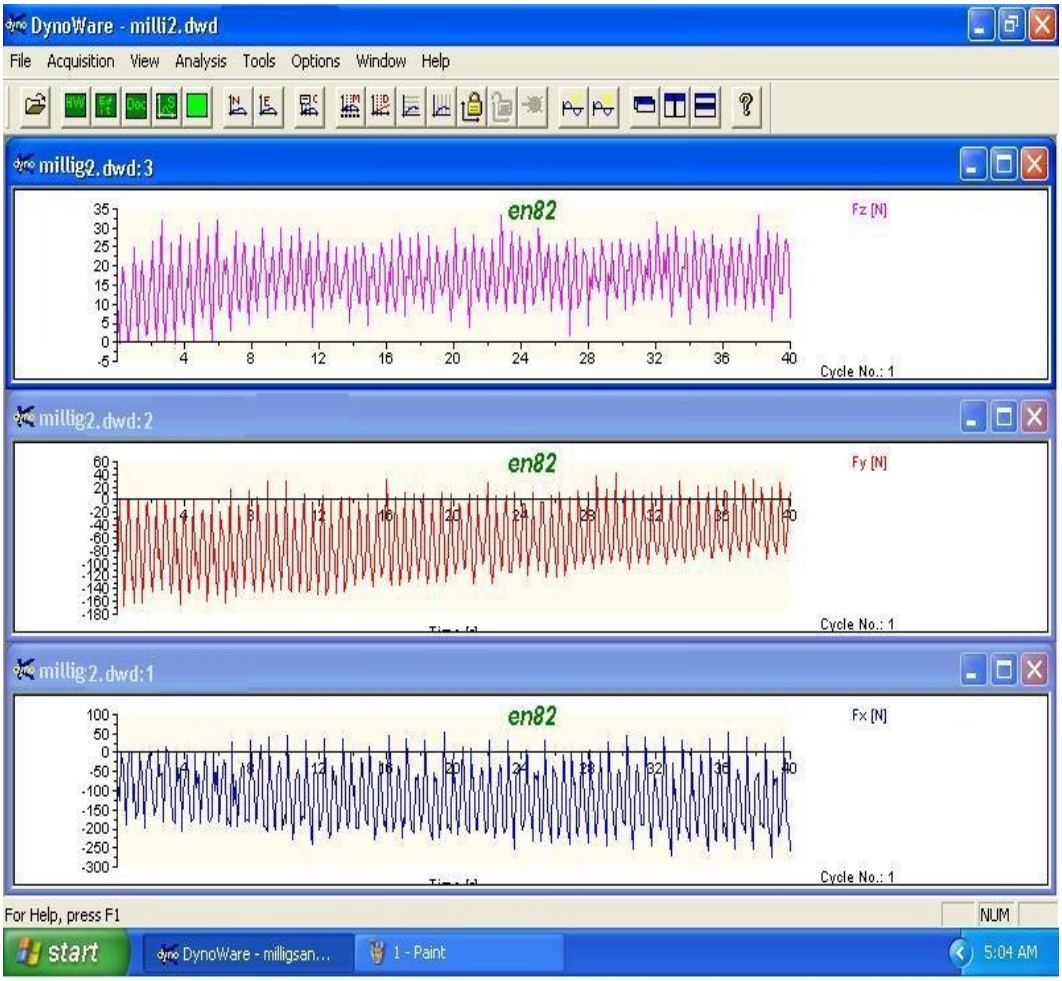

Figure 4.9 Graphical Representation of Force Variations of EN8

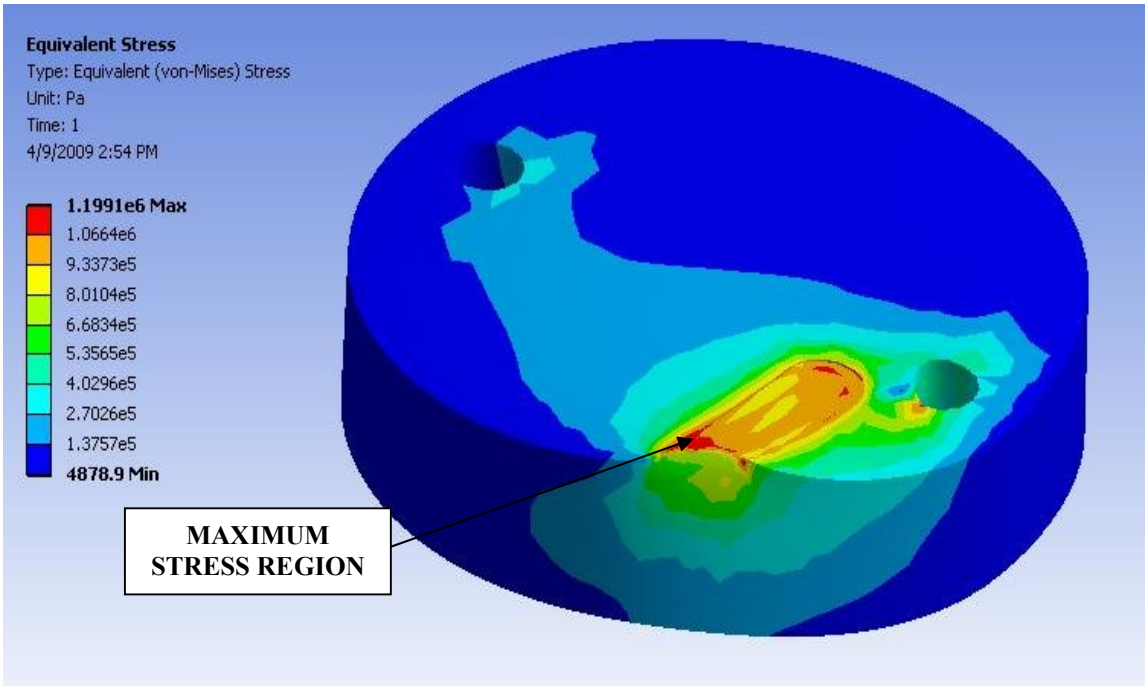

Figure 4.10 Analysis of EN 8 (V=102,F=35,A=0.25)

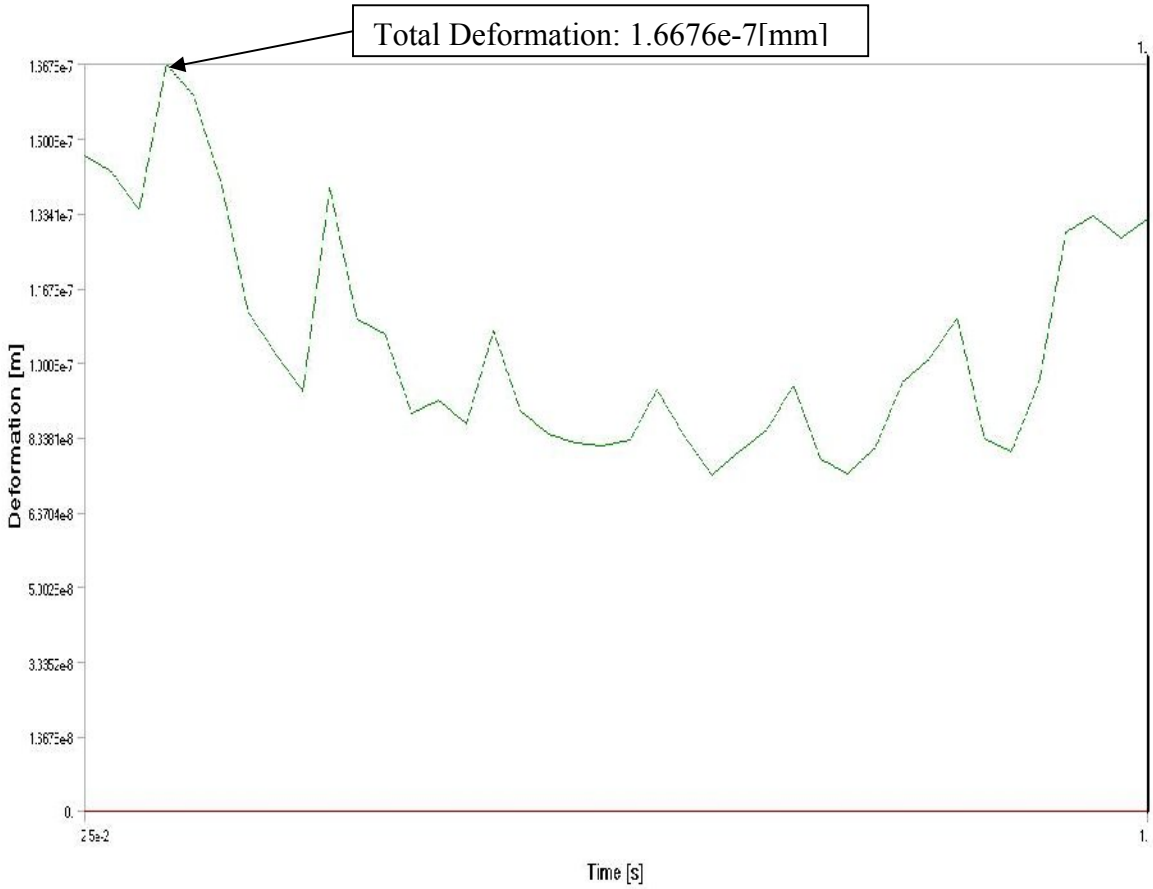

Figure 4.11 Total deformation of EN8 (V=102,F=35,A=0.25)

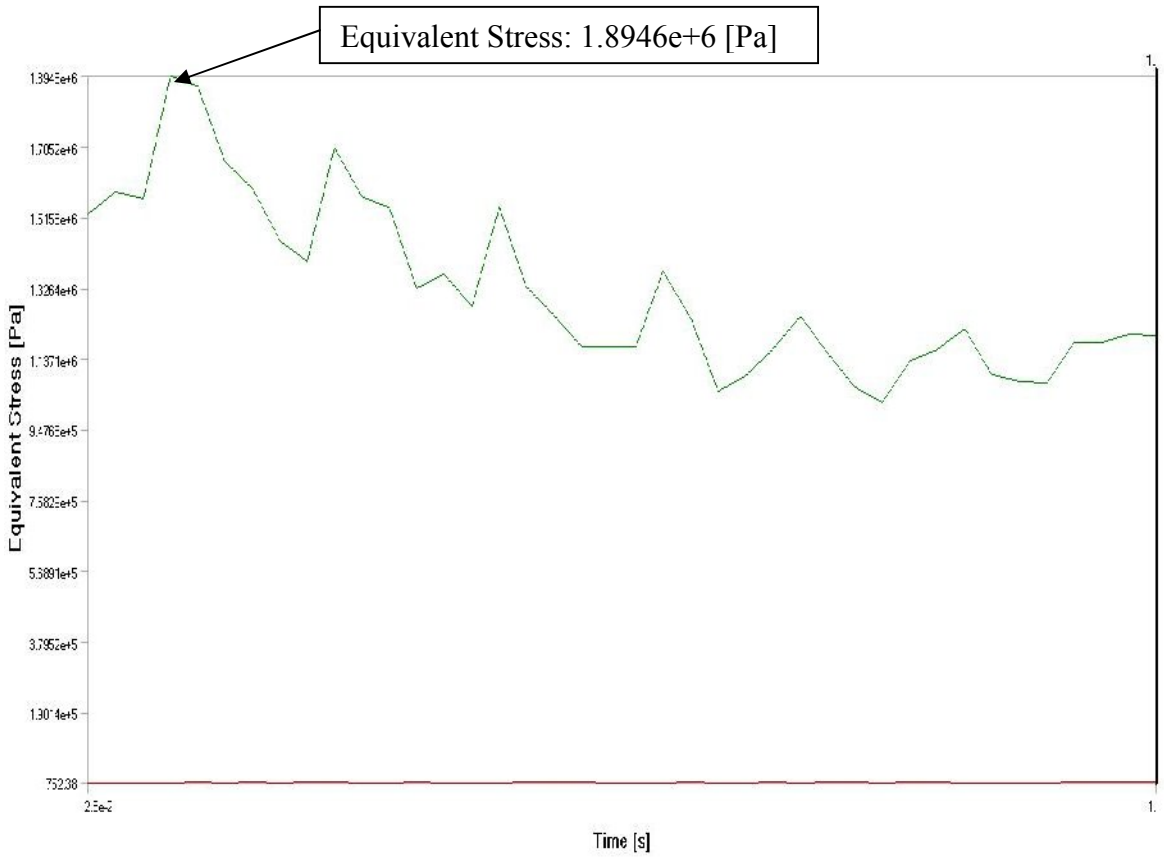

Figure 4.12 Equivalent Stress of EN8 (V=102,F=35,A=0.25)

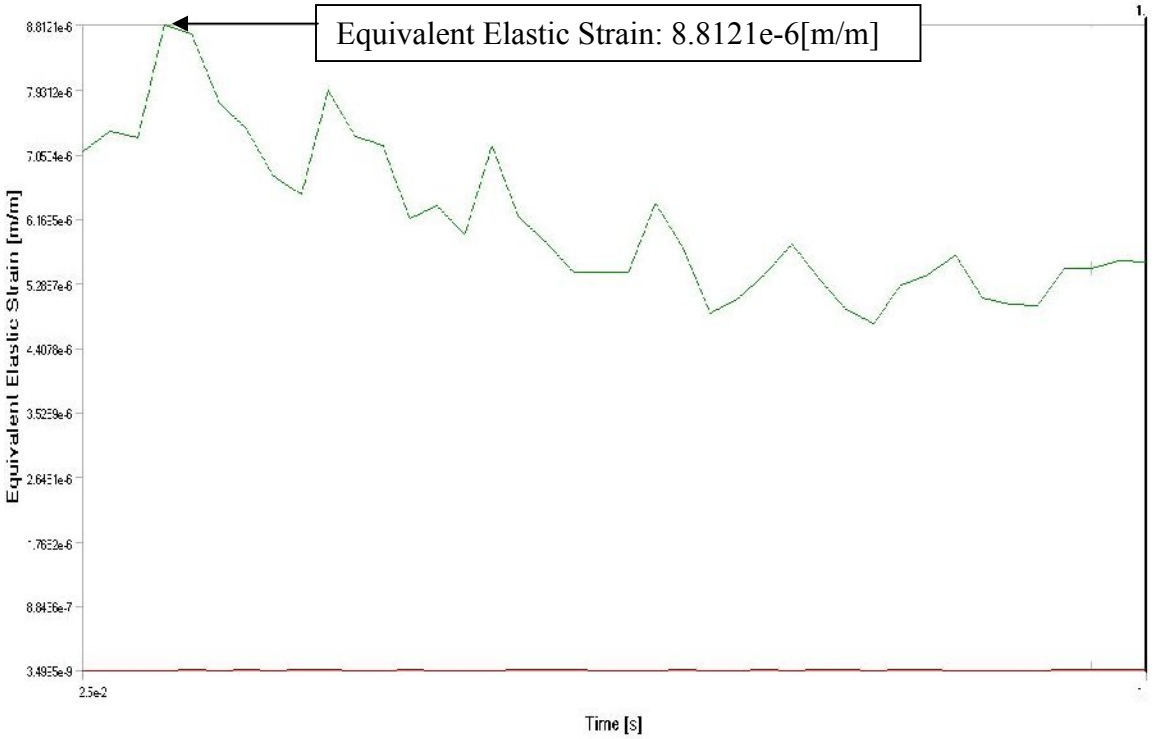

Figure 4.13 Equivalent Elastic Strain of EN8 (V=102,F=35,A=0.25)

4.2.1.3

Table 4.9 Machining parameters of EN8

SPEED	102	r.p.m
FEED	65	mm/min
DOC	0.25	mm

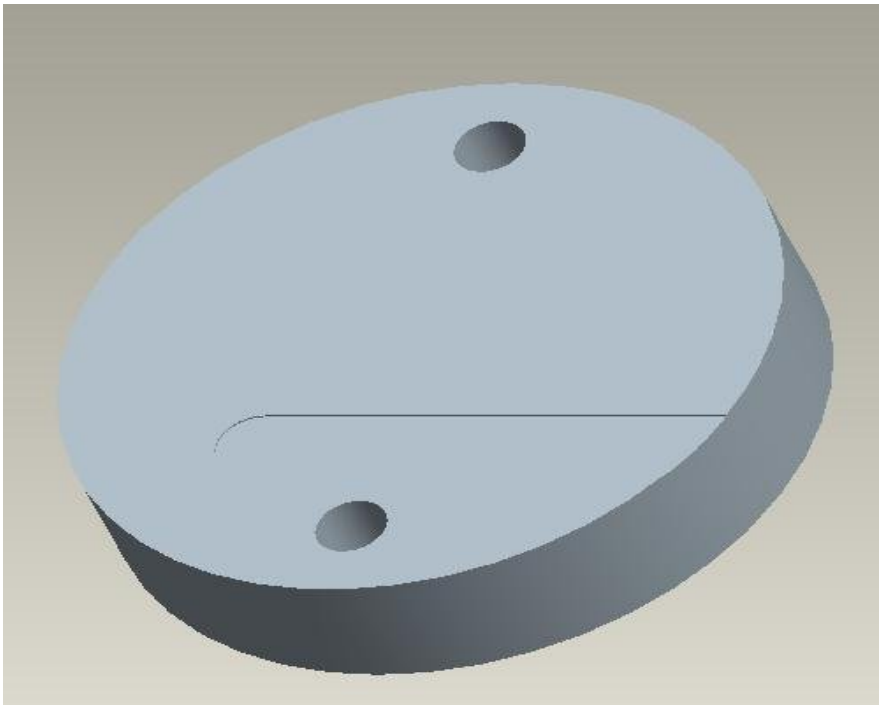

Figure 4.14 Pro-E Model of specimen of EN8 (V=102,F=65,A=0.25)

Table 4.10 Force Values (Kistler\DynoWare)

File Type:			
Path:	C:\Kistler\DynoWare\Data\		
Filename:	millig2.dwd		
Config ID:	millig2.cfg		
Sampling rate [Hz]:	10		
Measuring time [s]:	40		
Delay time [s]:	0		
Cycle time [s]:	0		
Cycles:	1		
Samples per channel:	401		
Cycle interval:	0		
Channel enabled:	1	1	1
Cycle No:	1		
Time [s]	Fx	Fy	Fz

0	-21.0388	50.2808	-99.7803
1	27.3376	37.9395	-31.9519
2	-98.1812	37.6099	-107.135
3	-3.05786	65.1855	-101.08
4	6.92139	33.4839	-56.6895
5	-103.812	44.0308	-145.734
6	10.7941	49.8047	-81.5796
7	2.1698	25.6226	-69.4702
8	-91.3422	44.0308	-177.545
9	10.3821	45.6909	-88.7024
10	21.698	18.8721	-36.1877
11	-63.8489	47.4609	-175.775
12	6.86646	30.9937	-99.8413
13	26.6144	17.9077	-3.50342
14	-10.8856	29.1016	-103.955
15	30.5878	30.188	-62.8845
16	8.78906	9.46045	0.823975
17	-0.93384	39.0625	-111.89
18	38.6902	30.249	-30.9692
19	-19.2352	16.9922	-38.6047
20	17.9535	45.1782	-111.591
21	38.15	29.9072	-17.0044
22	-29.718	24.1455	-69.3909
23	32.5928	49.4629	-89.3982
24	35.907	49.2798	-24.8779
25	-14.6942	22.0581	-69.0552
26	50.235	56.7383	-99.1211
27	28.1616	24.8291	-90.3687
28	-8.99963	38.5986	-129.926
29	51.2787	53.3691	-75.8301
30	35.4584	22.4487	-44.0125
31	15.097	39.9658	-158.661
32	56.7719	35.1074	-127.643
33	23.0896	15.686	-9.14307
34	31.7505	28.1616	-100.934
35	63.3179	33.7891	-93.7805
36	7.86438	10.6812	2.38037
37	49.7406	35.3394	-99.3408
38	25.4517	26.8311	-108.844
39	8.24E-02	2.91748	-1.65405
40	14.0533	38.3057	-103.18

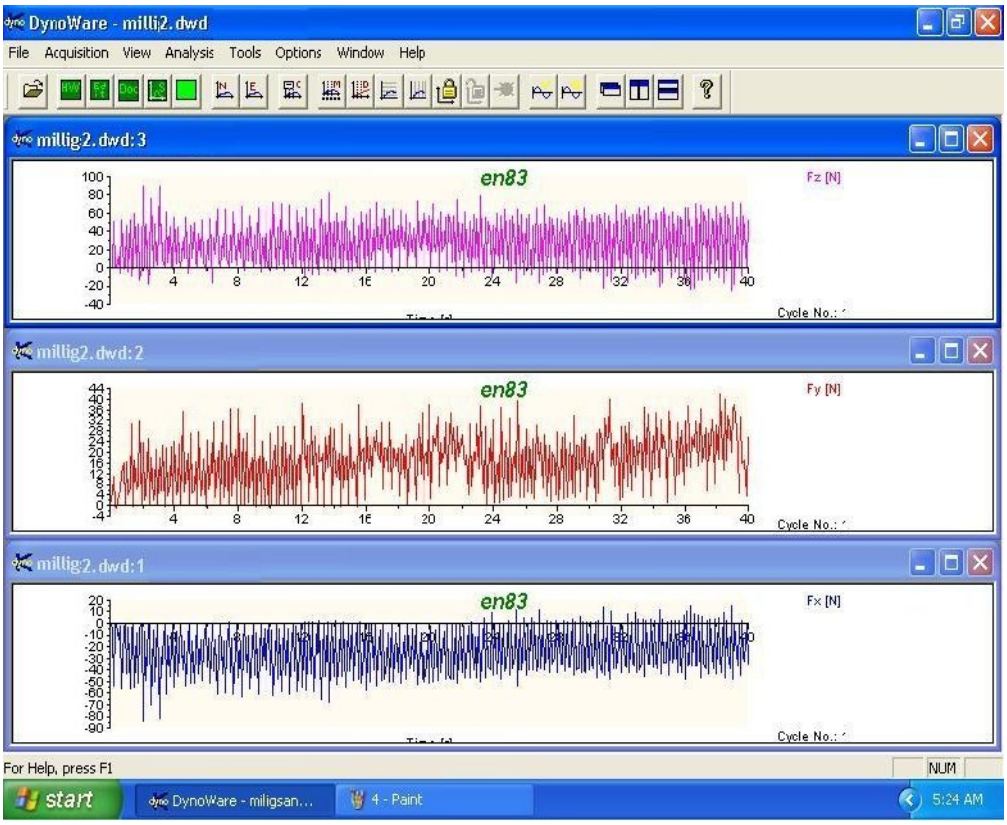

Figure 4.15 Graphical Representations of Force Variations of EN8

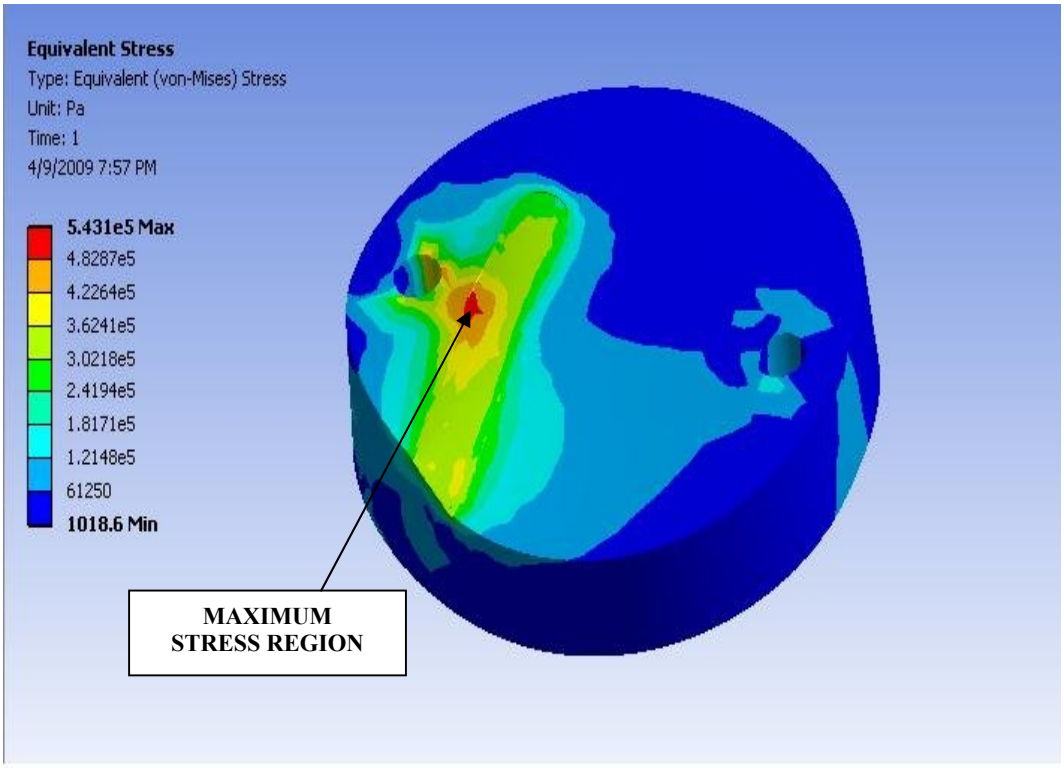

Figure 4.16 Analysis of EN8 (V=102,F=65,A=0.25)

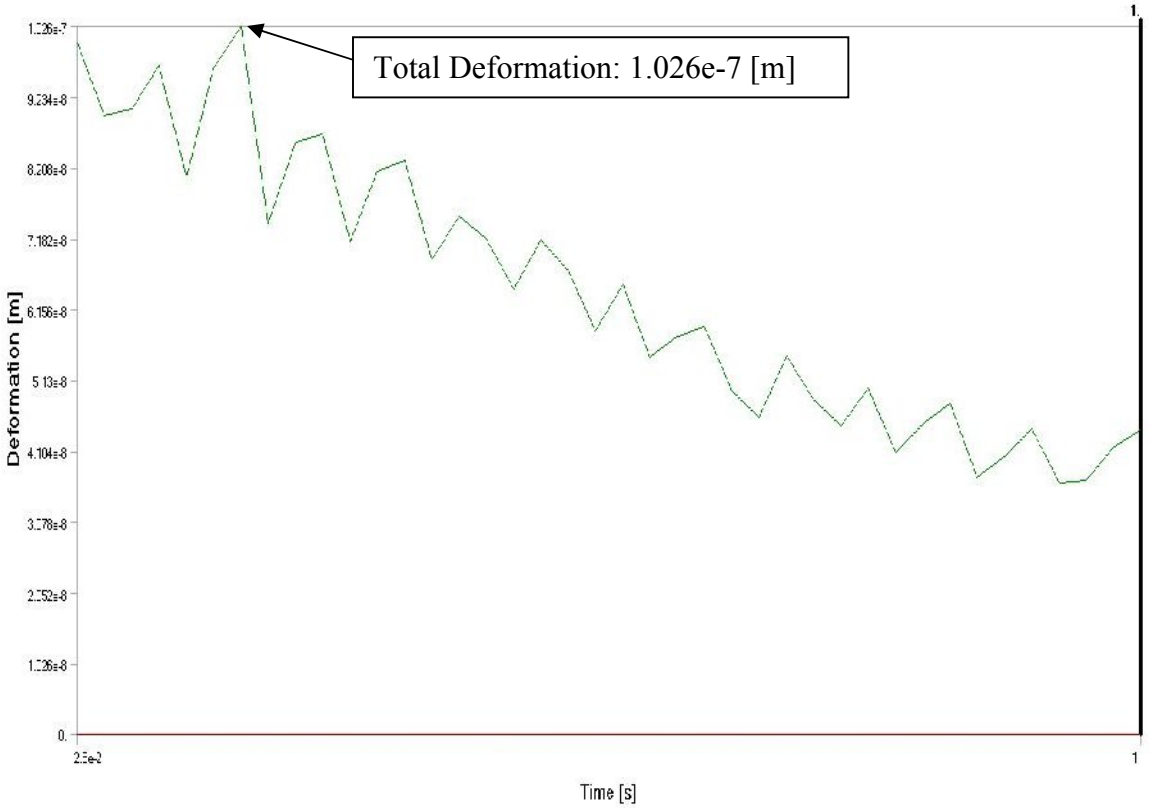

Figure 4.17 Total Deformation of EN8 (V=102,F=65,A=0.25)

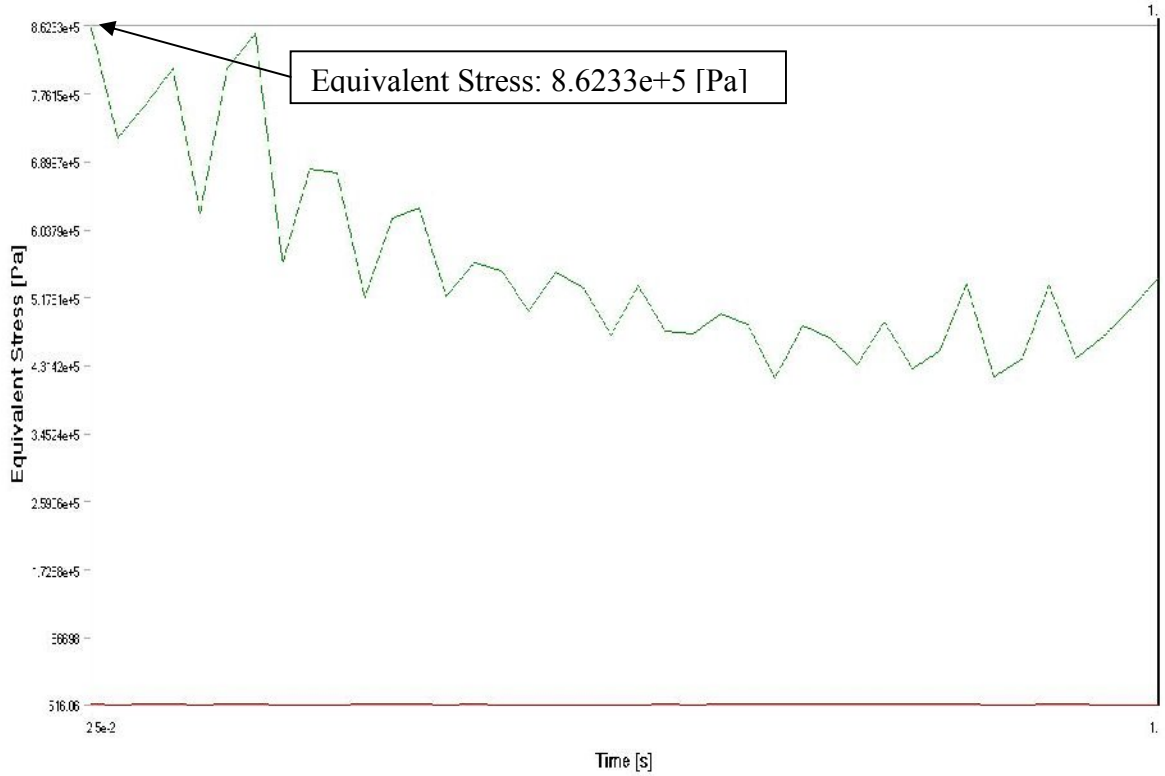

Figure 4.18 Equivalent Stress of EN8 (V=102,F=65,A=0.25)

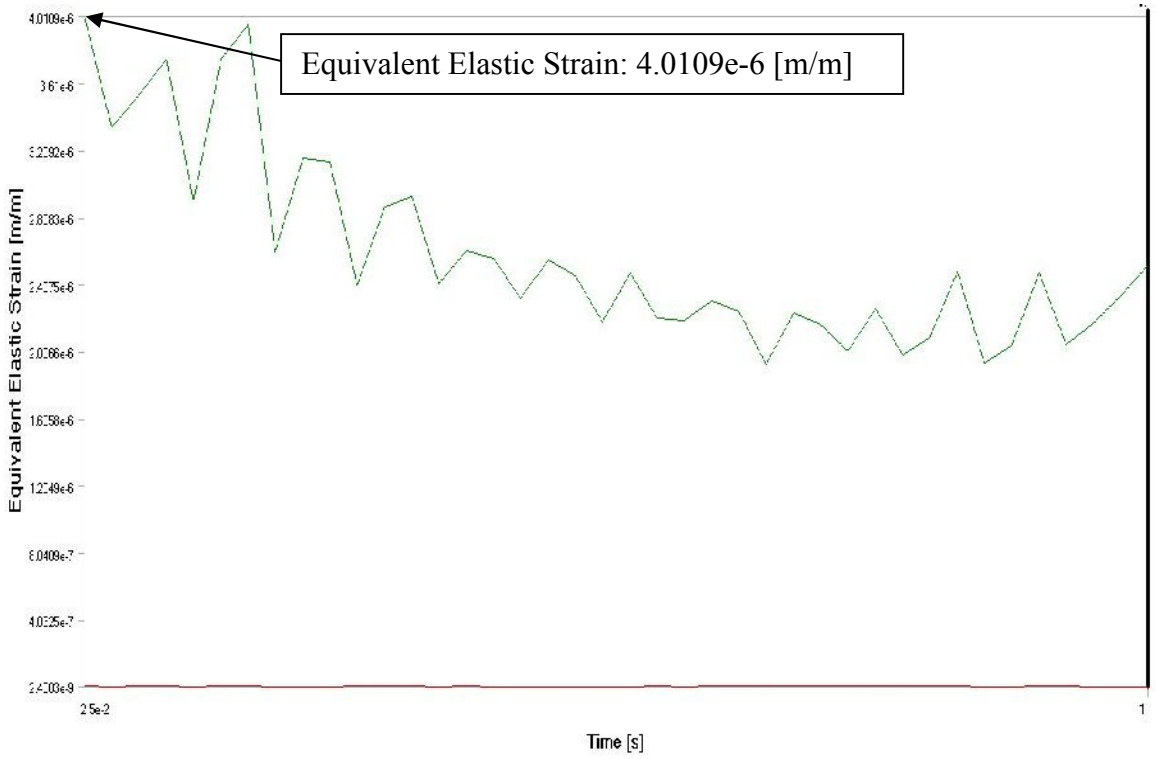

Figure 4.19 Equivalent Elastic Strain of EN8 (V=102,F=65,A=0.25)

4.2.1.4

Table 4.11 Machining parameter of EN8

SPEED	204	r.p.m
FEED	20	mm/min
DOC	0.25	mm

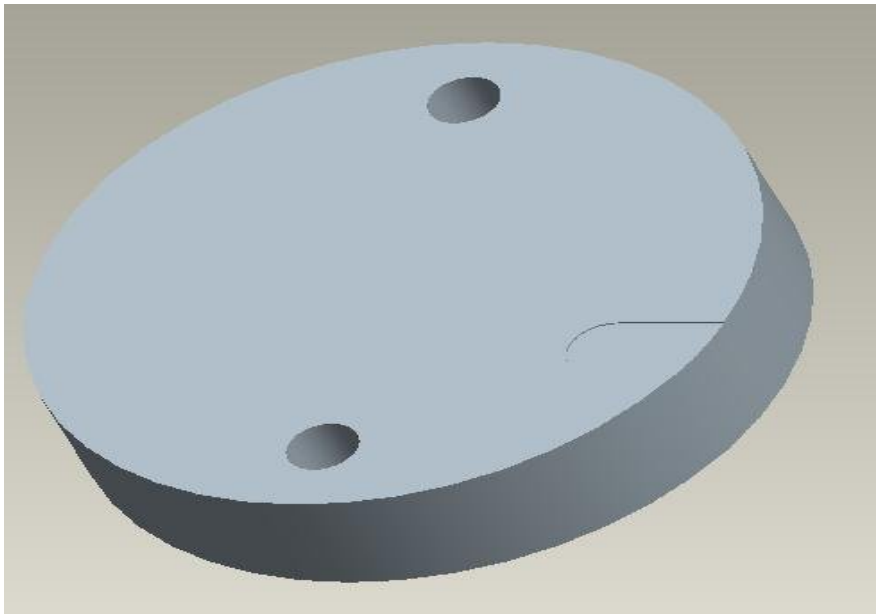

Figure 4.20 Pro-E model of Specimen of EN8 (V=204,F=20,A=0.25)

Table 4.12 Force Values (Kistler\DynoWare)

File Type:			
Path:	C:\Kistler\DynoWare\Data\		
Filename:	millig2.dwd		
Config ID:	millig2.cfg		
Sampling rate [Hz]:	10		
Measuring time [s]:	40		
Delay time [s]:	0		
Cycle time [s]:	0		
Cycles:	1		
Samples per channel:	401		
Cycle interval:	0		
Channel enabled:	1	1	1
Cycle No:	1		
Time [s]	Fx	Fy	Fz
0	-68.6005	-101.685	15.7104
1	-152.289	0.305176	3.61938
2	-108.508	-103.052	7.23267
3	0.714111	-52.6123	14.325
4	-106.476	2.63672	2.97852
5	-58.8043	-78.7476	5.88989
6	-1.84021	-17.4438	14.6301
7	-122.635	1.53809	0.866699
8	-36.5479	-54.6387	4.73633
9	-1.66626	-7.84912	13.562
10	-100.342	0.305176	4.88E-02
11	-3.31421	-84.9121	15.1855
12	-48.4406	30.9937	14.447
13	-123.55	-3.77197	1.25732
14	-5.96008	-72.0703	16.449
15	-59.1339	23.4375	14.5935
16	-113.69	-45.52	3.95508
17	3.16772	-31.8481	16.5771
18	-114.468	42.5903	15.8813
19	-95.1508	-75.2808	8.47778
20	-37.5092	-33.4229	13.7268
21	-130.536	5.48096	7.86133
22	-102.356	-97.1558	7.95288
23	-28.2166	-8.8623	17.2485
24	-160.803	1.72119	5.31616

25	-87.8448	-92.6636	10.2539
26	-8.04749	-28.0396	17.8345
27	-167.789	9.36279	6.10352
28	-92.3859	-80.2979	7.93457
29	9.79614	-27.6367	13.2568
30	-121.573	7.21436	2.54517
31	-69.5984	-70.105	8.41064
32	2.41699	-2.6001	10.7849
33	-139.993	1.14746	1.2085
34	-23.9136	-54.3457	12.2681
35	2.34375	22.8271	11.3586
36	-117.709	4.06494	1.70898
37	-9.62219	-43.8477	16.7908
38	-71.0815	35.2051	13.092
39	-115.082	-49.707	9.7229
40	6.6925	-15.2832	12.2131

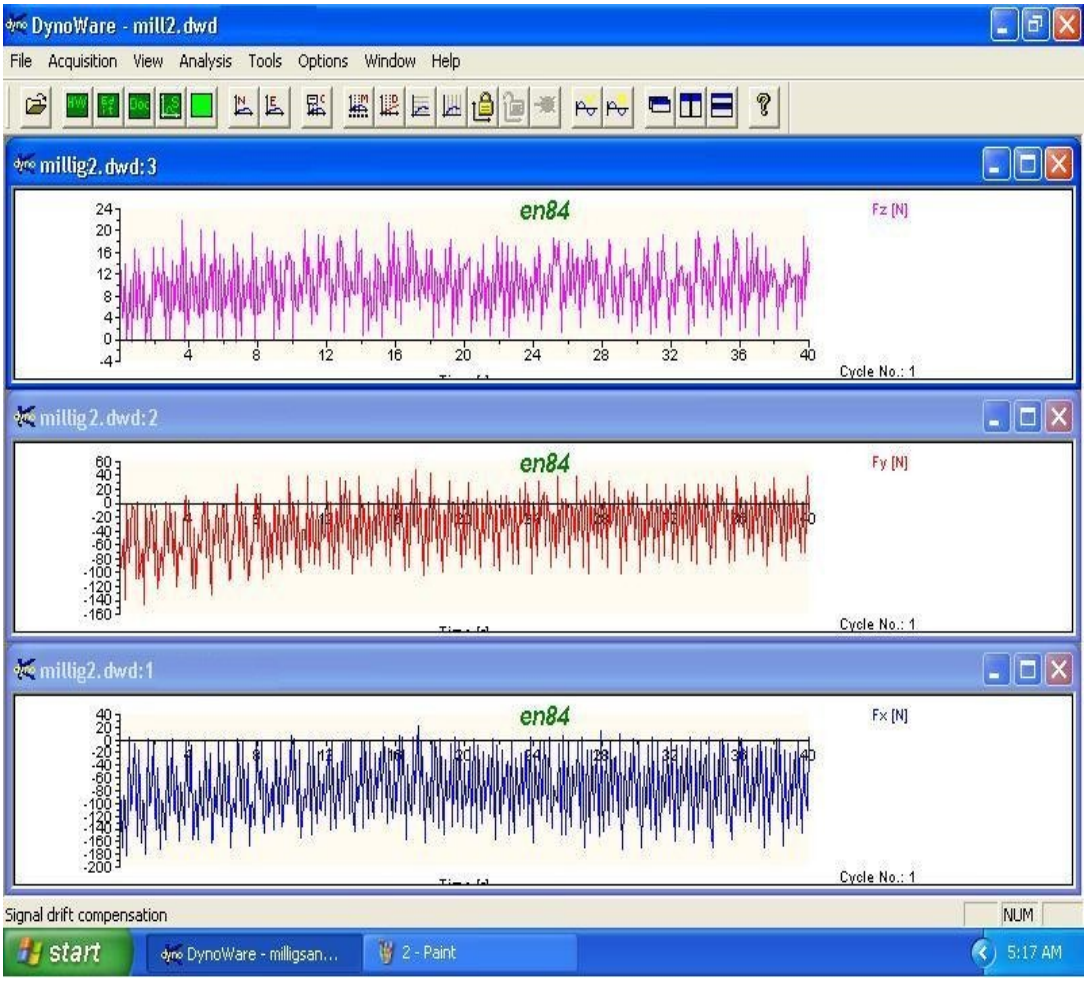

Figure 4.21 Graphical representation of Force Variations of EN8

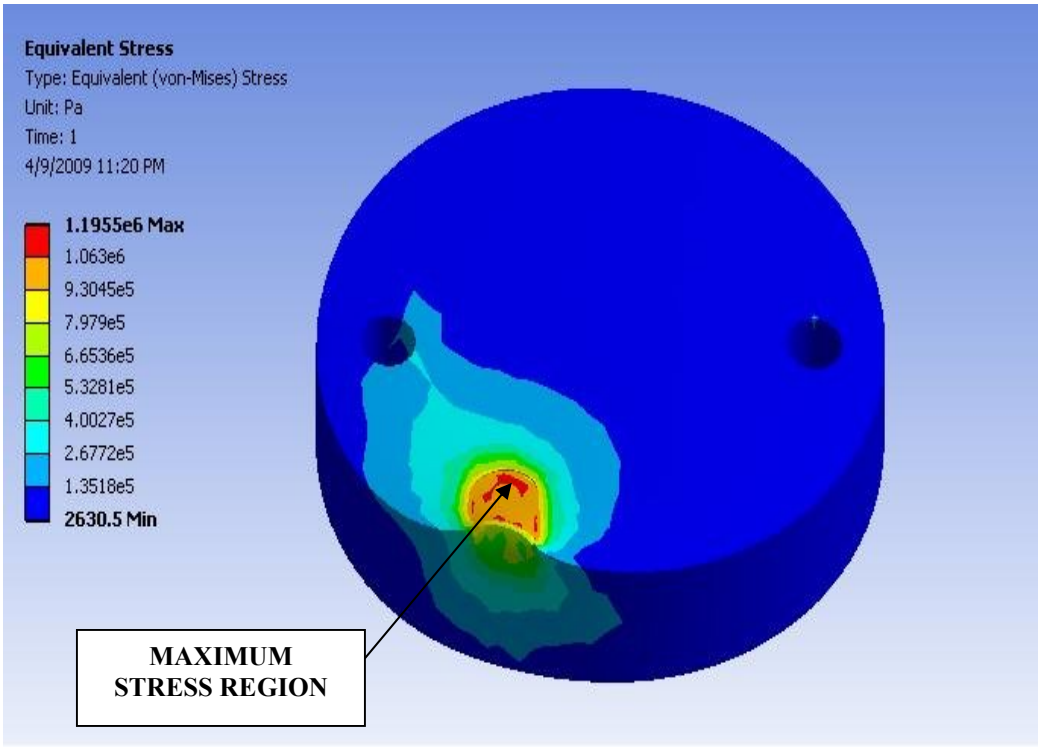

Figure 4.22 Analysis of EN8 (V=204,F=20,A=0.25)

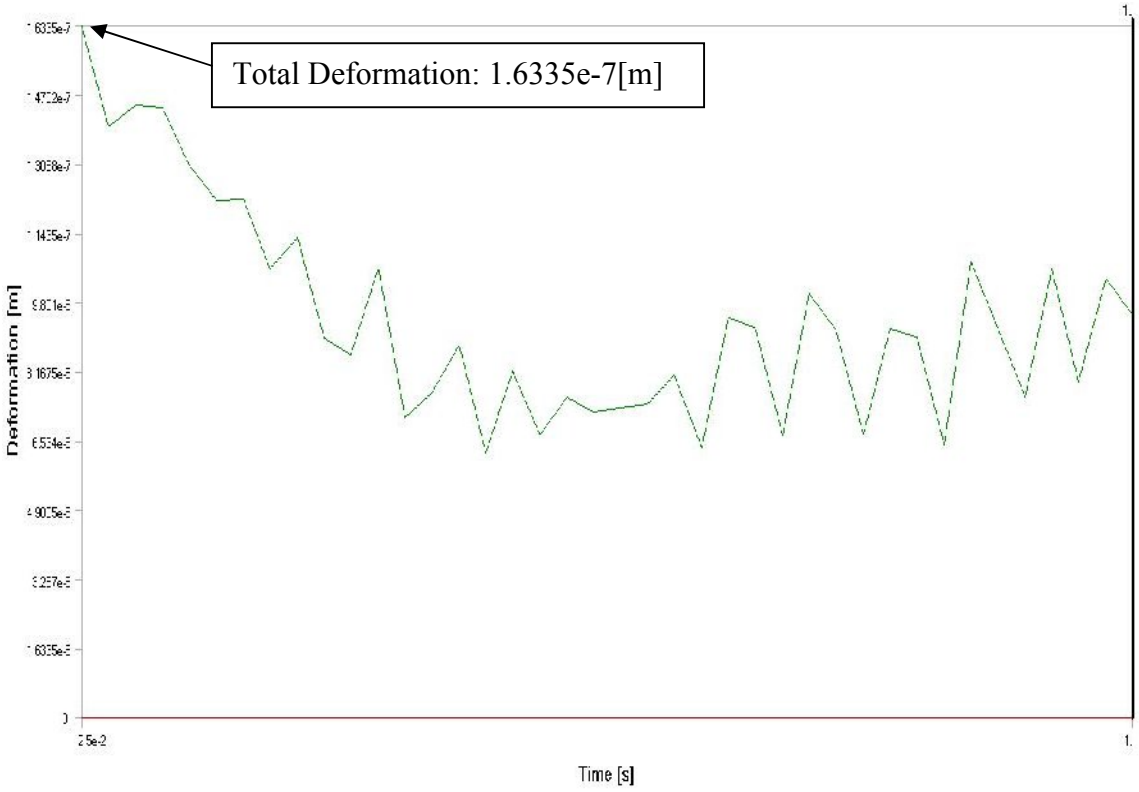

Figure 4.23 Total Deformation of EN8 (V=204,F=20,A=0.25)

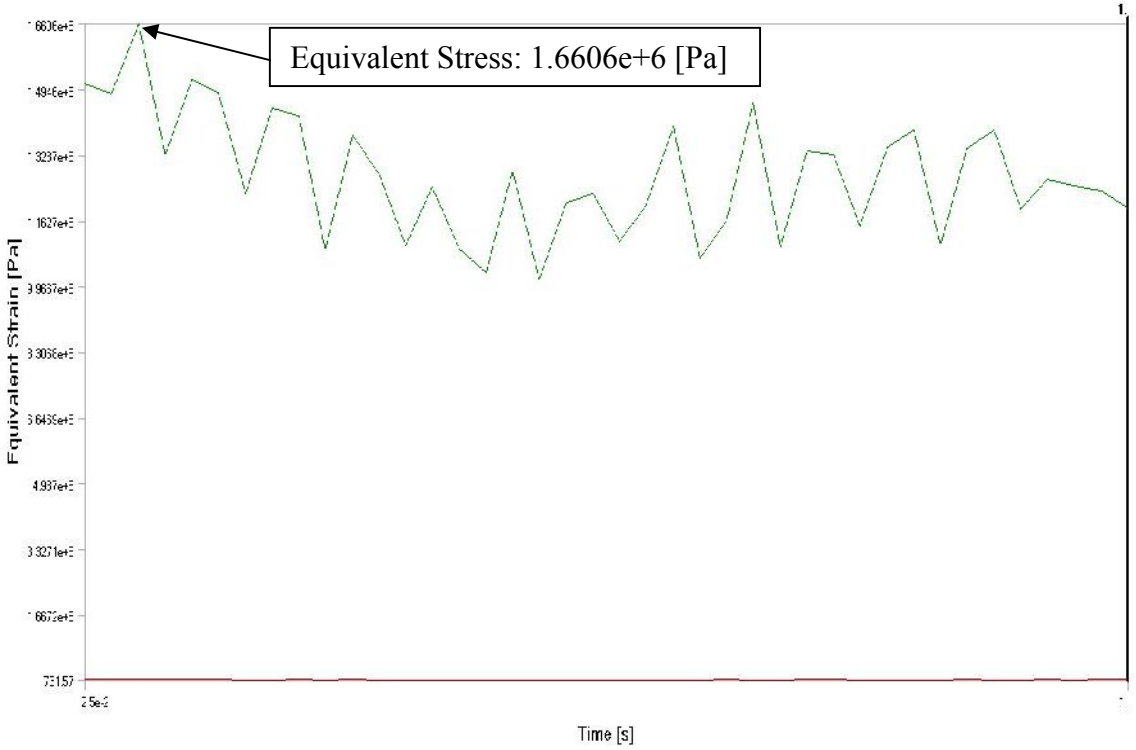

Figure 4.24 Equivalent Stress of EN8 (V=204,F=20,A=0.25)

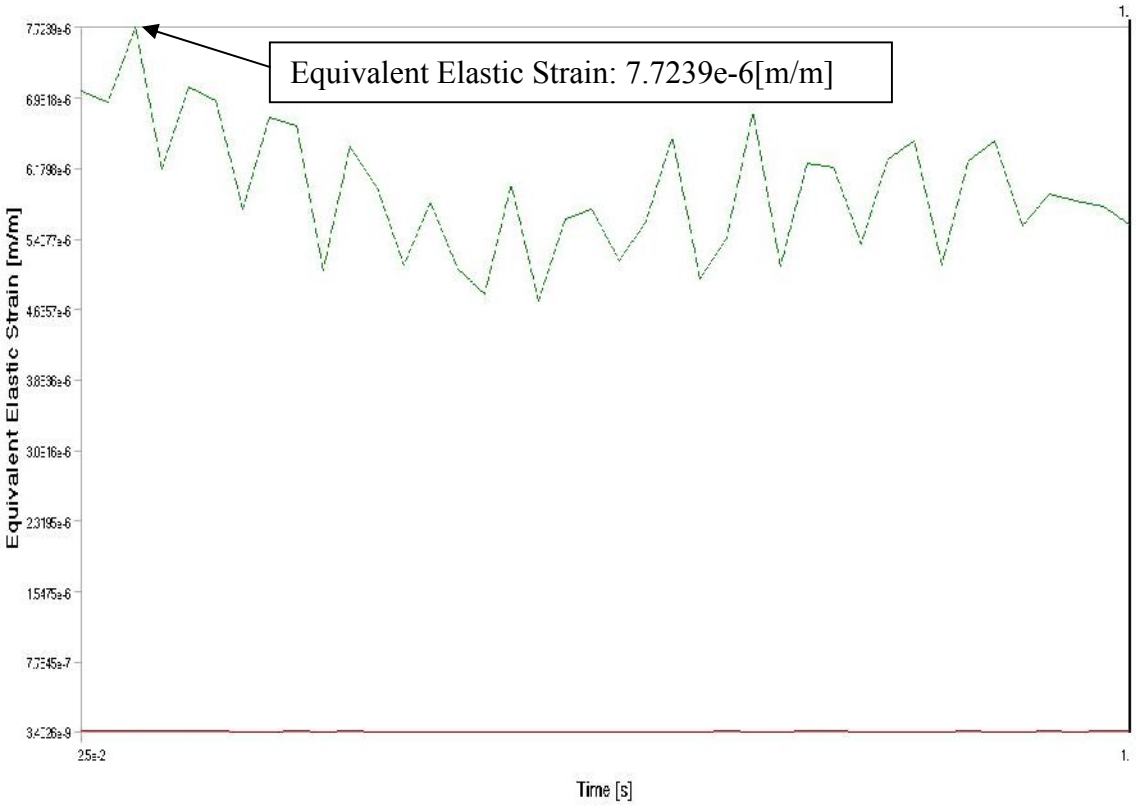

Figure 4.25 Equivalent Elastic Strain of EN8 (V=204,F=20,A=0.25)

Table 4.13 Material composition of EN19

C	Si	Mn	S	P	Cr	Mo
0.35-0.45	0.10-0.35	0.5-0.8	0.05max	0.05max	0.9-1.5	0.2-0.4

Table 4.14 Mechanical properties of EN19

Tensile Strength	1150 N/mm²
Yield Stress	850 N/mm²
Reduction of Area	12%
Elongation	14-17%
Modulus of elasticity	210 000 N/mm²
Density	7.8 Kg/m3
Hardness	55 HRC

Figure 4.26 Specimen details of EN19

4.2.2.1

Table 4.15 Machining parameters of EN19

SPEED	102	r.p.m
FEED	20	mm/min
DOC	0.25	mm

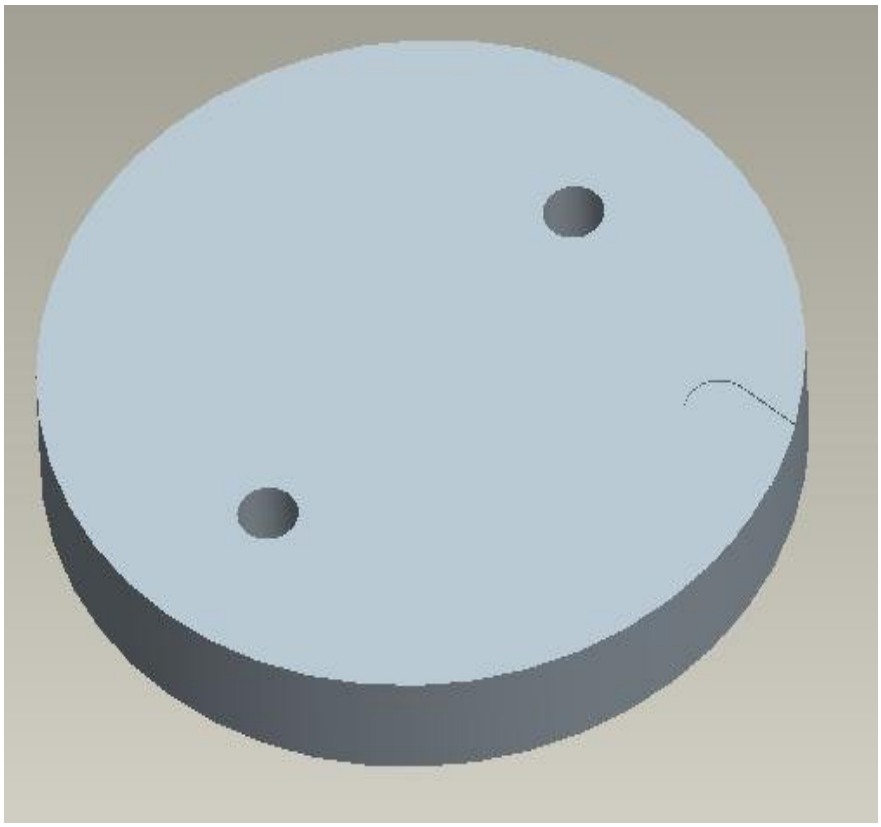

Figure 4.27 Pro-E model of specimen of EN19 (V=102,F=20,A=0.25)

Table 4.16 Force Values (Kistler\DynoWare)

File Type:			
Path:	C:\Kistler\DynoWare\Data\		
Filename:	millig2.dwd		
Config ID:	millig2.cfg		
Sampling rate [Hz]:	10		
Measuring time [s]:	40		
Delay time [s]:	0		
Cycle time [s]:	0		
Cycles:	1		
Samples per channel:	401		
Cycle interval:	0		
Channel enabled:	1	1	1
Cycle No:	1		
Time [s]	Fx	Fy	Fz
0	-17.2028	10.7056	-3.97949
1	-22.6593	2.69775	-16.1133
2	-40.3748	5.70068	-28.0273

3	-122.241	26.6846	-97.467
4	-85.6567	17.749	-51.1841
5	-96.2128	23.4619	-71.2891
6	-26.3397	7.42188	-20.9839
7	-52.2034	10.6934	-61.6577
8	-32.0618	6.11572	-21.1487
9	-104.764	22.4487	-88.916
10	-75.0732	34.7534	-62.0789
11	-54.4281	20.6787	-42.2058
12	-20.8191	3.93066	-19.8608
13	-49.3561	8.76465	-50.7446
14	-80.722	23.3032	-87.5122
15	-116.016	21.1548	-105.054
16	-71.6034	32.6294	-60.9741
17	-37.6373	18.9453	-25.6348
18	-22.1832	5.27344	-26.3062
19	-42.0593	7.56836	-40.6616
20	-88.504	21.6675	-87.3901
21	-83.9722	25.061	-76.6113
22	-62.0453	29.187	-55.8228
23	-24.6094	10.3149	-17.1997
24	-23.0896	7.60498	-34.436
25	-40.7867	13.8062	-51.2329
26	-87.2772	21.521	-94.0002
27	-77.8564	28.6743	-73.4802
28	-56.076	20.459	-52.6733
29	-12.5793	5.18799	-11.1633
30	-28.3722	9.06982	-38.0615
31	-62.8967	20.166	-73.6511
32	-85.9222	25.2808	-93.7256
33	-56.3599	32.0557	-48.8342
34	-45.639	24.2065	-36.438
35	-8.3313	4.27246	-12.2498
36	-36.9965	11.1206	-44.8364
37	-58.8593	21.7896	-72.0459
38	-77.417	27.1606	-82.7148
39	-55.3986	32.3486	-54.9988
40	-30.5603	25.2686	-19.7021

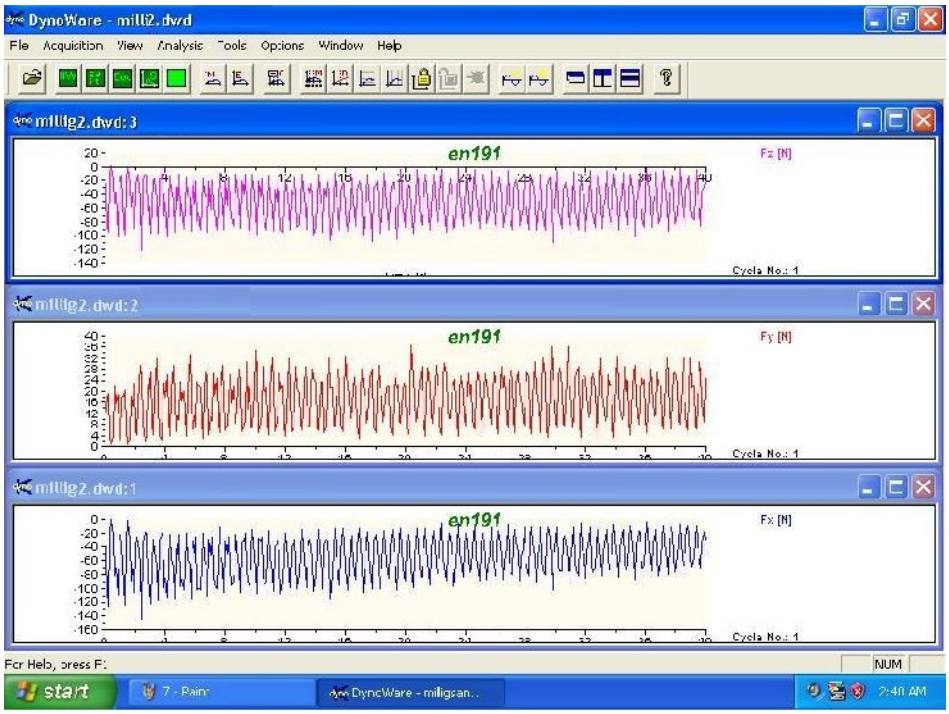

Figure 4.28 Graphical representations of force variations of EN19

- **Analysis of EN19**

Analysis software: ANSYS V11.0 (WORKBENCH INTERFACE)

Analysis type : TRANSIENT (40 Sec)

Inputs : IGES (PRO-E), SOLID ELEMENT TETRAHEDRAL 8-NODES

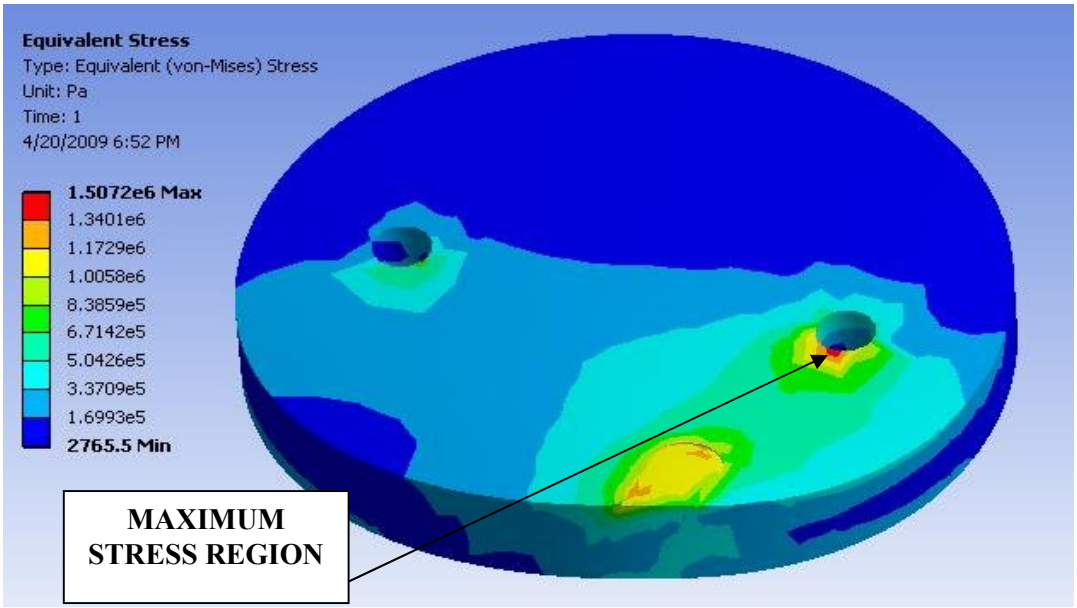

Figure 4.29 Analysis of EN19(V=102,F=20,A=0.25)

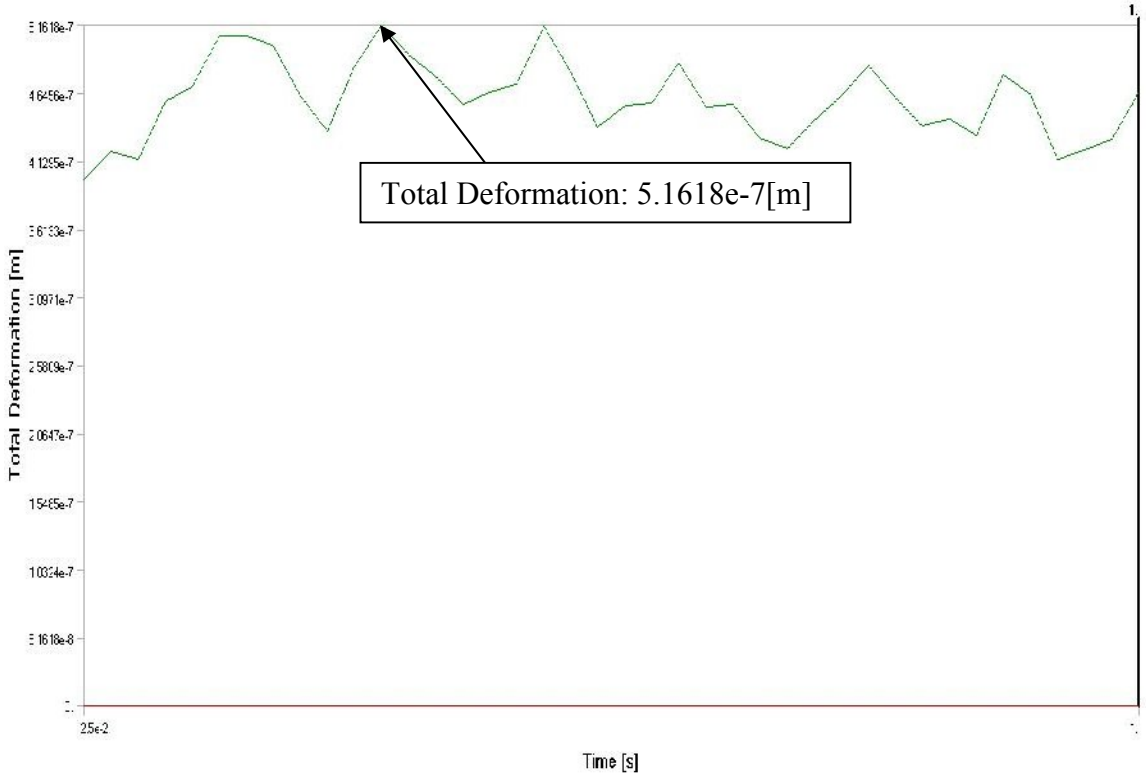

Figure 4.30 Total Deformation of EN19(V=102,F=20,A=0.25)

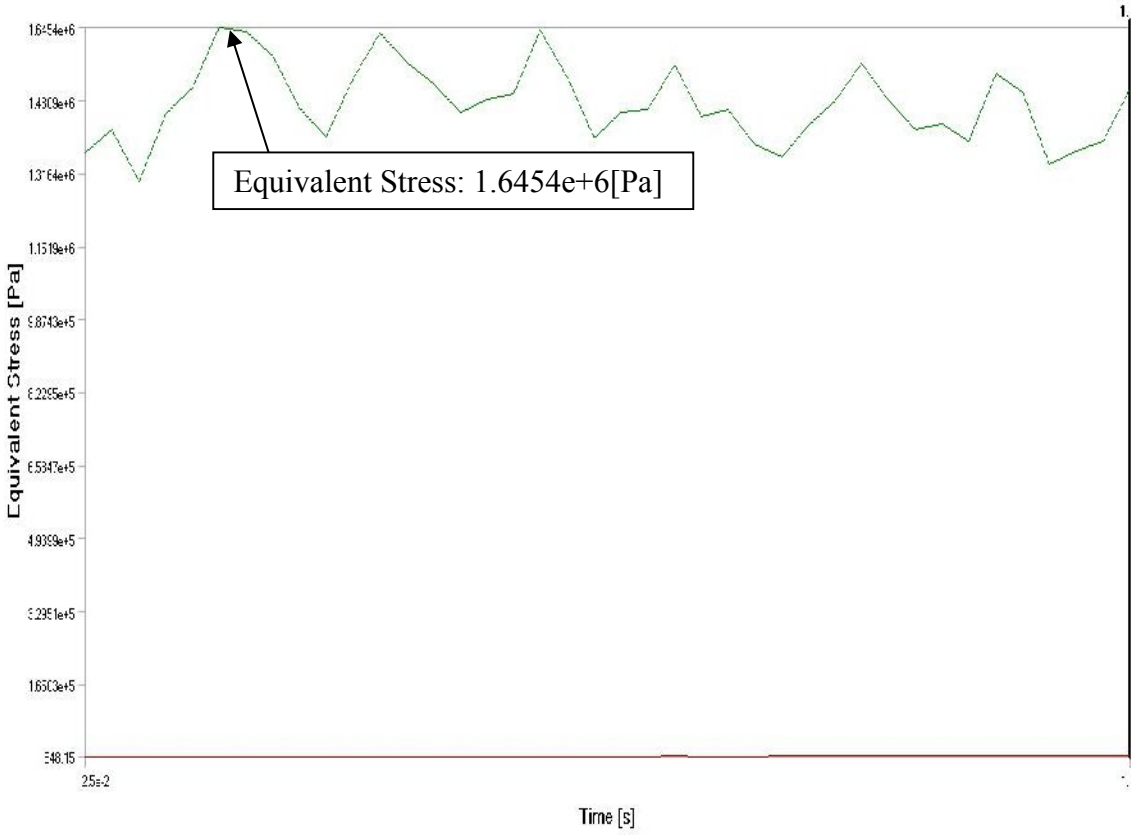

Figure 4.31 Equivalent Stress of EN19(V=102,F=20,A=0.25)

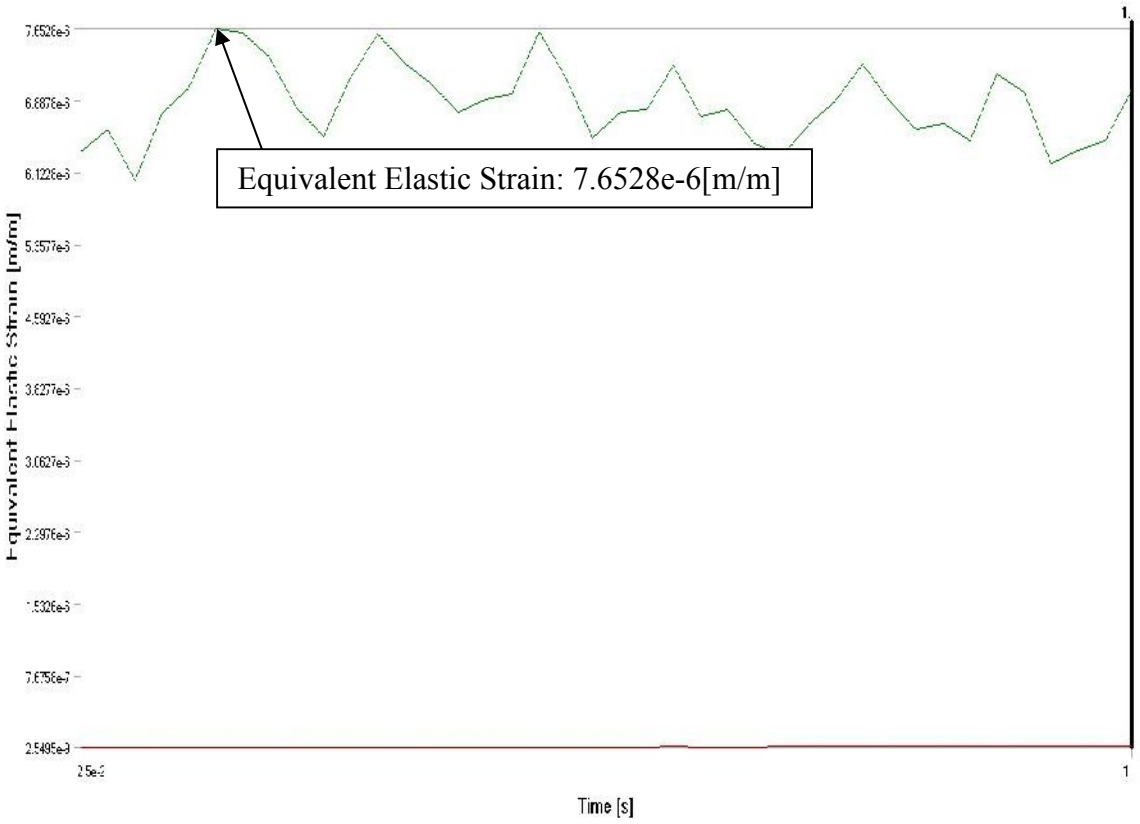

Figure 4.32 Equivalent Elastic Strain of EN19(V=102,F=20,A=0.25)

4.2.2.2

Table 4.17 Machining parameters of EN19

SPEED	102	r.p.m
FEED	35	mm/min
DOC	0.25	mm

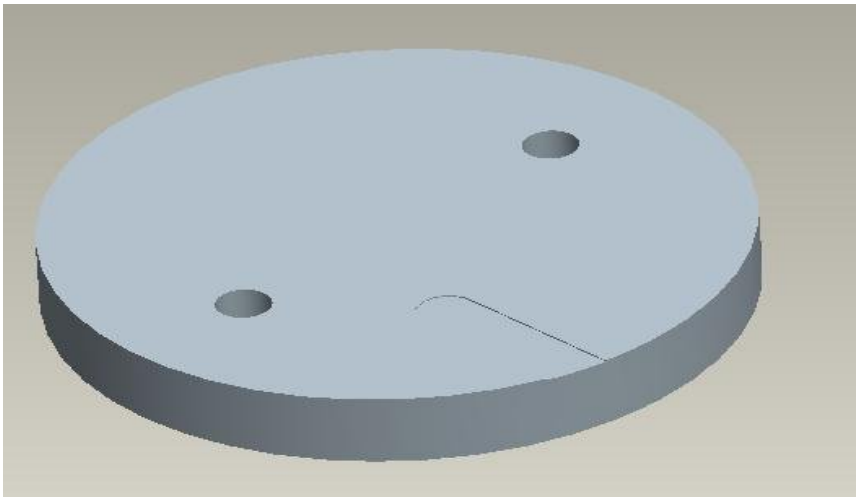

Figure 4.33 Pro-E model of specimen of EN19

Table 4.18 Force Values (Kistler\DynoWare)

File Type:			
Path:	C:\Kistler\DynoWare\Data\		
Filename:	millig2.dwd		
Config ID:	millig2.cfg		
Sampling rate [Hz]:	10		
Measuring time [s]:	40		
Delay time [s]:	0		
Cycle time [s]:	0		
Cycles:	1		
Samples per channel:	401		
Cycle interval:	0		
Channel enabled:	1	1	1
Cycle No:	1		
Time [s]	Fx	Fy	Fz
0	58.8684	-12.2314	53.4302
1	45.6116	-12.4512	44.5679
2	-2.10571	12.9456	-13.3484
3	-26.0193	11.9568	-42.865
4	12.4329	24.4446	-18.6035
5	37.0789	7.06787	2.34375
6	83.606	-11.1694	71.7224
7	44.8242	-9.50317	39.9536
8	15.8203	9.55811	4.77905
9	-9.75952	10.8765	-33.0872
10	48.3215	20.1965	9.35669
11	36.6211	18.988	2.45361
12	101.697	-6.00586	86.7004
13	67.3096	-14.2639	56.8542
14	41.9495	-1.83E-02	24.5728
15	-8.82568	15.9119	-43.9453
16	33.0872	25.4883	-10.2173
17	30.3406	12.1399	-15.1062
18	101.88	0.567627	76.8311
19	76.2268	-15.2344	69.3237
20	51.178	-1.57471	28.4363
21	14.3921	9.10034	-20.4712
22	47.0947	24.9573	-4.26636
23	34.9182	12.9089	-17.3401
24	98.8586	0.128174	73.4253

25	92.157	-10.9863	79.7974
26	59.3628	-0.97046	38.7451
27	21.7712	15.1062	-27.356
28	55.8838	19.7937	9.375
29	42.4438	18.5669	-17.3401
30	94.8486	-6.26221	68.9575
31	81.5552	-12.6892	68.4265
32	67.4194	-6.57349	43.7439
33	37.0239	9.77783	-12.4695
34	59.5093	13.5864	3.16772
35	64.8376	21.8079	-3.53394
36	99.7375	-1.7395	69.0491
37	79.9072	-13.3667	66.2659
38	80.6213	-10.3271	64.9292
39	44.3115	11.4624	-15.7288
40	66.4307	17.981	2.12402

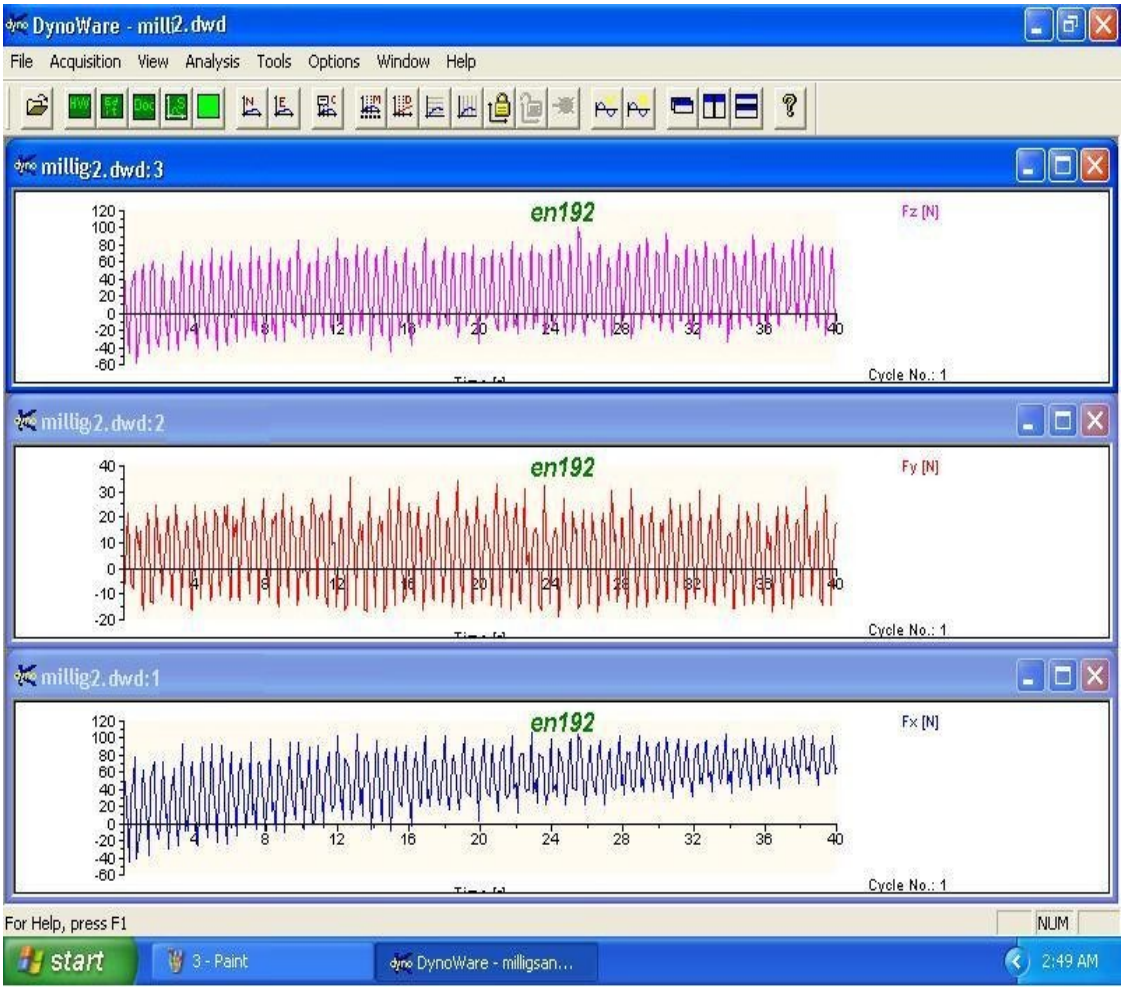

Figure 4.34 Graphical Representation of Force Variation of EN19

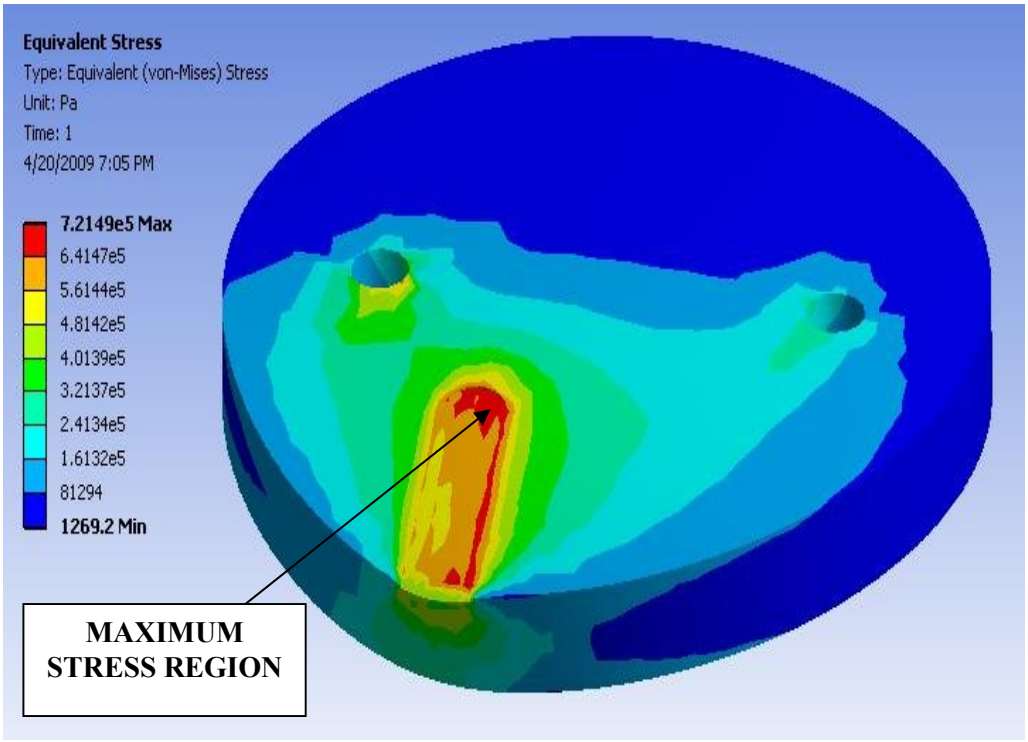

Figure 4.35 Analysis of EN19(V=102,F=35,A=0.25)

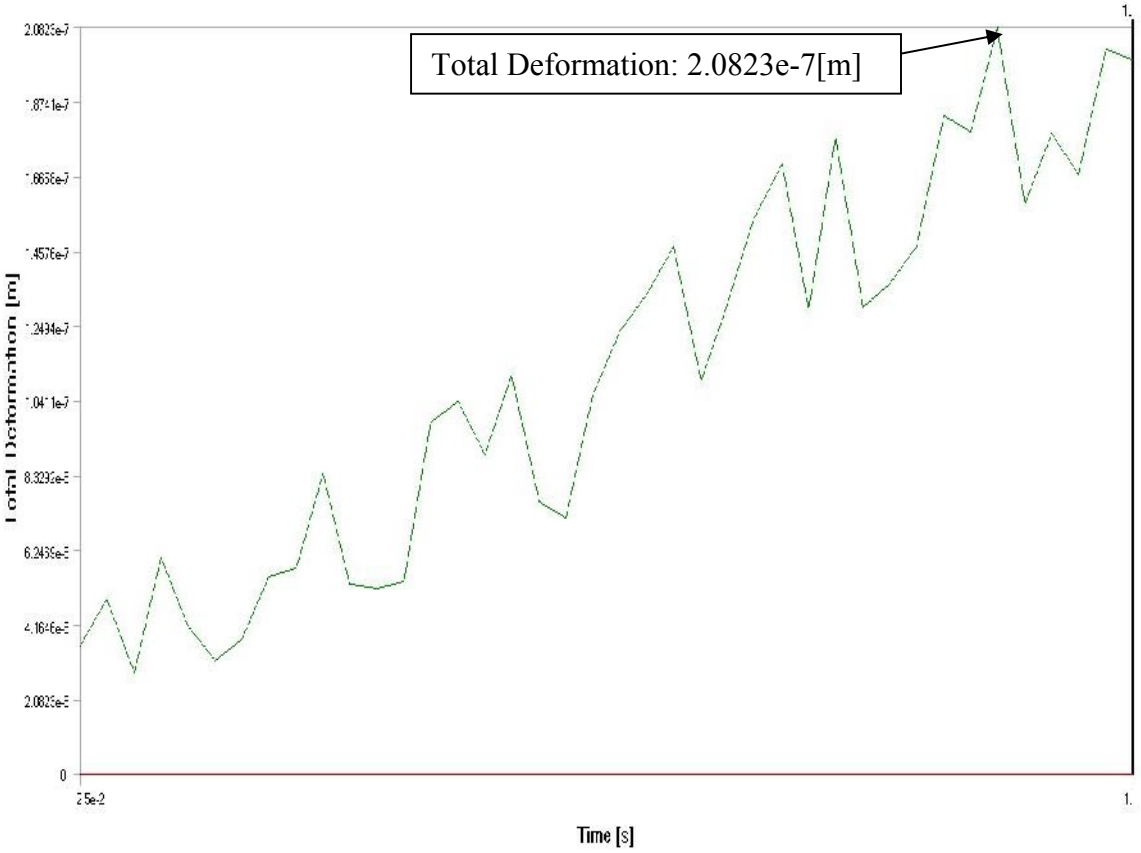

Figure 4.36 Total Deformation of EN19(V=102,F=20,A=0.25)

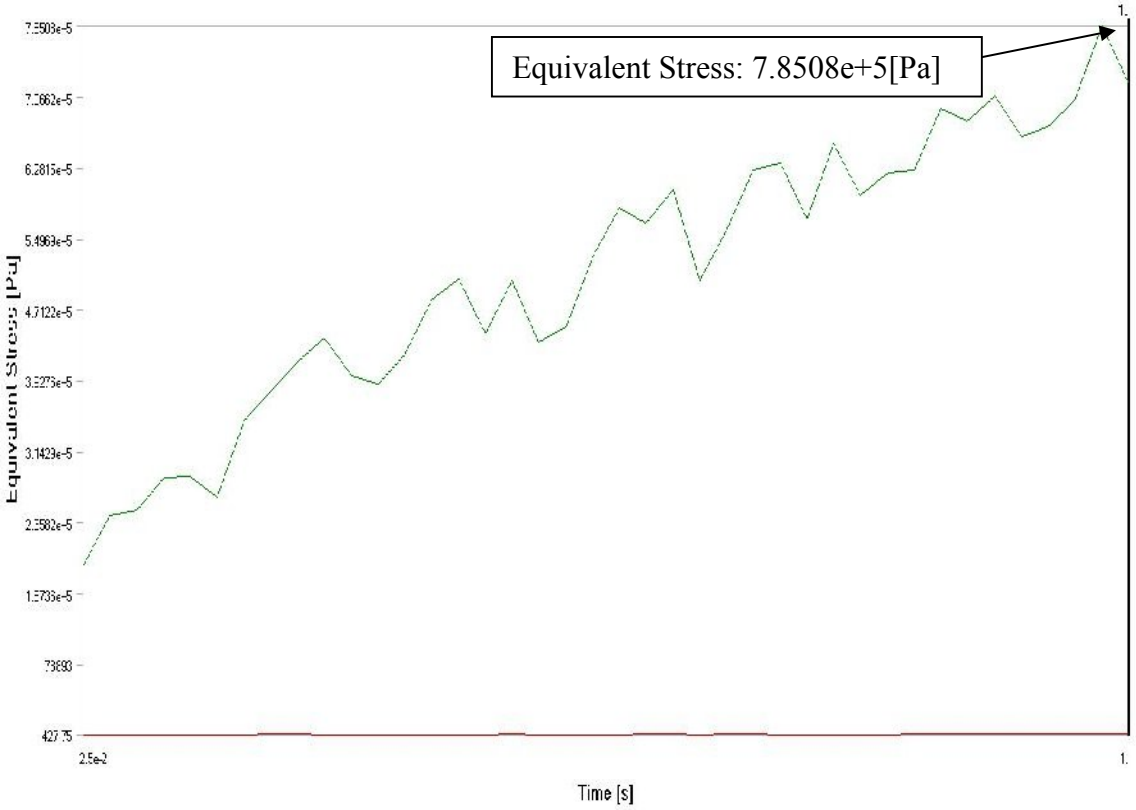

Figure 4.37 Equivalent Stress of EN19(V=102,F=20,A=0.25)

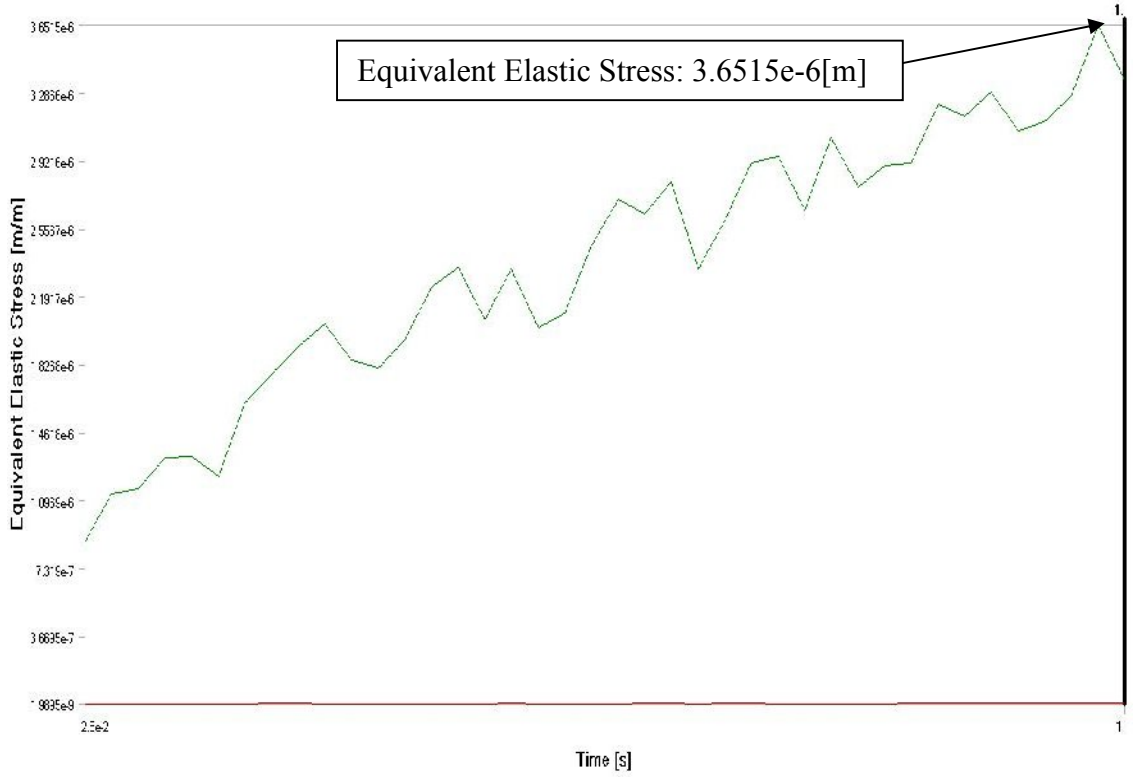

Figure 4.38 Equivalent Elastic Stress of EN19

4.2.2.3

Table 4.19 Machining parameters of EN19

SPEED	102	r.p.m
FEED	65	mm/min
DOC	0.25	mm

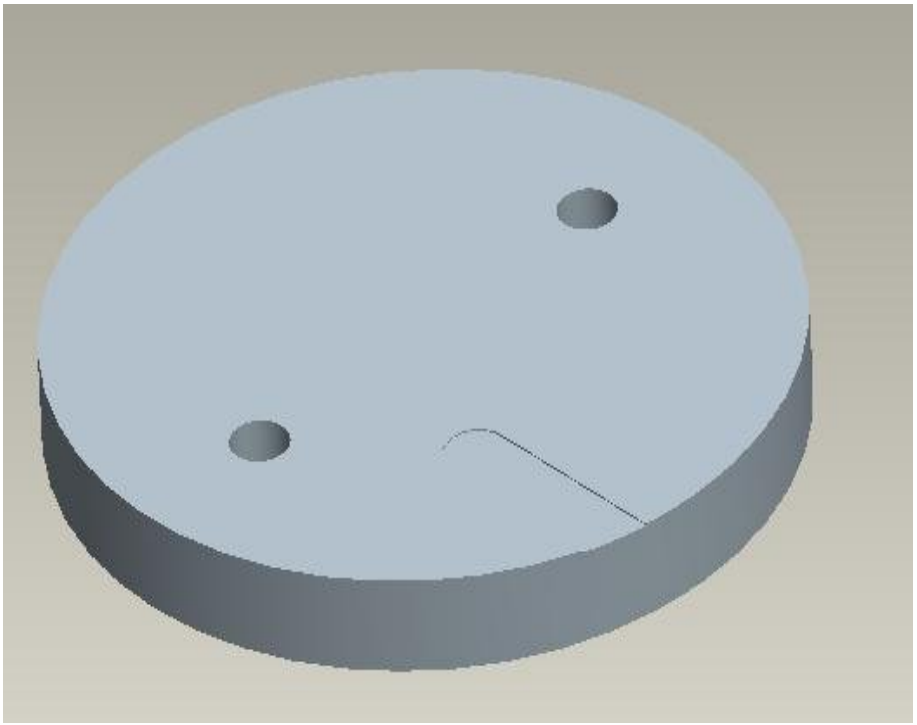

Figure 4.39 Pro-E Model of Specimen

Table 4.20 Force Values (Kistler\DynoWare)

File Type:			
Path:	C:\Kistler\DynoWare\Data\		
Filename:	millig2.dwd		
Config ID:	millig2.cfg		
Sampling rate [Hz]:	10		
Measuring time [s]:	40		
Delay time [s]:	0		
Cycle time [s]:	0		
Cycles:	1		
Samples per channel:	401		
Cycle interval:	0		
Channel enabled:	1	1	1
Cycle No:	1		
Time [s]	Fx	Fy	Fz

0	-99.0784	-30.6152	10.4736
1	-127.826	-63.6658	26.3855
2	-146.631	-100.836	25.7446
3	-112.225	-93.8965	45.0806
4	3.22266	-78.3508	15.2344
5	-19.7388	14.8865	10.2356
6	-71.228	-4.83398	5.49E-02
7	-109.68	-10.7666	23.8403
8	-118.158	-53.1372	22.7966
9	-101.495	-58.1726	42.1692
10	10.3638	-52.7893	17.5232
11	4.37622	7.30591	18.6035
12	-34.8083	11.0779	-6.68335
13	-71.8506	9.44824	3.73535
14	-79.9255	-20.05	10.0891
15	-113.104	-40.7227	28.3813
16	-14.7949	-28.4363	26.0925
17	26.5869	2.41699	21.3867
18	1.83105	19.4458	-8.12988
19	-49.4751	20.8008	-10.7849
20	-65.0024	8.97217	8.95386
21	-110.193	5.31006	16.4246
22	-36.8042	-12.5793	25.47
23	30.9998	3.05786	19.5007
24	17.6147	26.4038	-8.5144
25	-11.2976	26.4038	-12.6343
26	-34.1675	36.7126	9.24683
27	-80.9326	24.9023	12.0117
28	-43.7622	11.0779	21.1121
29	30.5603	14.1357	20.4529
30	33.1055	27.3376	-12.5244
31	29.2603	31.9519	-4.26636
32	-2.45361	36.969	0.897217
33	-60.791	28.8208	-4.44946
34	-27.6306	31.6223	12.561
35	34.3506	27.063	-4.13818
36	44.7144	27.7222	1.13525
37	22.3572	27.2278	-13.7695
38	29.425	32.2449	-4.08325
39	-32.5378	30.1025	-7.61719
40	-28.8025	39.8987	7.80029

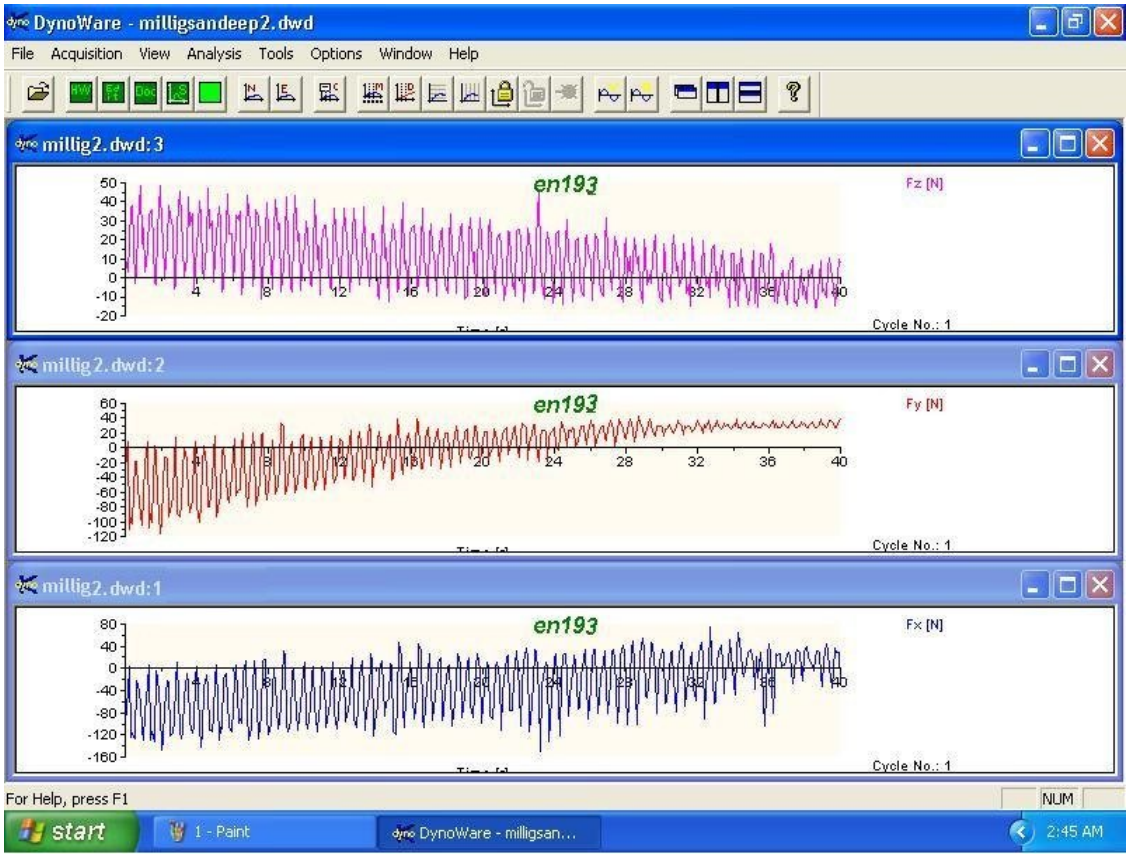

Figure 4.40 Graphical Representation of Force Variation of EN19

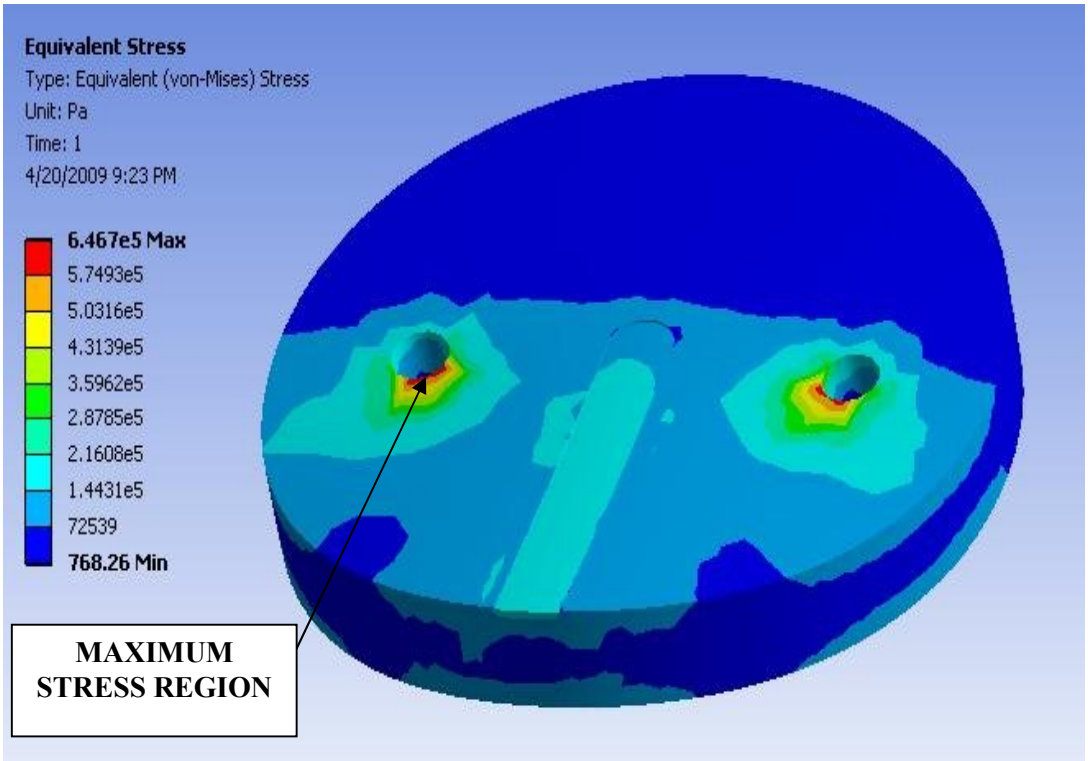

Figure 4.41 Analysis of EN19(V=102,F=65,A=0.25)

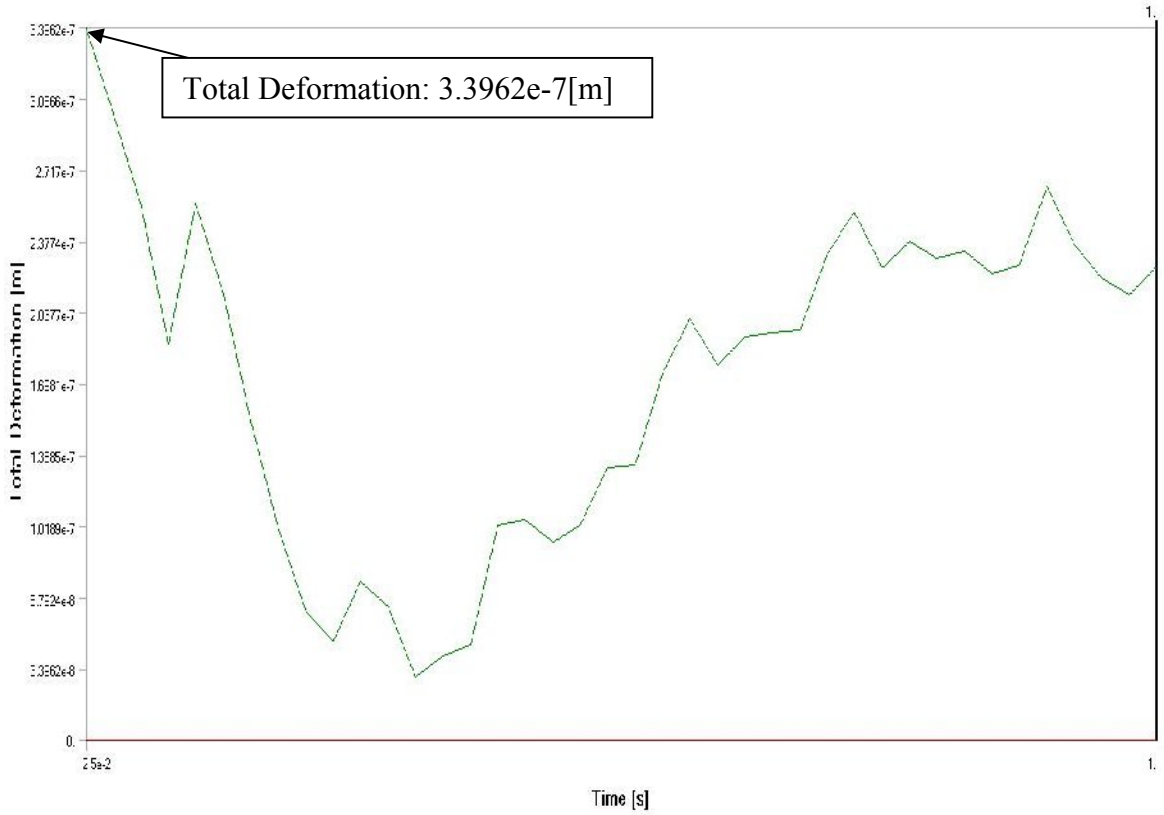

Figure 4.42 Total Deformation of EN19(V=102,F=65,A=0.25)

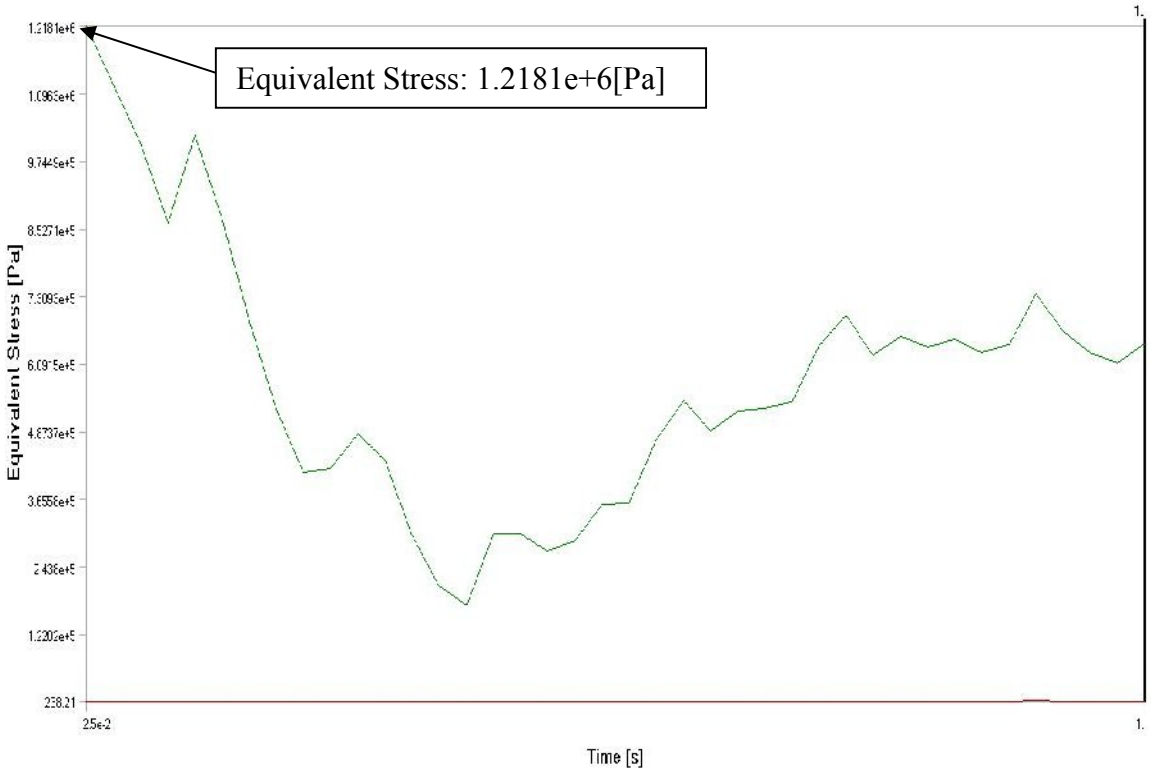

Figure 4.43 Equivalent Stress of EN19(V=102,F=65,A=0.25)

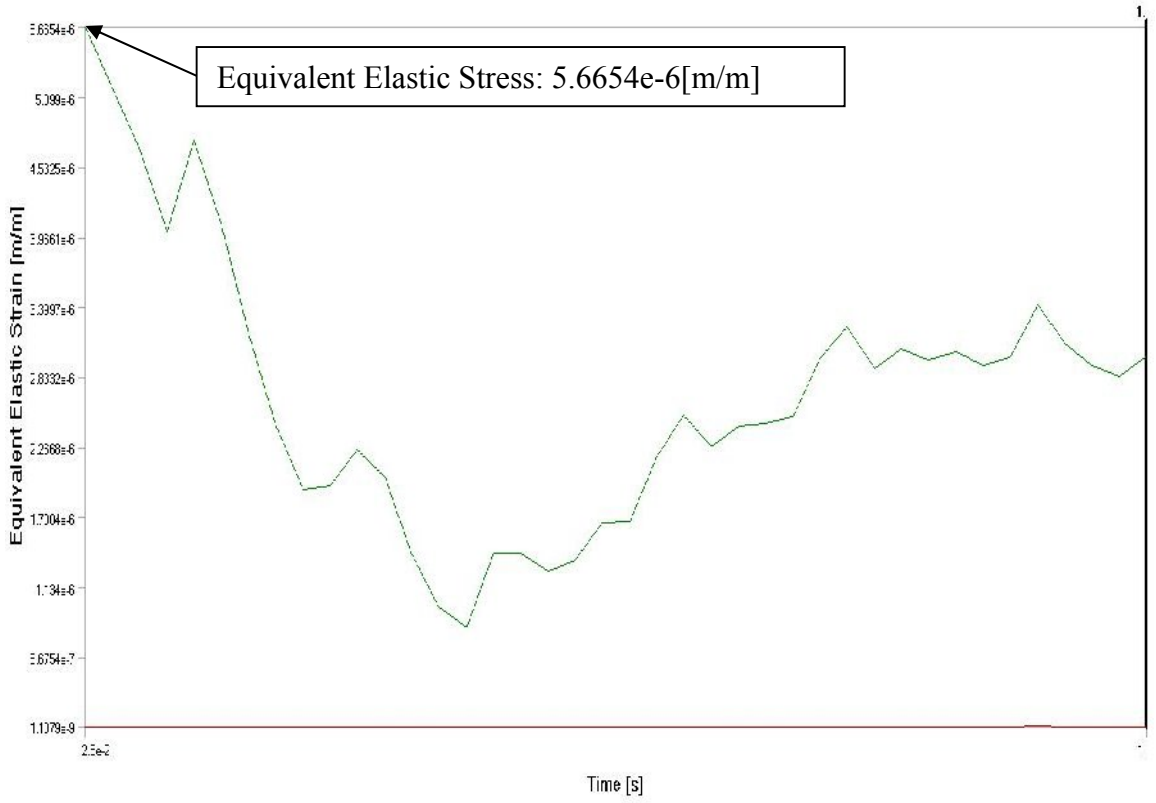

Figure 4.44 Equivalent Elastic Stress of EN19(V=102,F=65,A=0.25)

4.2.2.4

Table 4.21 Machining parameters of EN19

SPEED	204	r.p.m
FEED	35	mm/min
DOC	0.25	mm

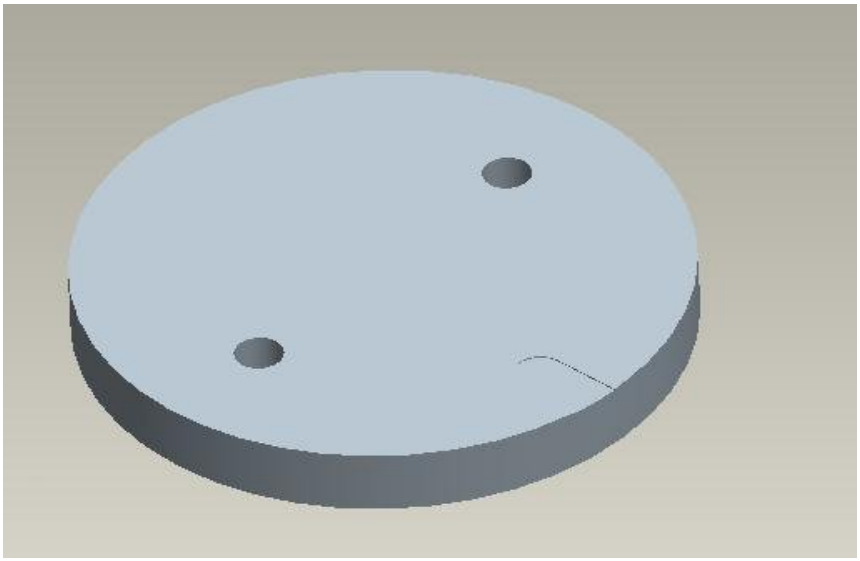

Figure 4.45 Pro-E Model of Specimen of EN19(V=204,F=35,A=0.25)

Table 4.22 Force Values (Kistler\DynoWare)

File Type:			
Path:	C:\Kistler\DynoWare\Data\		
Filename:	milligp2.dwd		
Config ID:	millig2.cfg		
Sampling rate [Hz]:	10		
Measuring time [s]:	40		
Delay time [s]:	0		
Cycle time [s]:	0		
Cycles:	1		
Samples per channel:	401		
Cycle interval:	0		
Channel enabled:	1	1	1
Cycle No:	1		
Time [s]	Fx	Fy	Fz
0	-0.62256	-0.18311	-0.73242
1	-35.7422	9.92432	-28.2532
2	-0.8606	-0.12817	-2.10571
3	-56.8359	9.75952	-57.0923
4	-31.0364	12.4512	-28.7659
5	-3.20435	0.640869	-3.91846
6	-64.7644	11.9202	-61.6699
7	-15.4541	10.0159	-18.5303
8	-10.8582	1.64795	-10.1257
9	-58.8135	10.0891	-60.4248
10	-9.33838	9.97925	-12.3596
11	-6.97632	1.79443	-6.71997
12	-35.8521	9.94263	-45.7397
13	-0.58594	5.7312	-5.16357
14	-19.5007	6.35376	-19.2444
15	-12.6343	13.8977	-25.177
16	6.26221	5.76782	6.48193
17	-42.8101	8.22144	-43.2678
18	-3.93677	11.6821	-15.564
19	-1.83E-02	0.787354	0.128174
20	-62.677	10.5835	-67.7673
21	-14.9231	16.9373	-24.7742
22	0.292969	1.2085	1.30005
23	-60.7727	10.8765	-67.2546
24	-18.219	11.7371	-23.9136

25	-11.1511	1.33667	-10.2905
26	-49.2737	10.6018	-58.0444
27	-11.4441	9.77783	-18.4021
28	-12.6526	1.68457	-15.7104
29	-37.5549	11.6821	-53.4668
30	-1.24512	4.13818	-6.55518
31	-10.9131	2.56348	-14.5386
32	-14.6118	14.3555	-31.9702
33	1.22681	1.99585	-2.47192
34	-34.6252	8.05664	-37.3718
35	-4.59595	15.6189	-20.5444
36	-0.36621	1.31836	-0.12817
37	-47.2961	12.5427	-54.3274
38	-6.7749	18.8599	-21.1487
39	-1.57471	1.66626	-2.91138
40	-49.3103	14.3921	-65.5151

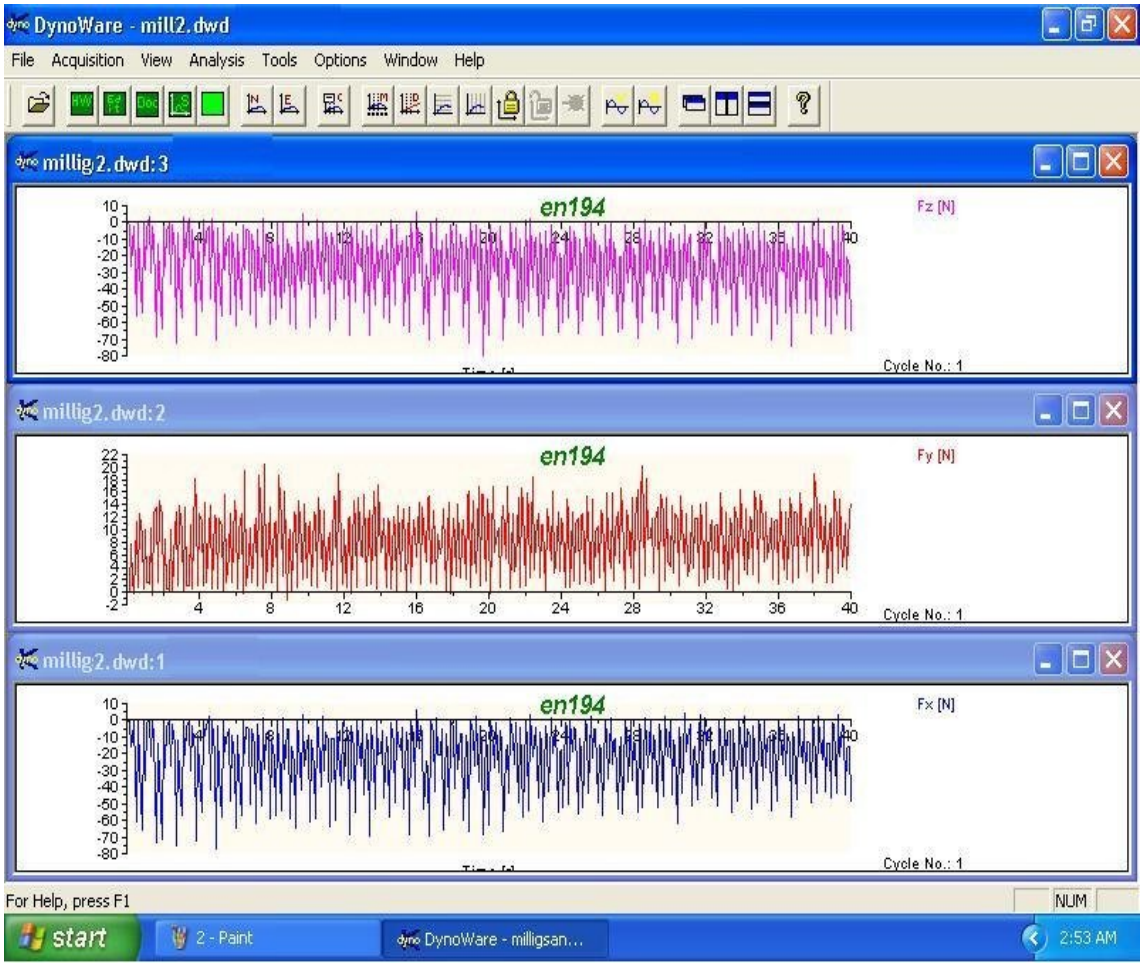

Figure 4.46 Graphical Representation of Force Variation of EN19

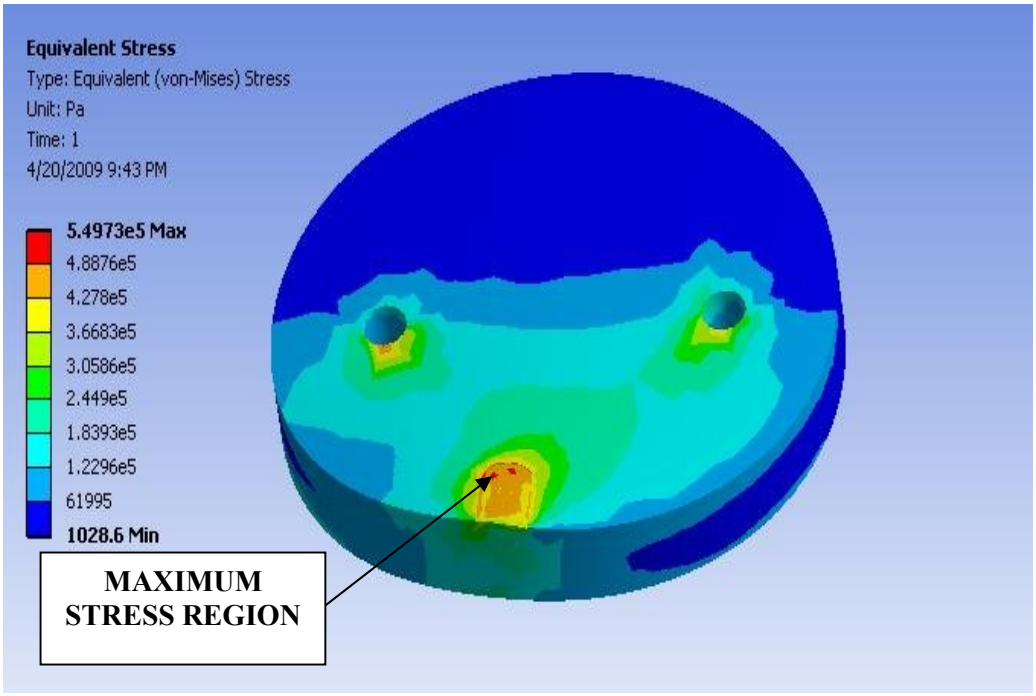

Figure 4.47 Analysis of EN19(V=102,F=65,A=0.25)

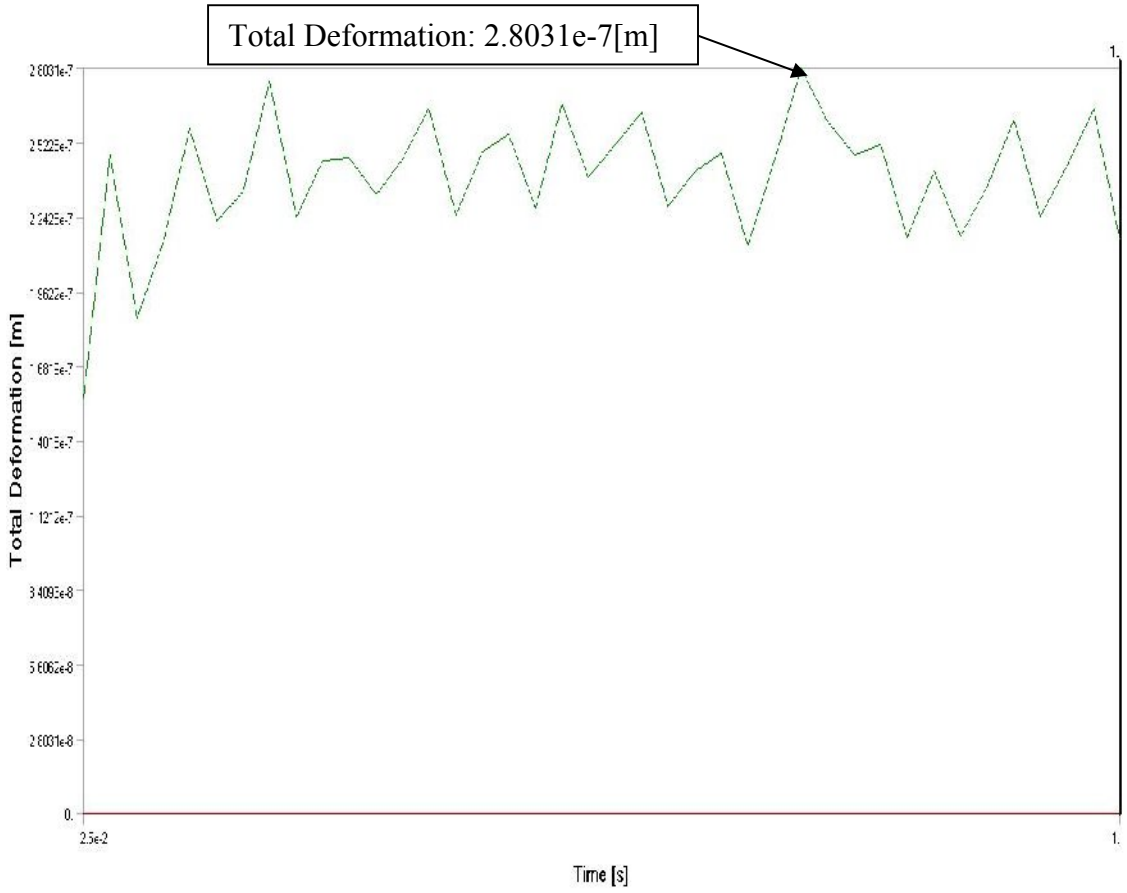

Figure 4.48 Total Deformation of EN19(V=102,F=65,A=0.25)

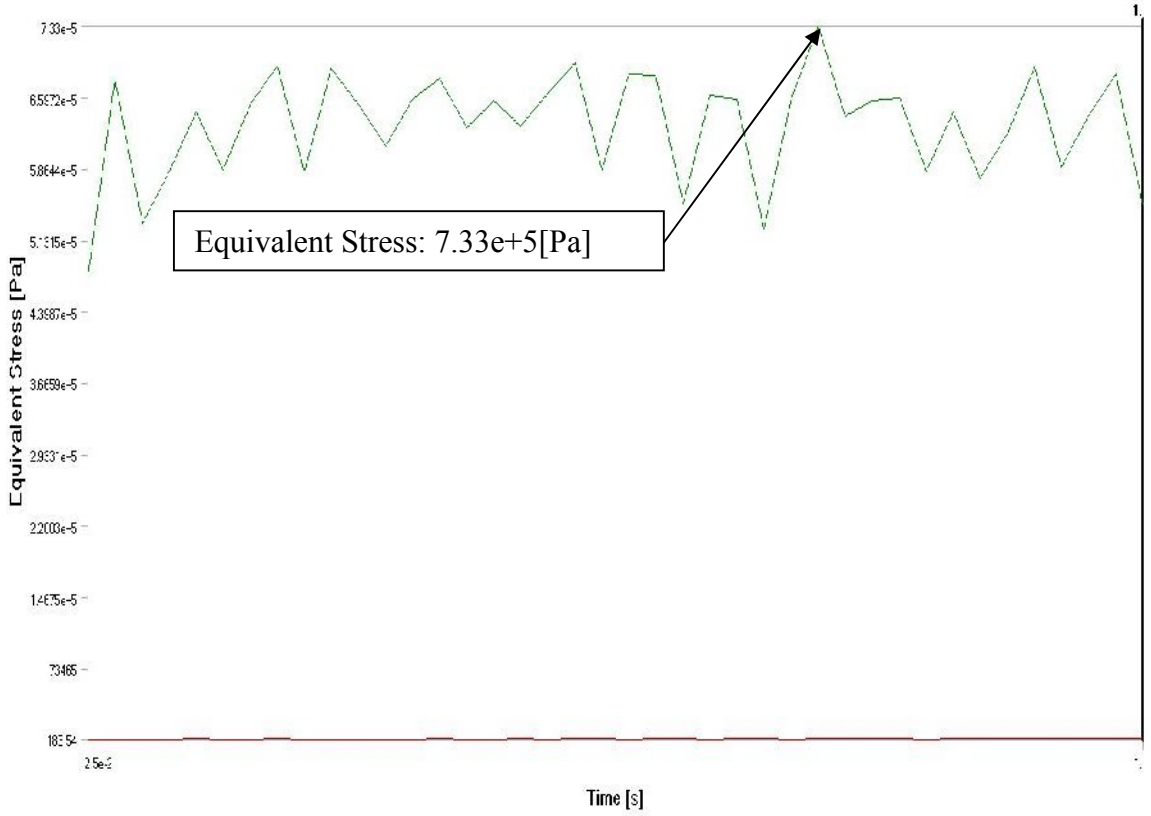

Figure 4.49 Equivalent Stress of EN19(V=102,F=65,A=0.25)

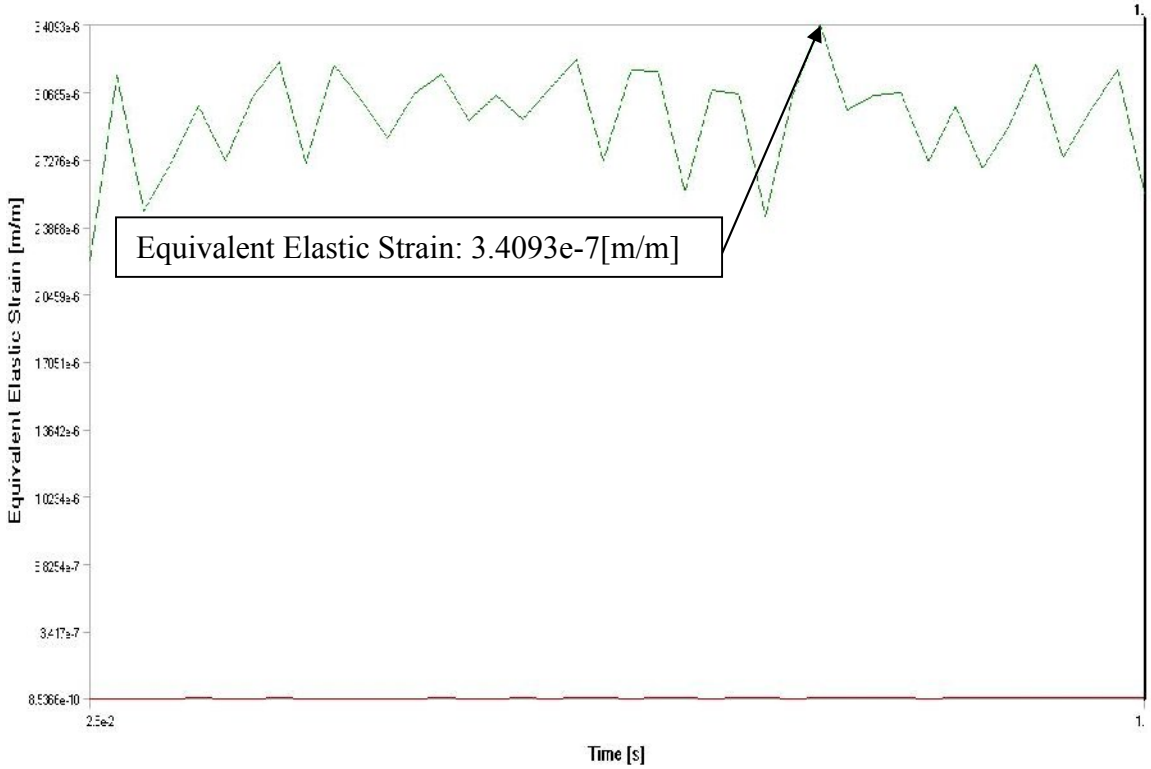

Figure 4.50 Equivalent Elastic Strain of EN19(V=102,F=65,A=0.25)

4.2.3 Analysis of EN31

Table 4.23 Material composition of EN31

C	Si	Mn	S	P	Cr
0.9-1.2	0.10-0.35	0.3-0.75	0.05max	0.05max	1.0-1.4

Table 4.24 Mechanical properties of EN31

Tensile Strength	750 N/mm²
Yield Stress	450 N/mm²
Reduction of Area	45%
Elongation	30%
Modulus of elasticity	215 000 N/mm²
Density	7.8 Kg/m3
Hardness	63 HRC

Figure 4.51 Specimen Details of EN31

4.2.3.1

Table 4.25 Machining parameters of EN31

SPEED	102	r.p.m
FEED	20	mm/min
DOC	0.25	mm

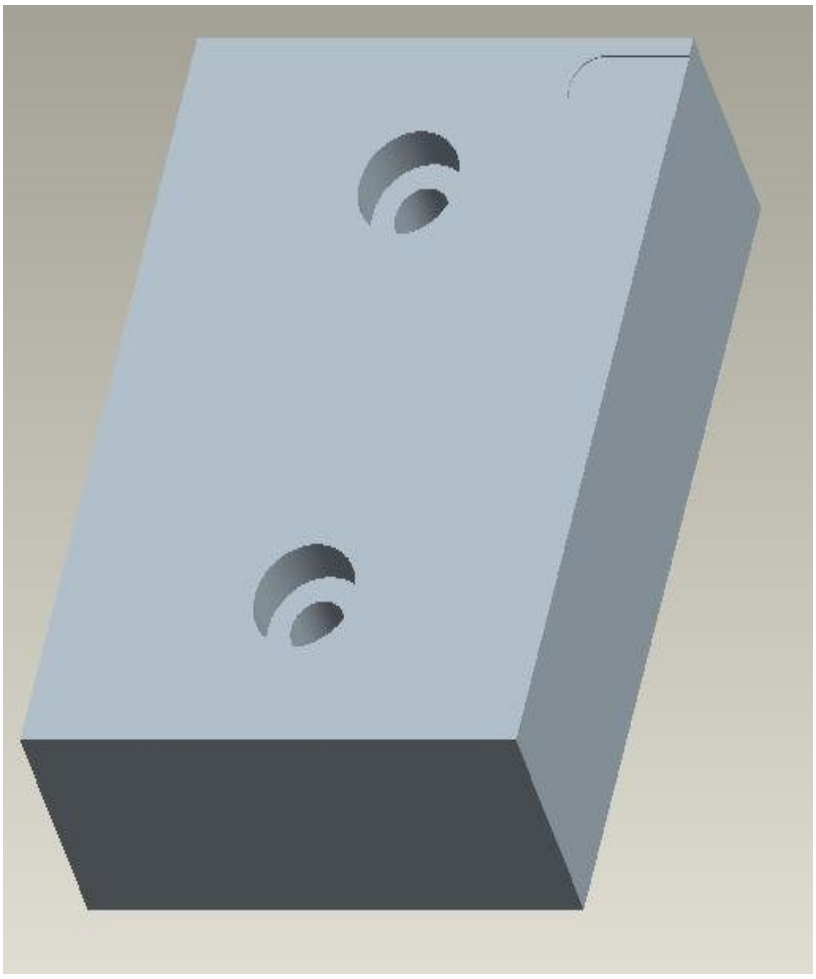

Figure 4.52 Pro-E Model of Specimen of EN31

Table 4.26 Force Values (Kistler\Dyno Ware)

File Type:			
Path:	C:\Kistler\DynoWare\Data\		
Filename:	millig2.dwd		
Config ID:	millig2.cfg		
Sampling rate [Hz]:	10		
Measuring time [s]:	40		
Delay time [s]:	0		
Cycle time [s]:	0		
Cycles:	1		
Samples per channel:	401		
Cycle interval:	0		
Channel enabled:	1	1	1
Cycle No:	1		
Time [s]	Fx	Fy	Fz
0	-125.693	44.1284	-98.9075

1	-198.505	36.4868	-133.783
2	-97.3389	45.2393	-38.9954
3	-77.2156	19.104	-32.4585
4	-9.16E-03	0.793457	-3.60107
5	-46.1609	24.3286	-93.2678
6	-96.9177	39.624	-101.453
7	-106.018	41.7847	-56.1707
8	-94.986	33.3618	-37.738
9	-81.5277	18.0176	-51.7883
10	0.595093	-0.87891	-1.94702
11	-18.6676	22.2412	-92.5171
12	-67.2638	39.6606	-102.319
13	-120.557	51.416	-66.5344
14	-116.327	33.9111	-70.3247
15	-81.1707	33.8257	-32.9224
16	-27.8137	13.4277	-3.24097
17	-7.35168	30.7617	-126.404
18	-111.255	33.8257	-127.96
19	-123.688	52.9541	-83.9233
20	-153.461	31.5063	-99.7314
21	-66.4215	32.0923	0.20752
22	-30.0476	10.9375	-7.77588
23	40.0909	30.6519	-112.36
24	-77.2705	36.853	-155.145
25	-118.35	50.2686	-129.755
26	-100.204	50.0366	-71.5942
27	-98.877	38.5986	-26.3672
28	-64.6179	17.7002	-44.0491
29	9.60388	30.7495	-57.959
30	-52.4048	37.3901	-167.352
31	-89.74	36.2671	-112.402
32	-120.511	51.7456	-71.3501
33	-115.53	31.8604	-46.1426
34	-53.9886	29.4067	-32.9895
35	-1.66626	5.61523	-7.93E-02
36	-8.60596	33.2153	-93.7134
37	-103.546	38.8672	-146.765
38	-109.286	51.5991	-104.321
39	-130.884	31.7749	-93.5486
40	-69.3604	36.1084	-8.06274

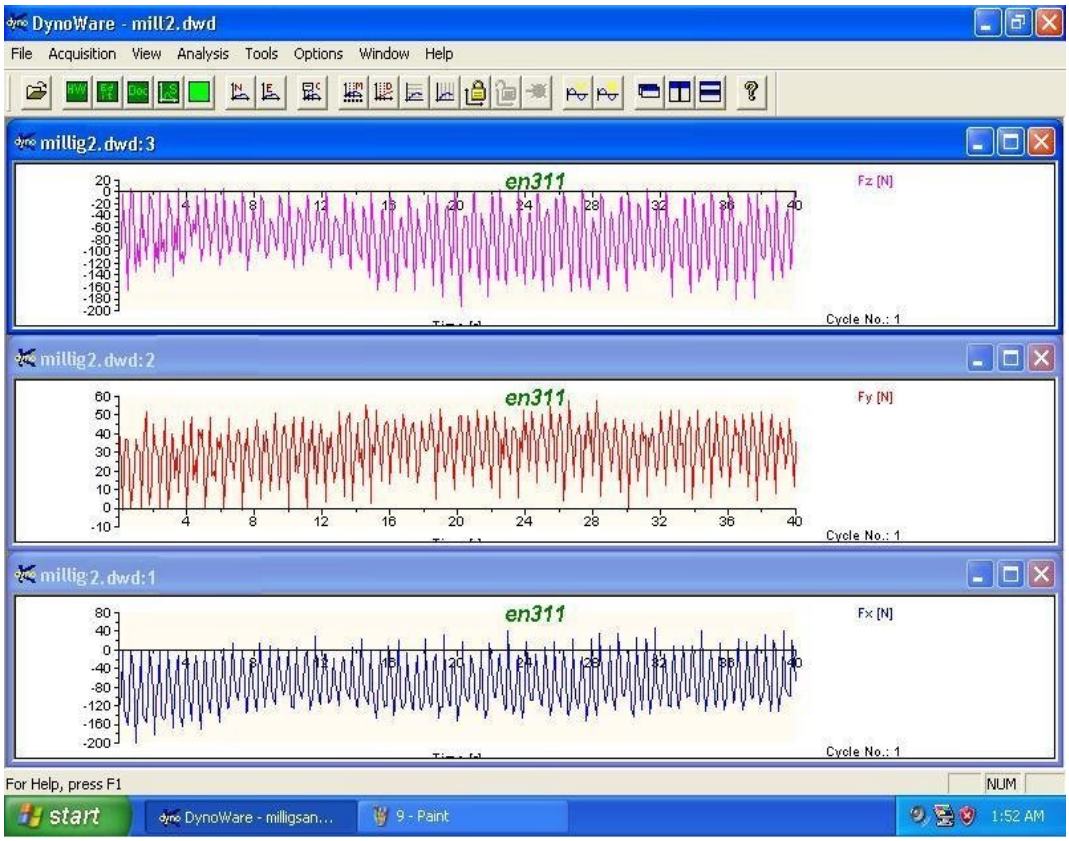

Figure 4.53 Graphical Representation of Force Variation of EN31

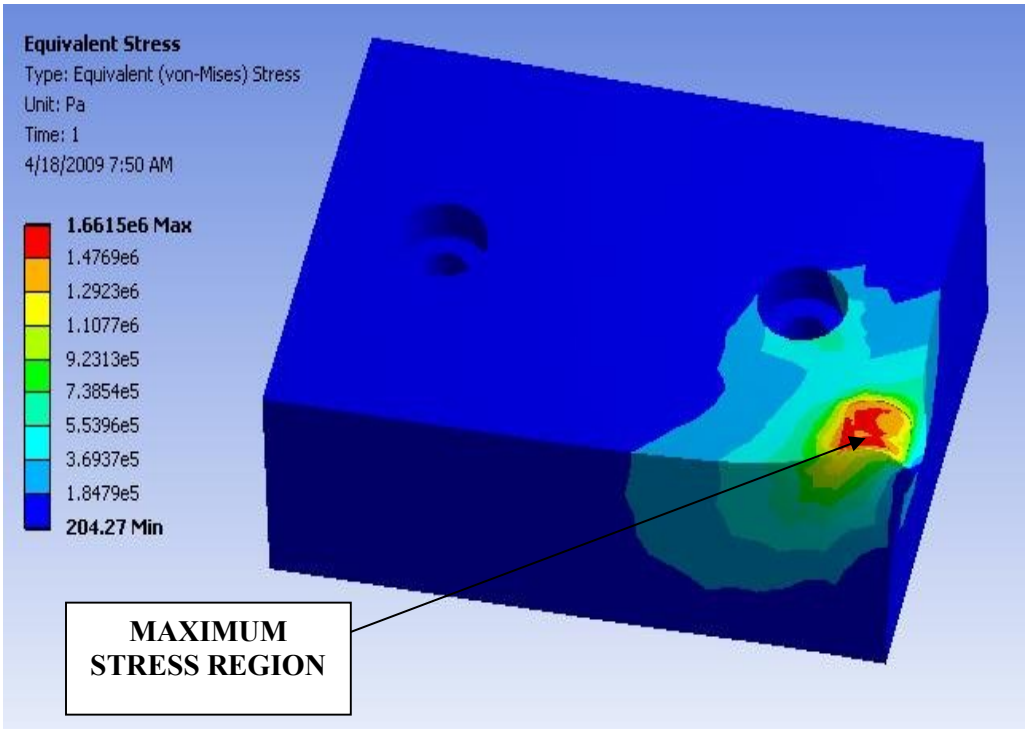

Figure 4.54 Analysis of EN31(V=102,F=20,A=0.25)

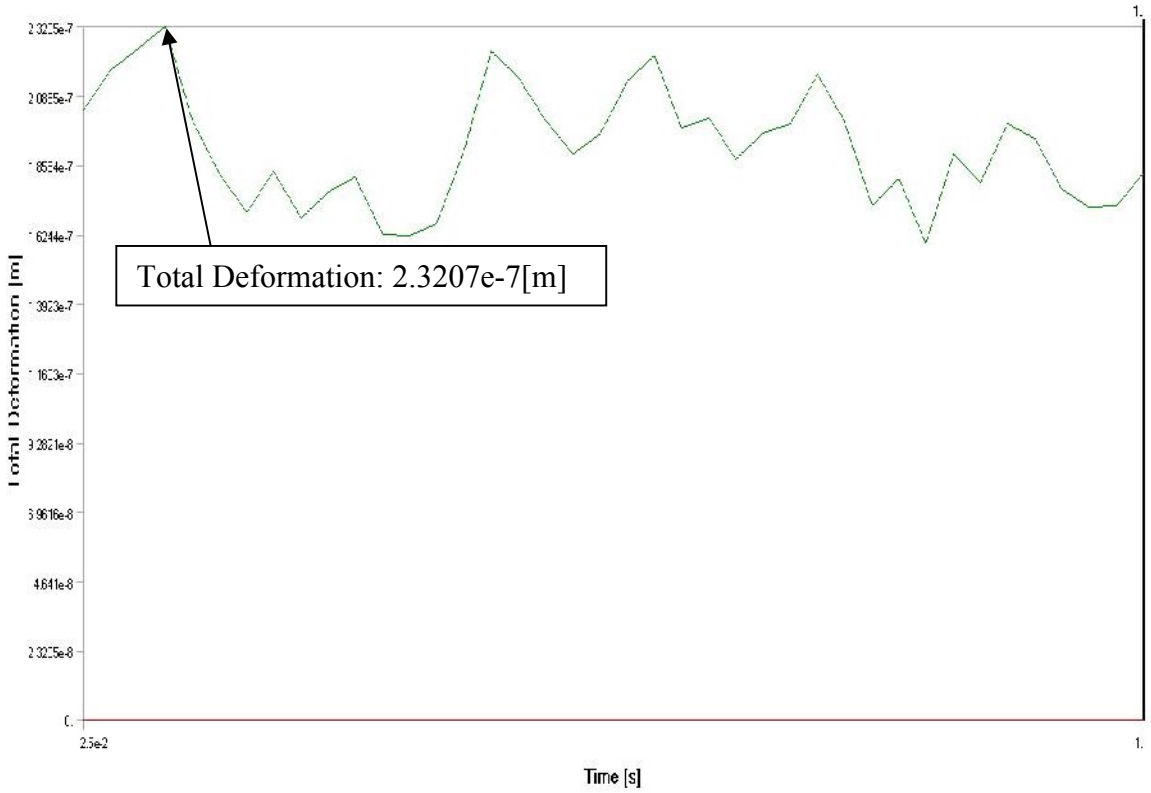

Figure 4.55 Total Deformation of EN31(V=102,F=20,A=0.25)

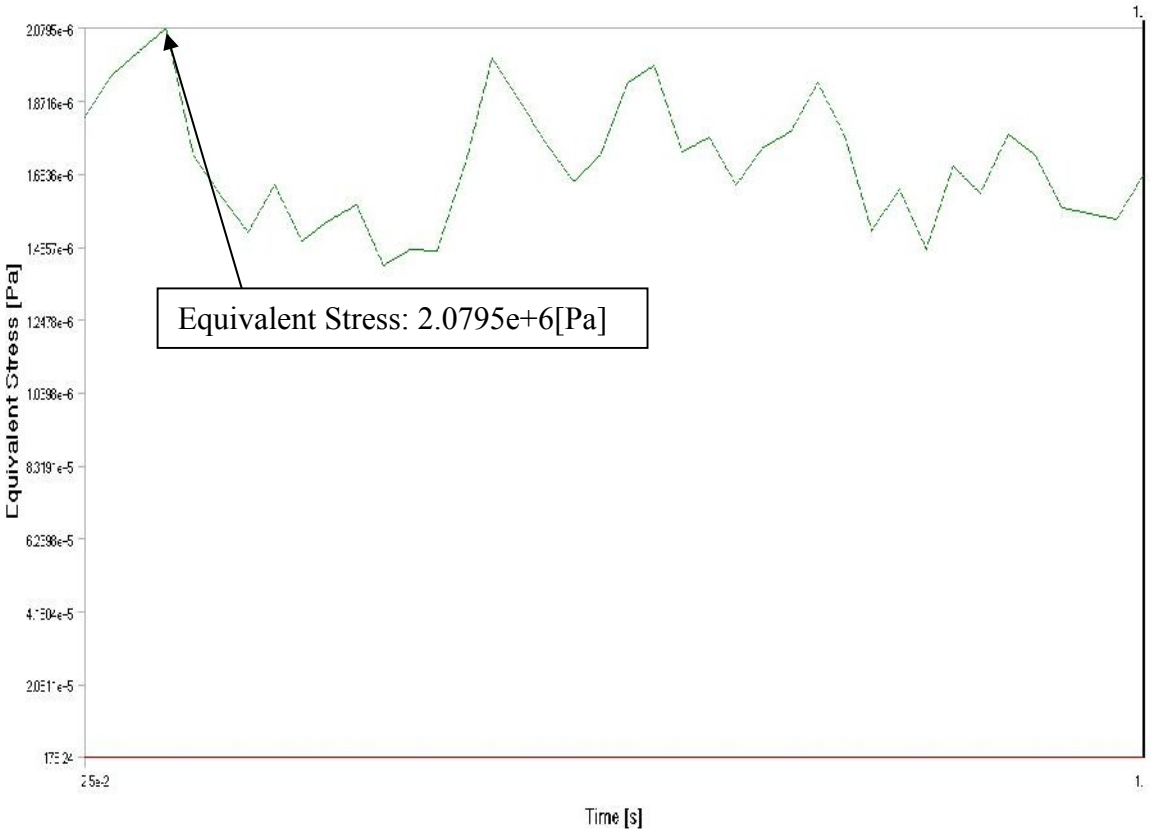

Figure 4.56 Equivalent Stress of EN31(V=102,F=20,A=0.25)

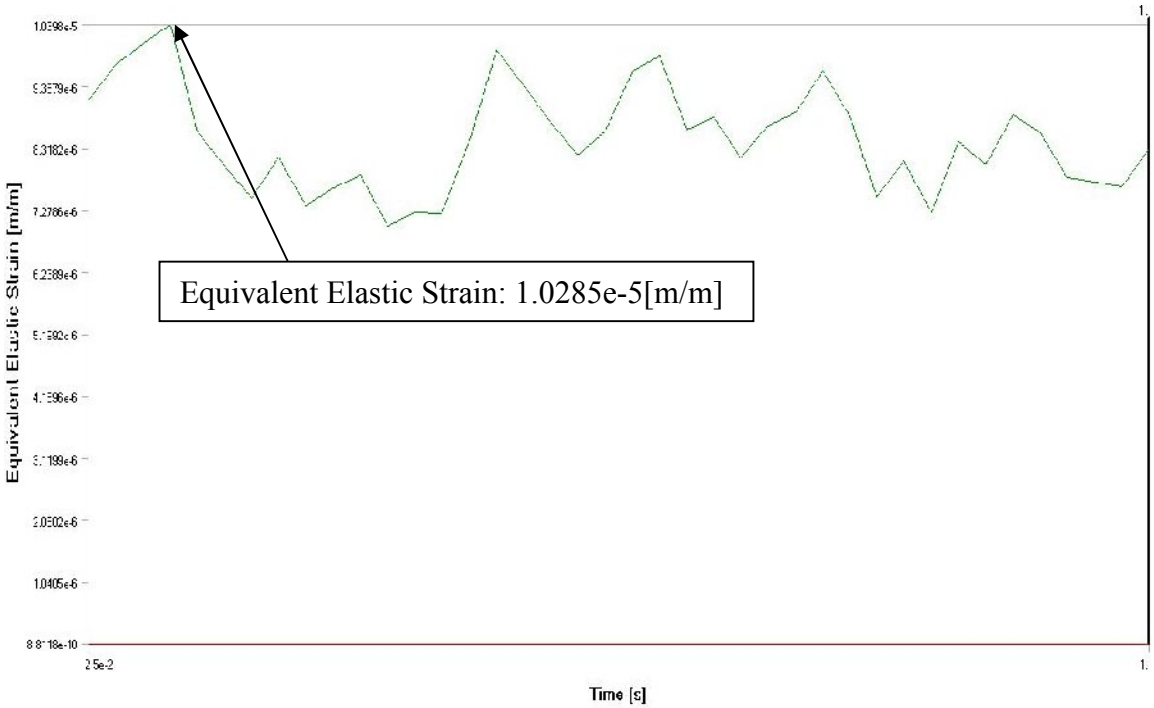

Figure 4.57 Equivalent Elastic Strain of EN31(V=102,F=20,A=0.25)

4.2.3.2

Table 4.27 Machining parameters of EN31

SPEED	102	r.p.m
FEED	35	mm/min
DOC	0.25	mm

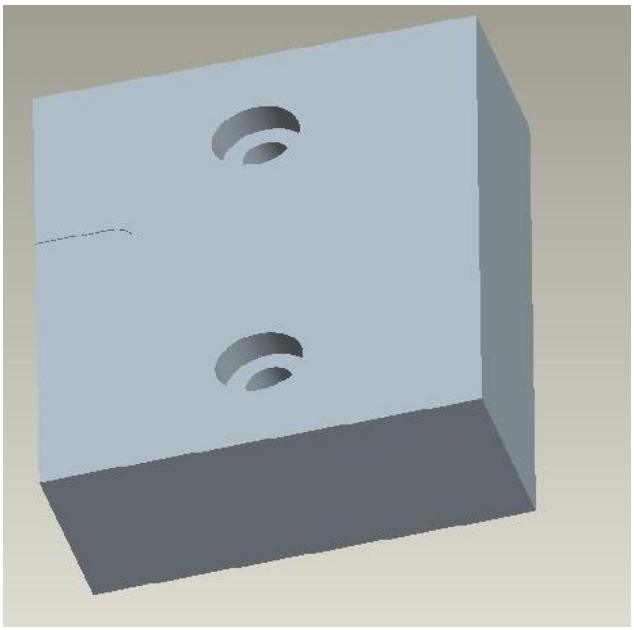

Figure 4.58 Pro-E Model of Specimen of EN31(V=102,F=35,A=0.25)

Tableb4.28 Force Values (Kistler\Dyno Ware)

File Type:			
Path:	C:\Kistler\DynoWare\Data\		
Filename:	millig2.dwd		
Config ID:	millig2.cfg		
Sampling rate [Hz]:	10		
Measuring time [s]:	40		
Delay time [s]:	0		
Cycle time [s]:	0		
Cycles:	1		
Samples per channel:	401		
Cycle interval:	0		
Channel enabled:	1	1	1
Cycle No:	1		
Time [s]	Fx	Fy	Fz
0	-44.9524	25.1312	69.3237
1	-0.90027	-1.53E-02	5.27344
2	-91.0492	32.1045	119.714
3	-31.5399	14.0686	52.4658
4	-96.756	34.256	126.66
5	-35.2783	41.6412	67.5293
6	-42.3126	28.244	64.7949
7	-2.36511	0.213623	8.59375
8	-70.0073	27.0386	94.5557
9	-61.9659	43.1824	90.0879
10	-68.5577	46.6919	107.312
11	-32.8827	36.499	60.3271
12	-35.4156	34.2255	62.2192
13	-14.7552	14.7858	20.1172
14	-71.1212	28.3051	99.7681
15	-71.5485	46.9666	117.151
16	-36.1786	39.978	71.6553
17	-8.37708	33.5083	37.5244
18	-22.0947	18.2495	24.9878
19	-23.941	16.8304	29.6021
20	-79.1626	38.8794	120.789
21	-64.4379	44.7998	111.963
22	-38.1927	46.7529	78.3081
23	-17.2577	31.8298	40.2954
24	-13.9771	19.0582	33.5083
25	-22.995	20.874	32.2998

26	-56.0455	30.1361	87.2437
27	-55.7861	47.9736	107.959
28	-34.5154	47.5311	87.8662
29	1.297	31.2195	18.4204
30	-13.7329	20.9961	37.4146
31	-26.8707	22.1863	35.8521
32	-78.8116	56.1981	137.28
33	-54.2908	43.3807	111.67
34	-35.9955	45.929	89.7827
35	-5.84412	30.2734	28.0396
36	12.085	20.34	-14.8438
37	-26.5503	25.8026	58.6792
38	-65.033	59.9976	122.754
39	-46.9055	49.1791	101.868
40	-36.2244	50.1862	91.394

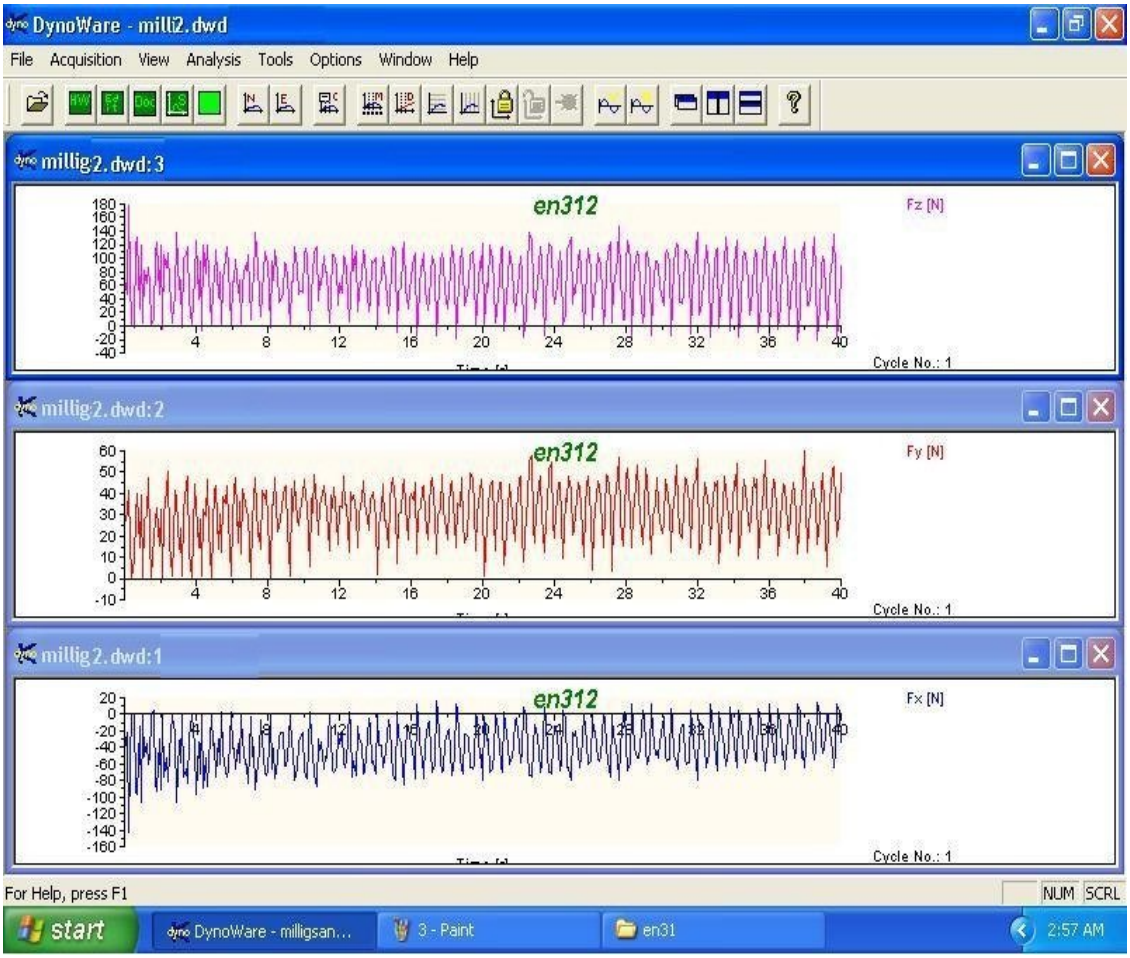

Figure 4.59 Graphical Representation of Force Variation of EN31

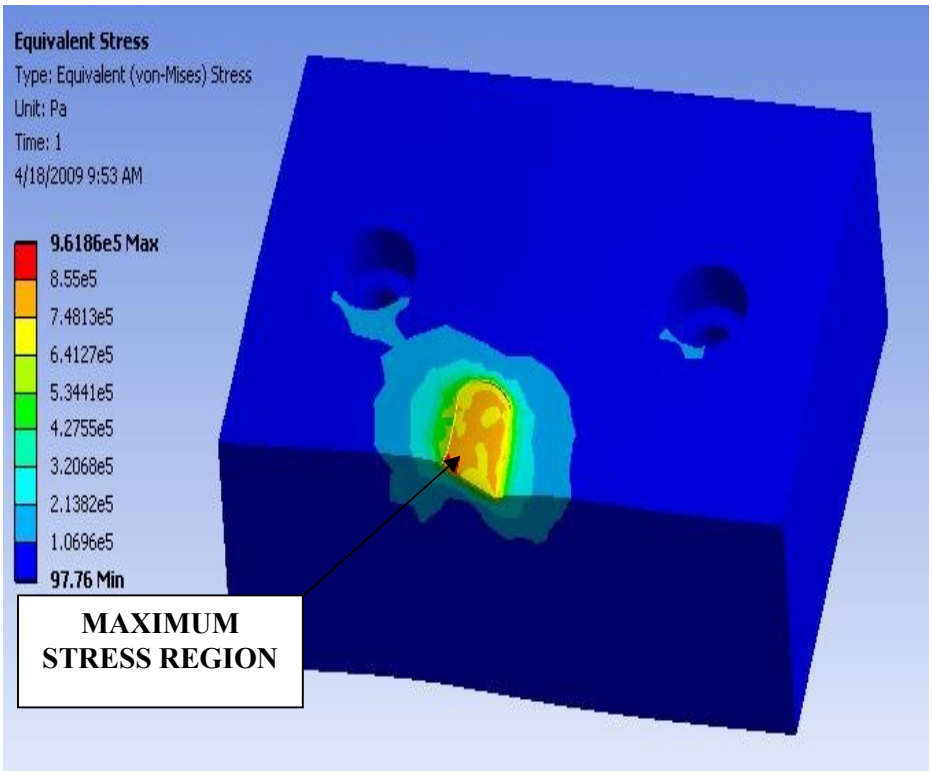

Figure 4.60 Analysis of EN31(V=102,F=35,A=0.25)

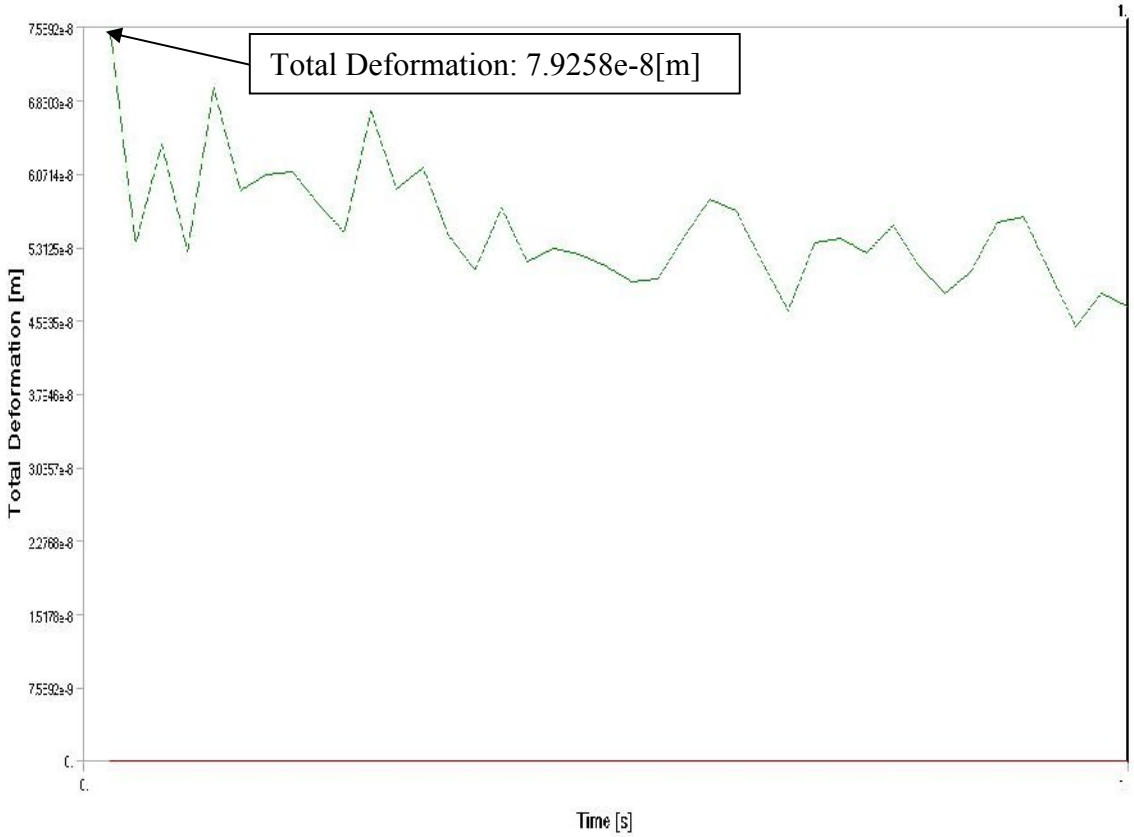

Figure 4.61 Total Deformation of EN31(V=102,F=35,A=0.25)

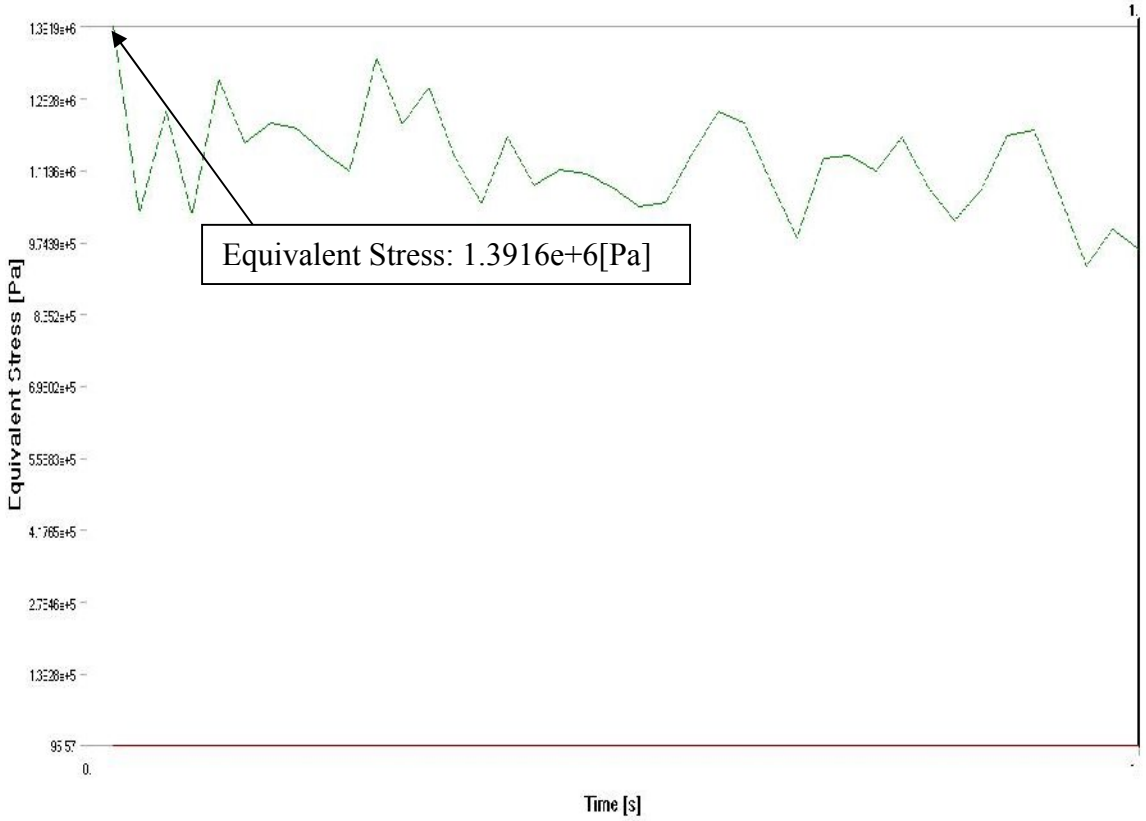

Figure 4.62 Equivalent Stress of EN31(V=102,F=35,A=0.25)

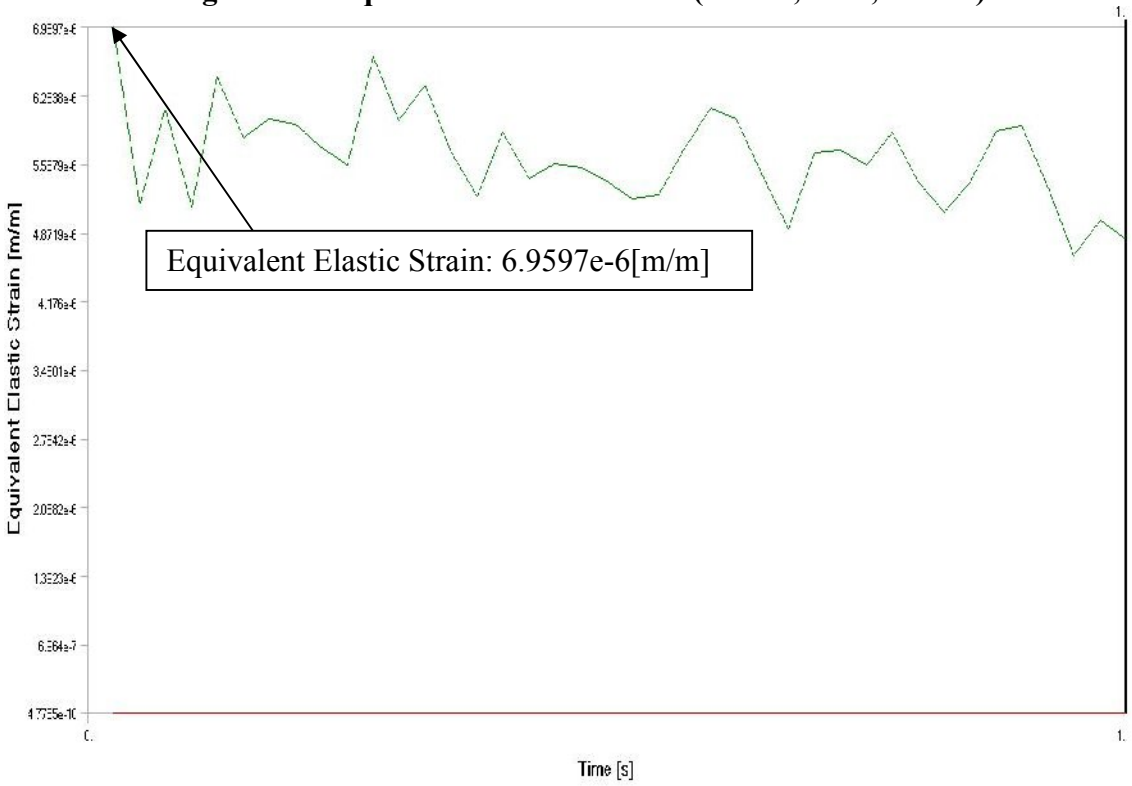

Figure 4.63 Equivalent Elastic Strain of EN31(V=102,F=35,A=0.25)

4.2.3.3

Table 4.29 Machining parameters of EN31

SPEED	102	r.p.m
FEED	65	mm/min
DOC	0.25	mm

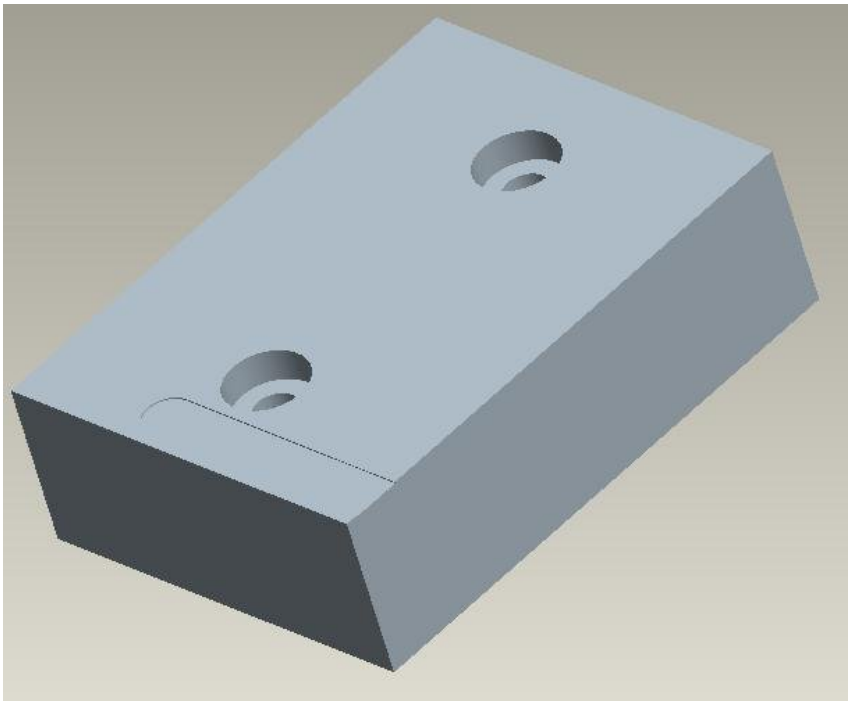

Figure 4.64 Pro-E Model of Specimen of EN31

Table 4.30 Force Values (Kistler\Dyno Ware)

File Type:			
Path:	C:\Kistler\DynoWare\Data\		
Filename:	millig2.dwd		
Config ID:	millig2.cfg		
Sampling rate [Hz]:	10		
Measuring time [s]:	40		
Delay time [s]:	0		
Cycle time [s]:	0		
Cycles:	1		
Samples per channel:	401		
Cycle interval:	0		
Channel enabled:	1	1	1
Cycle No:	1		
Time [s]	Fx	Fy	Fz
0	45.1202	44.5709	-80.4688

1	47.0886	29.8309	-55.9692
2	-142.944	40.39	-64.0991
3	-203.644	62.9883	-235.583
4	-75.6226	89.6149	-219.763
5	-19.6075	62.9883	-219.495
6	29.8004	58.8837	-118.347
7	50.5829	22.6898	-36.6089
8	-156.509	46.875	-74.6704
9	-93.9789	46.7377	-162.805
10	-49.6216	100.006	-247.18
11	16.4948	62.6068	-221.436
12	81.2531	45.5627	-93.1152
13	84.1827	26.7181	-31.9336
14	-179.337	53.4668	-110.974
15	-56.1066	44.4489	-91.5161
16	16.7542	95.7947	-230.823
17	86.441	53.9856	-178.113
18	98.5565	34.7137	-12.9395
19	166.031	57.3273	-134.851
20	-227.524	69.4275	-165.723
21	-41.6718	71.1517	-219.019
22	-13.2141	77.4078	-237.488
23	152.161	64.3158	-160.986
24	74.4476	43.7469	-91.4795
25	59.6924	21.4233	-2.99072
26	-210.892	78.9337	-216.125
27	-31.3721	58.5175	-172.107
28	75.47	96.6034	-267.053
29	173.859	55.4047	-126.66
30	139.725	89.4012	-220.251
31	144.043	32.5012	-16.4307
32	-151.382	79.1473	-214.441
33	50.4303	62.7136	-205.2
34	131.226	81.6498	-217.969
35	105.194	70.2972	-148.254
36	121.475	42.7856	-141.284
37	27.71	21.6064	0.683594
38	-79.6814	79.4678	-241.614
39	97.0154	64.0869	-181.287
40	152.206	87.6465	-233.289

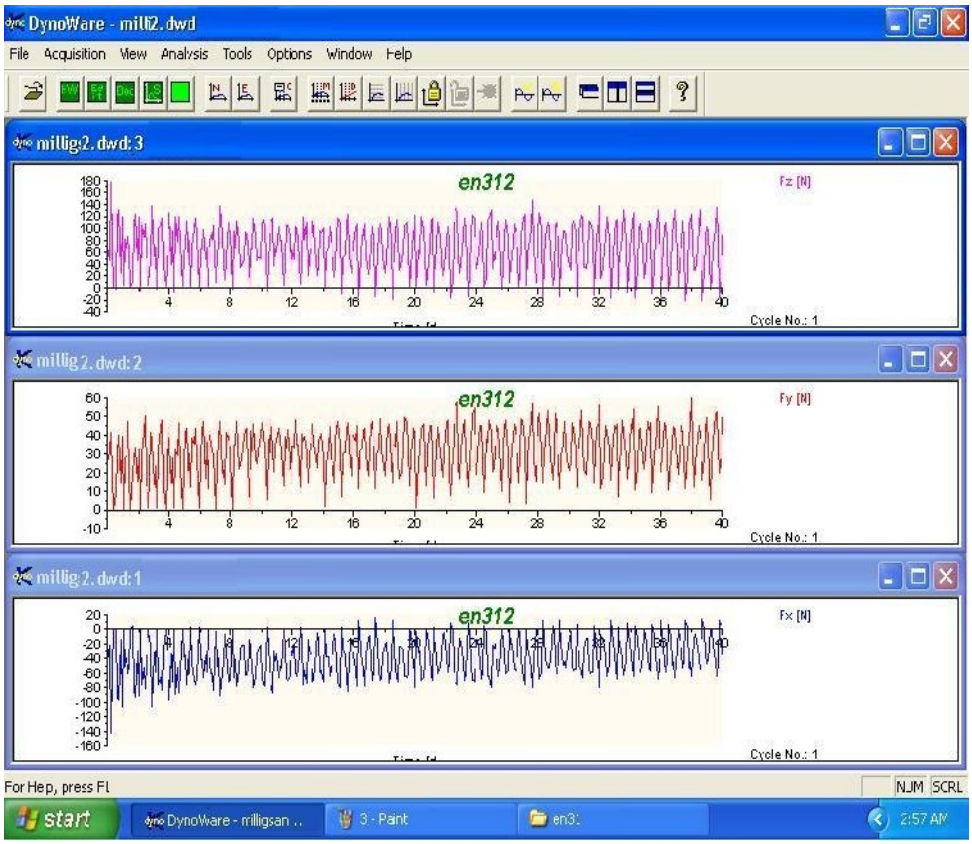

Figure 4.65 Graphical Representation of Force Variation of EN31

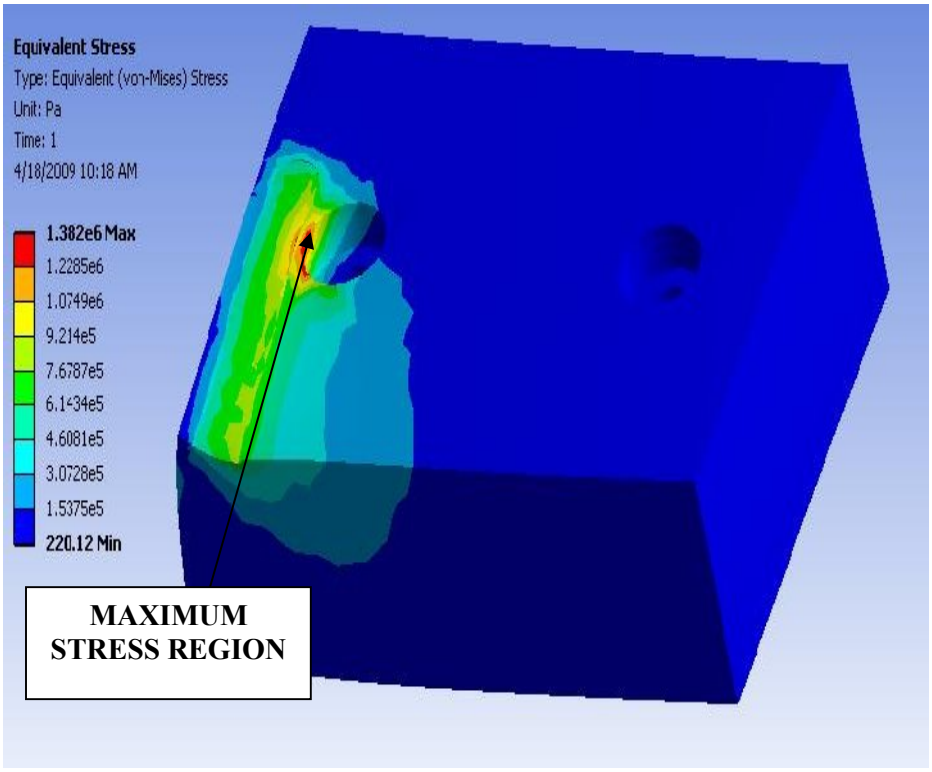

Figure 4.66 Analysis of EN31 (V=102,F=65,A=0.25)

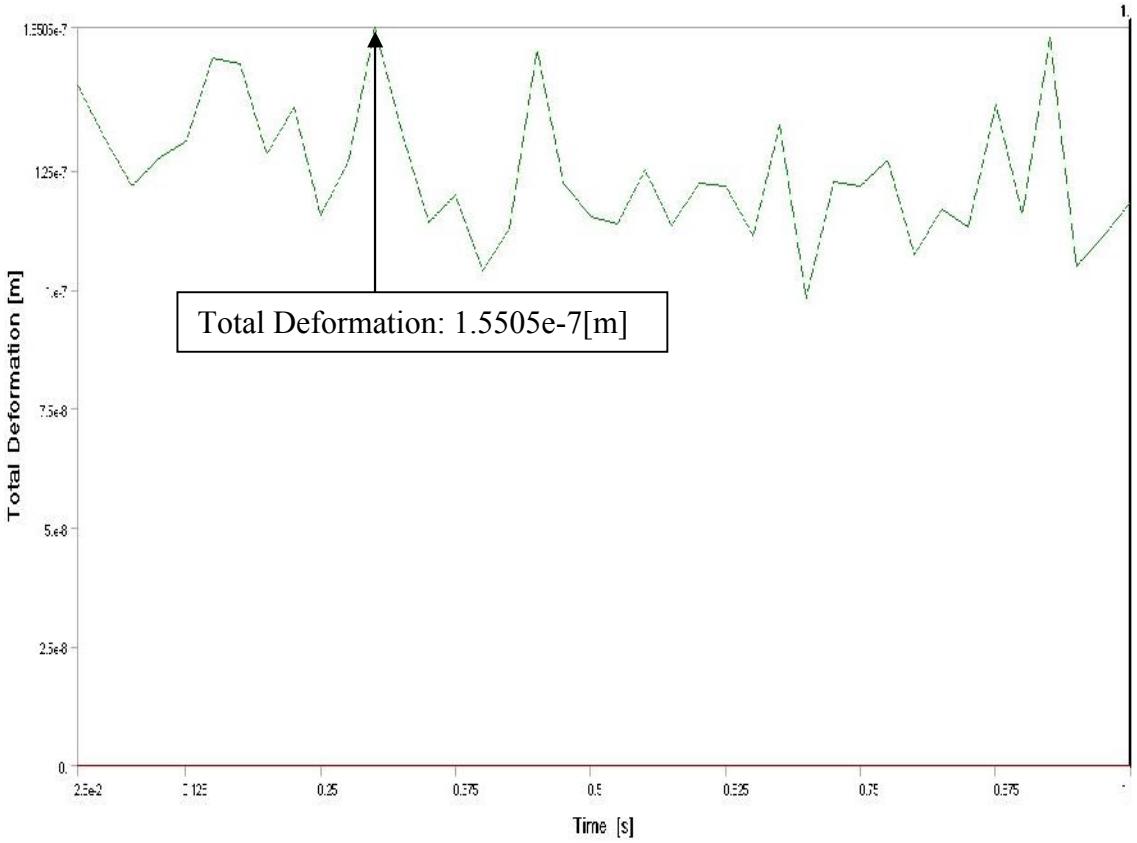

Figure 4.67 Total Deformation of EN31(V=102,F=65,A=0.25)

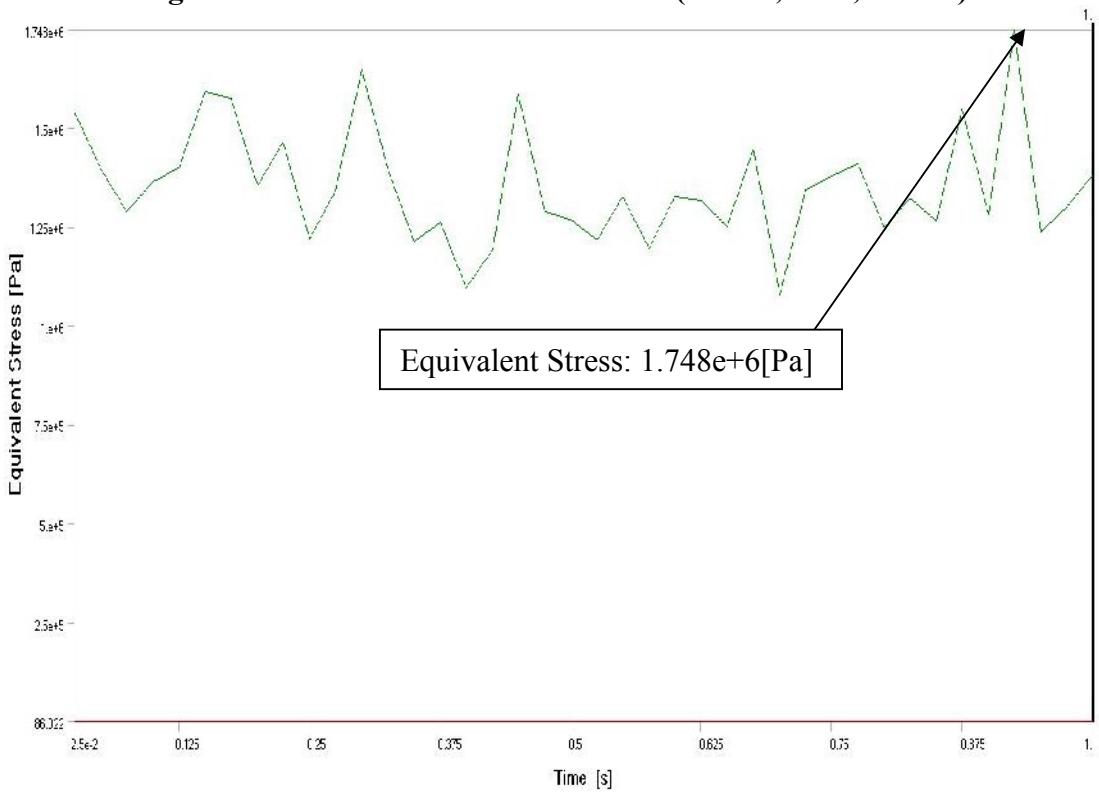

Figure 4.68 Equivalent Stress of EN31(V=102,F=65,A=0.25)

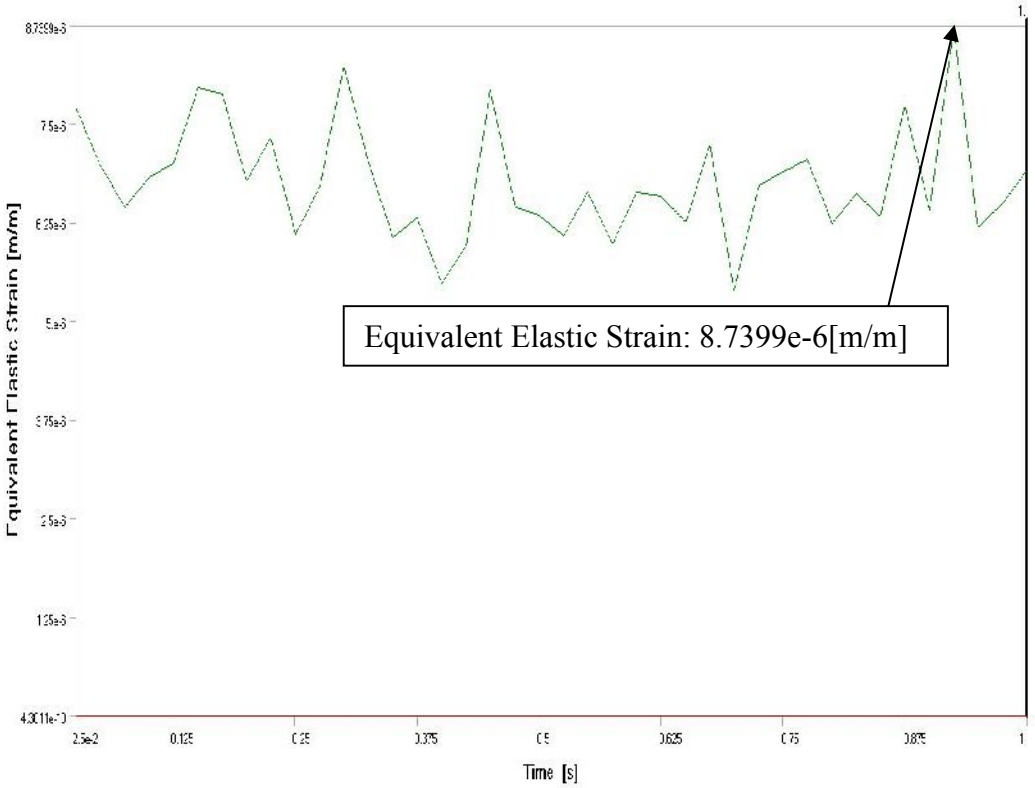

Figure 4.69 Equivalent Elastic Strain of EN31(V=102,F=65,A=0.25)

4.2.3.4

Table 4.31 Machining parameters of EN31

SPEED	204	r.p.m
FEED	20	mm/min
DOC	0.25	mm

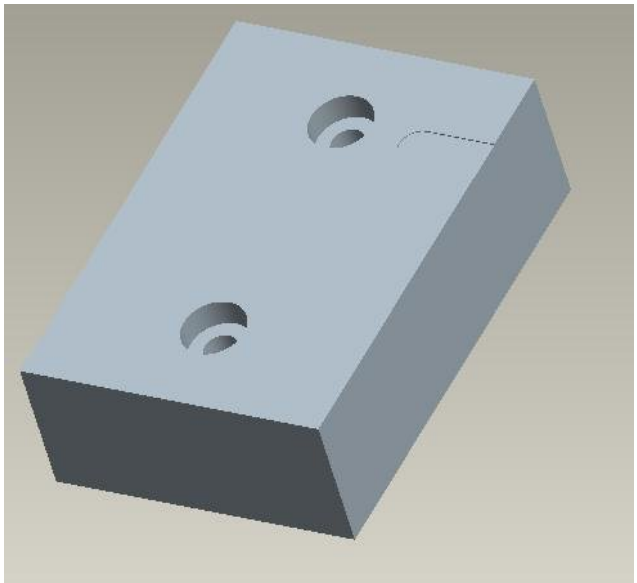

Figure 4.70 Pro-E Model of Specimen of EN31(V=204,F=20,A=0.25)

Table 4.32 Force Values (Kistler\Dyno Ware)

File Type:			
Path:	C:\Kistler\DynoWare\Data\		
Filename:	millig2.dwd		
Config ID:	millig2.cfg		
Sampling rate [Hz]:	10		
Measuring time [s]:	40		
Delay time [s]:	0		
Cycle time [s]:	0		
Cycles:	1		
Samples per channel:	401		
Cycle interval:	0		
Channel enabled:	1	1	1
Cycle No:	1		
Time [s]	Fx	Fy	Fz
0	-83.6884	17.2974	-44.1589
1	-120.914	17.8467	-125.659
2	-174.637	33.1299	-149.414
3	-46.3623	14.0015	-16.0706
4	-149.442	23.3887	-143.195
5	-157.013	28.894	-122.29
6	-31.2286	16.748	-6.52466
7	-145.45	22.9736	-141.937
8	-115.942	27.356	-68.2007
9	-15.4083	10.7422	-3.10059
10	-143.399	25.1221	-128.125
11	-95.3613	25.3662	-60.4614
12	-10.7391	6.92139	-10.0464
13	-138.977	32.4463	-128.68
14	-71.0632	39.0747	-24.9268
15	-9.75952	9.80225	-7.87964
16	-120.493	37.7197	-122.491
17	-73.9838	33.02	-46.759
18	-1.24512	2.7832	-2.02637
19	-106.924	39.1724	-109.296
20	-65.6433	37.7319	-40.1611
21	-0.41199	22.7295	-52.7161
22	-100.543	42.9443	-96.7773
23	-44.6228	59.3262	-9.08203
24	-10.0067	27.9297	-62.7075

25	-107.822	51.5991	-107.489
26	-47.4609	43.8843	-4.82178
27	-28.2532	25.8789	-101.447
28	-97.4304	44.5313	-100.861
29	-43.8629	42.1387	-14.6179
30	-37.1063	32.3608	-126.593
31	-105.991	41.5283	-96.8689
32	-42.6178	40.8447	-13.1958
33	-37.4084	30.5054	-117.706
34	-96.6431	45.4346	-93.9148
35	-42.0135	36.1694	-7.42188
36	-41.3452	31.9092	-136.163
37	-95.9473	46.9482	-97.8394
38	-44.6411	39.6851	-30.1941
39	-48.1842	28.3203	-137.878
40	-90.5365	42.4805	-86.5662

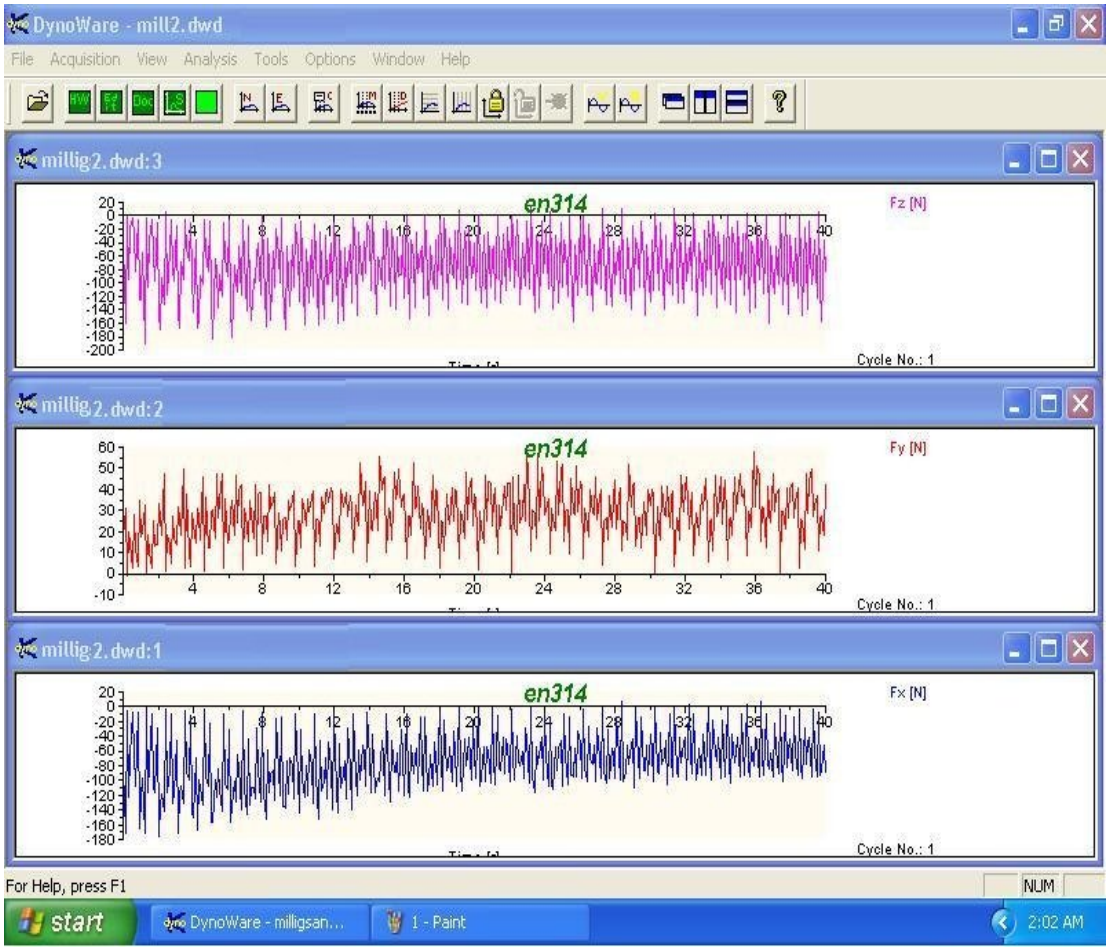

Figure 4.71 Graphical Representation of Force Variation of EN31

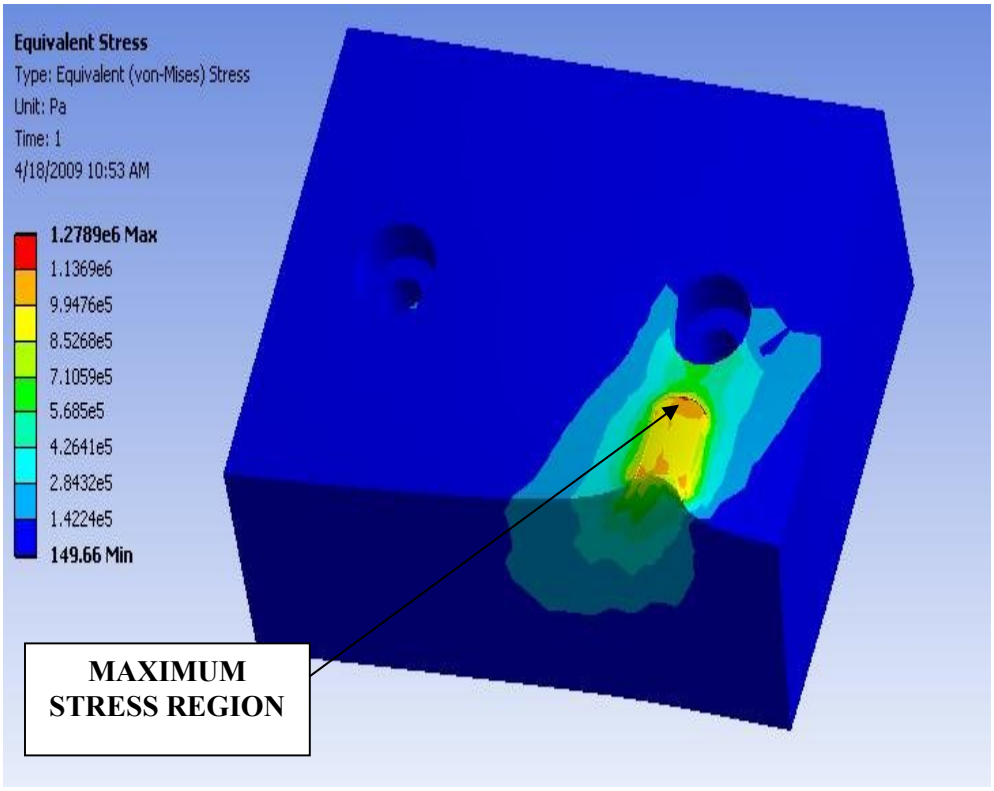

Figure 4.72 Analysis of EN31(V=204,F=20,A=0.25)

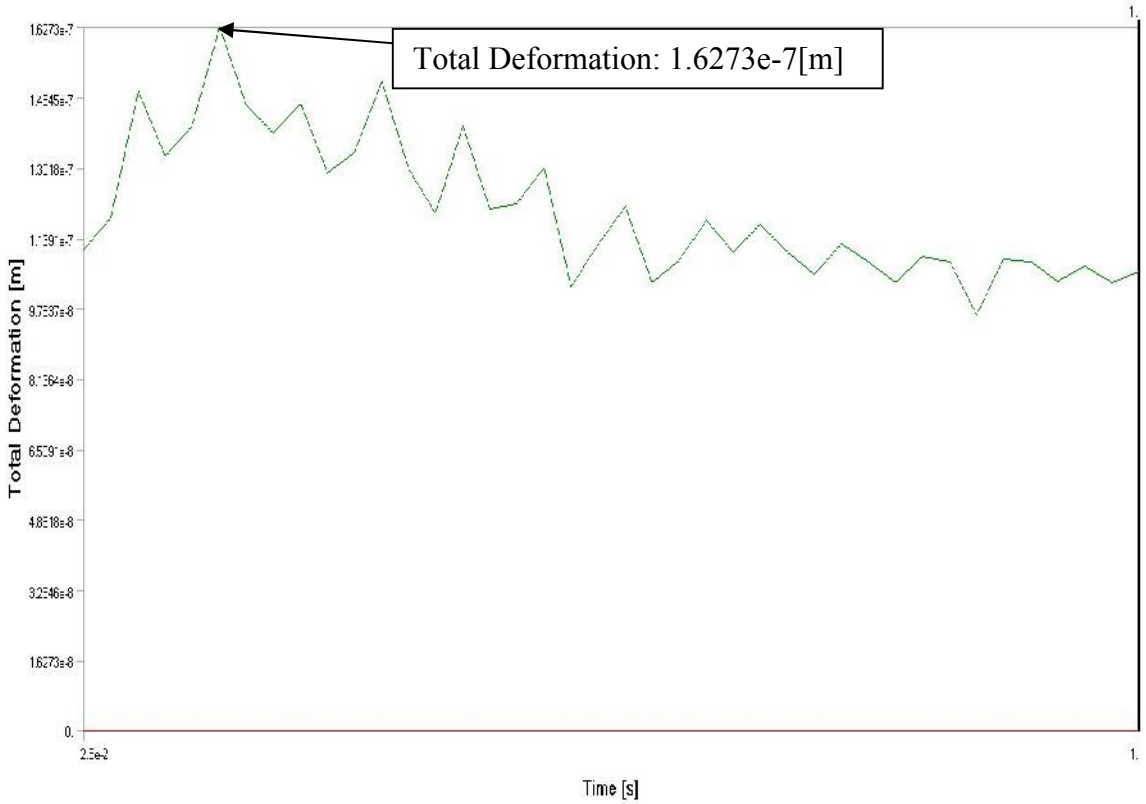

Figure 4.73 Total Deformation of EN31(V=204,F=20,A=0.25)

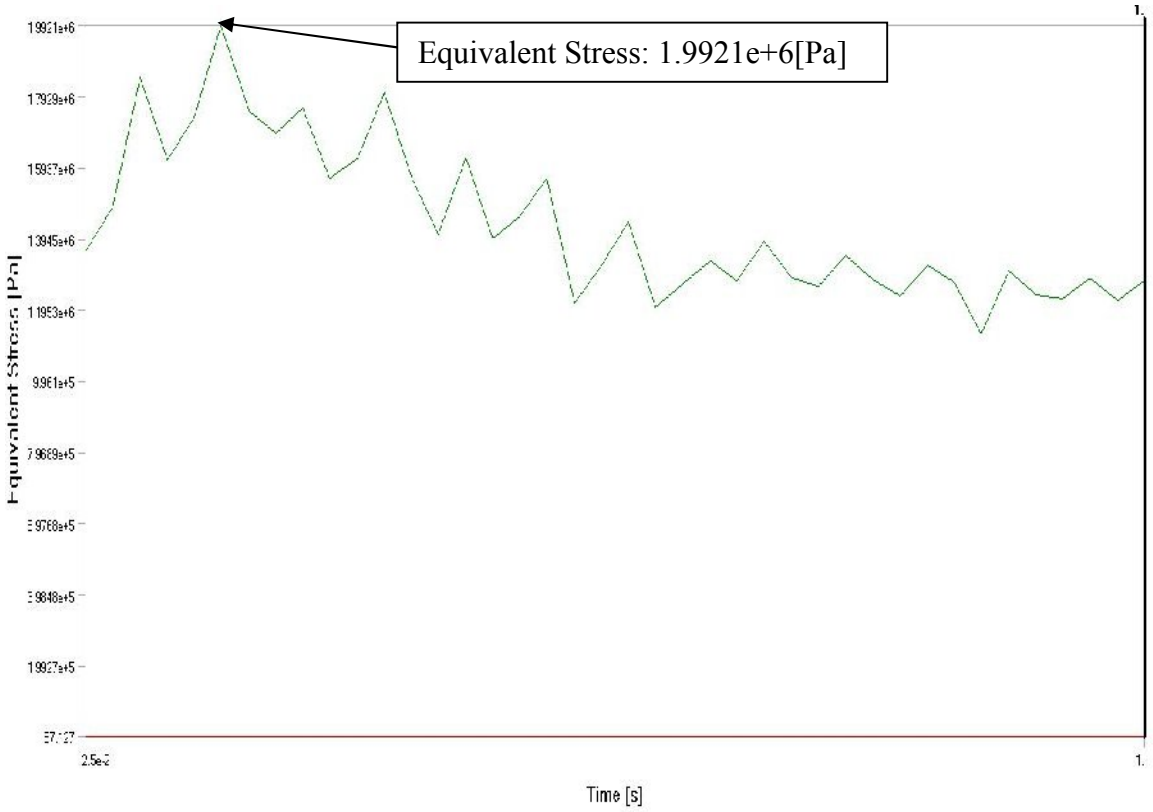

Figure 4.74 Equivalent Stress of EN31(V=204,F=20,A=0.25)

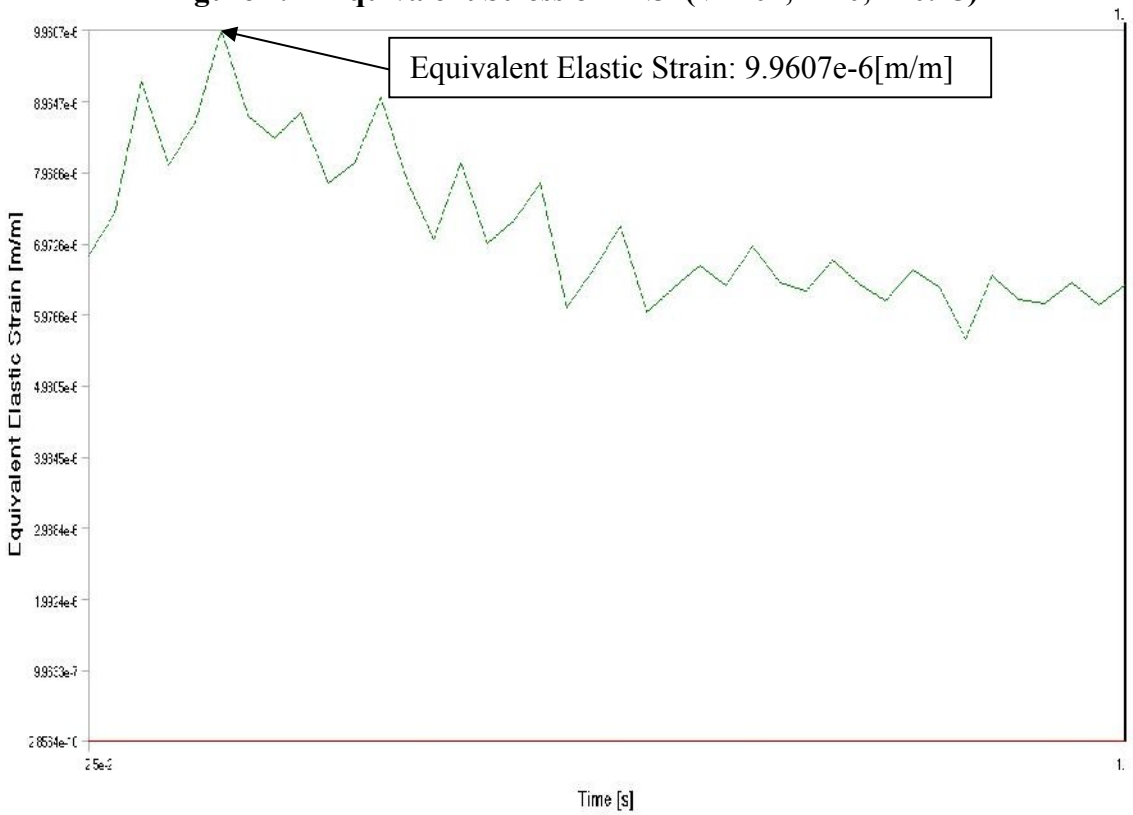

Figure 4.75 Equivalent Elastic Strain of EN31(V=204,F=20,A=0.25)

Table 4.33 Material composition of EN44

C	Si	Mn	S	P
0.9-1.05	0.35max	0.3-0.7	0.05max	0.05max

Table 4.34 Mechanical properties of EN44

Tensile Strength	656.7 N/mm²
Yield Stress	379.2 N/mm²
Reduction of Area	20.6 %
Elongation	13.0 %
Modulus of elasticity	210 000 N/mm²
Density	8.03Kg/m3
Hardness	65 HRC

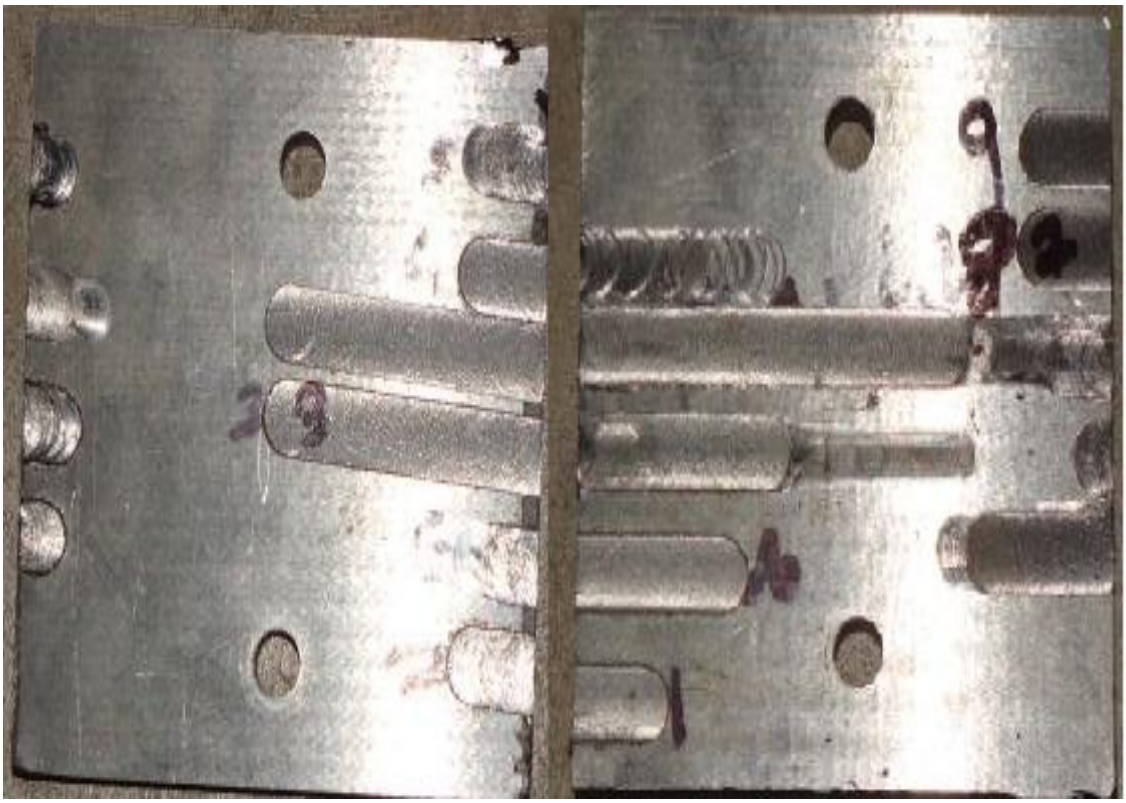

Figure 4.76 Specimen Details of EN44

4.2.4.1

Table 4.35 Machining parameters of EN44

SPEED	102	r.p.m
FEED	20	mm/min
DOC	0.25	mm

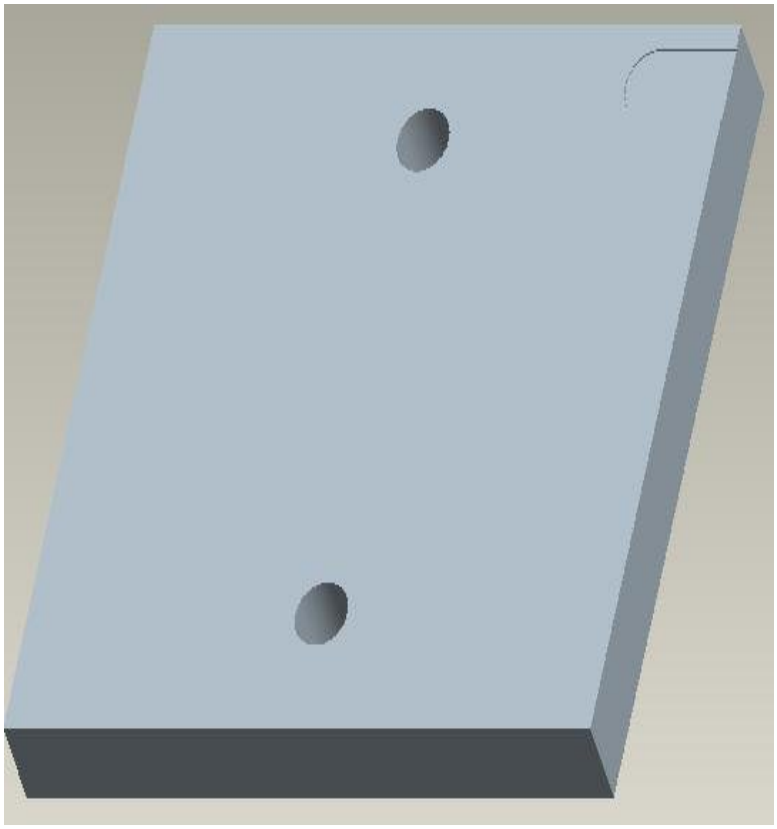

Figure 5 Pro-E Model of Specimen of EN44(V=102,F=20,A=0.25)

Table 4.36 Force Values (Kistler\Dayno Ware)

File Type:			
Path:	C:\Kistler\DynoWare\Data\		
Filename:	millig2.dwd		
Config ID:	millig2.cfg		
Sampling rate [Hz]:	10		
Measuring time [s]:	40		
Delay time [s]:	0		
Cycle time [s]:	0		
Cycles:	1		
Samples per channel:	401		
Cycle interval:	0		
Channel enabled:	1	1	1
Cycle No:	1		
Time [s]	Fx	Fy	Fz
0	-207.184	27.9236	-112.915
1	-0.13733	-6.72913	1.17188
2	-20.3857	-4.0741	-11.5967
3	-131.027	30.1971	-49.4995

4	-204.224	36.7279	-148.096
5	-154.51	43.2129	-45.3003
6	-161.041	25.0549	-82.3242
7	0.869751	-6.42395	1.47705
8	-159.409	37.4603	-176.331
9	-192.383	76.6907	-99.5605
10	-194.809	32.8827	-118.774
11	-88.4094	40.4358	-10.0586
12	-72.1436	12.6953	-18.5181
13	-30.777	27.4811	-107.031
14	-180.374	37.3383	-150.317
15	-161.56	43.1824	-78.1982
16	-169.144	33.432	-81.0791
17	-71.1975	39.0472	-8.56934
18	-24.1241	6.69861	3.93066
19	-50.3387	36.0718	-131.421
20	-157.12	35.2936	-117.322
21	-161.85	62.1796	-64.0381
22	-135.956	27.7557	-36.3892
23	-117.508	16.6321	-76.5015
24	-11.0931	3.44849	0.842285
25	-103.424	32.6691	-146.484
26	-165.878	38.8947	-117.993
27	-161.392	42.6178	-83.2642
28	-100.891	39.6423	-9.09424
29	-88.8672	15.4572	-36.853
30	-19.7144	26.7944	-77.063
31	-143.127	34.317	-158.972
32	-150.253	68.634	-77.1484
33	-164.505	37.2467	-94.1406
34	-63.9038	40.2527	7.49512
35	-48.5229	14.4806	-0.87891
36	-41.9464	33.7982	-131.934
37	-153.381	29.6173	-133.289
38	-138.763	64.8193	-61.8652
39	-134.811	34.3781	-46.8018
40	-81.6498	34.5306	-39.0015

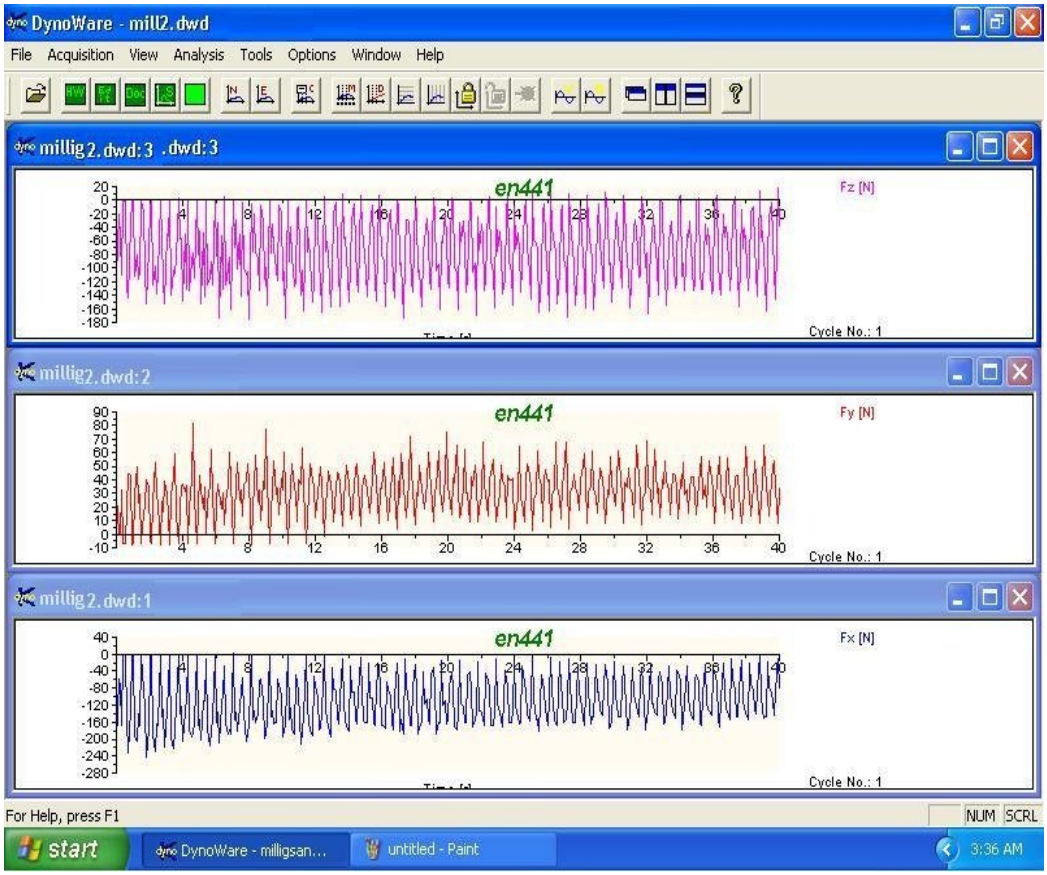

Figure 4.78 Graphical Representation of Force Variation of EN44

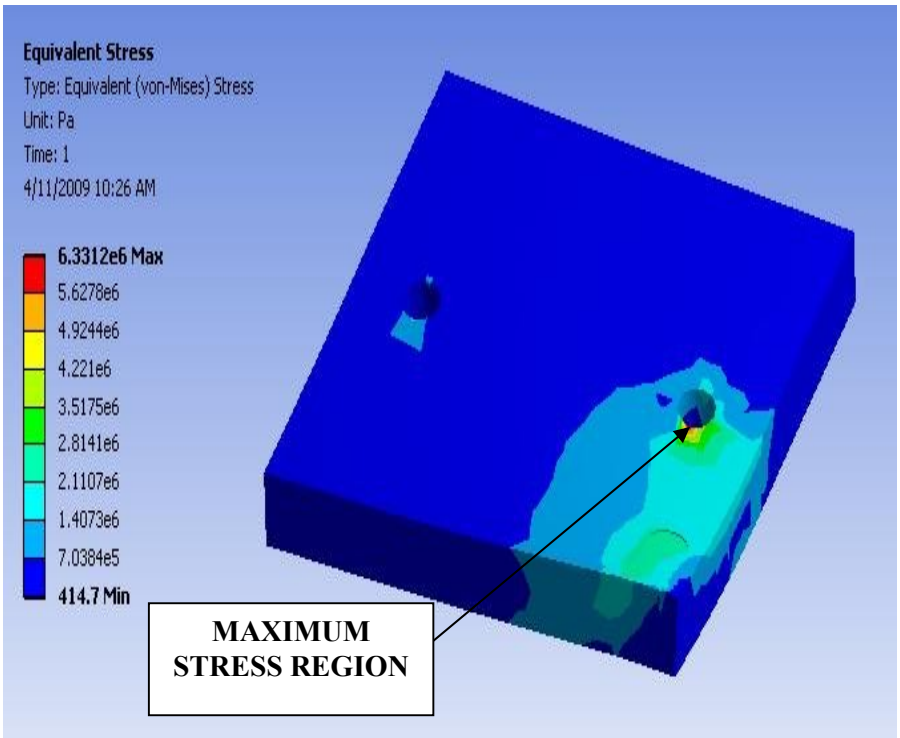

Figure 4.79 Analysis of EN44(V=102,F=20,A=0.25)

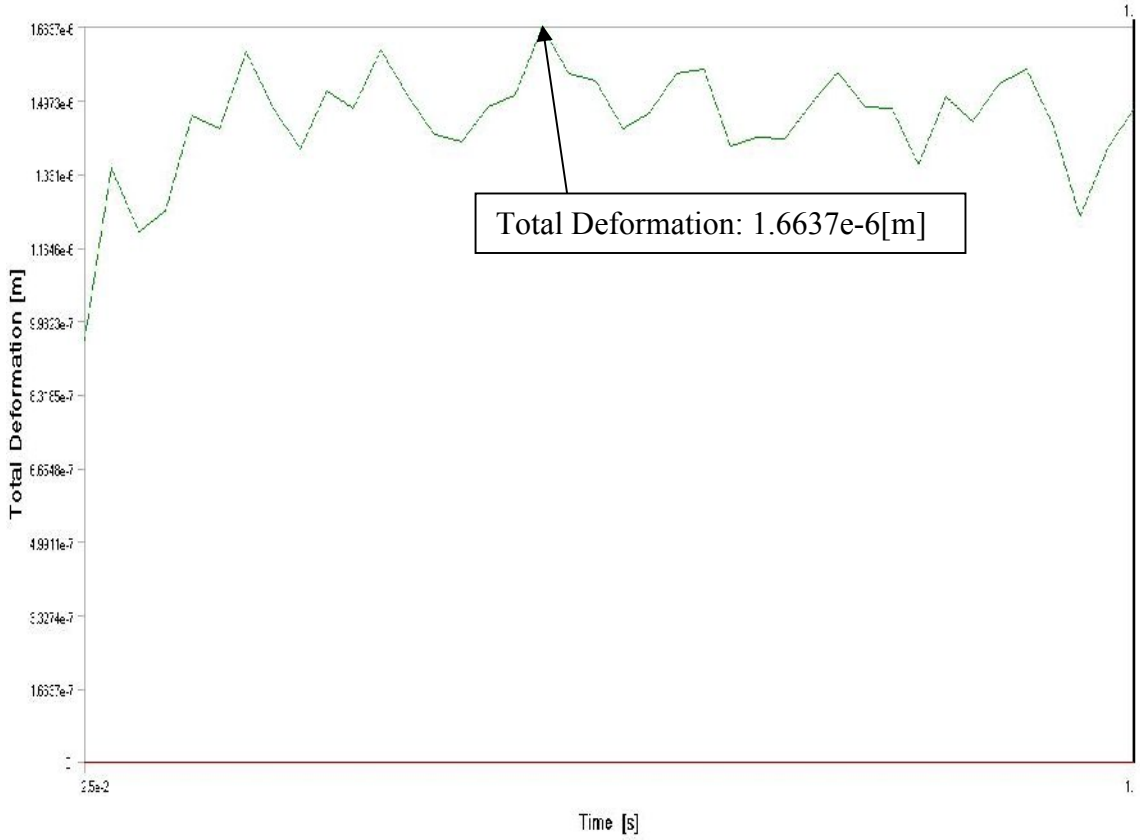

Figure 4.80 Total Deformation of EN44(V=102,F=20,A=0.25)

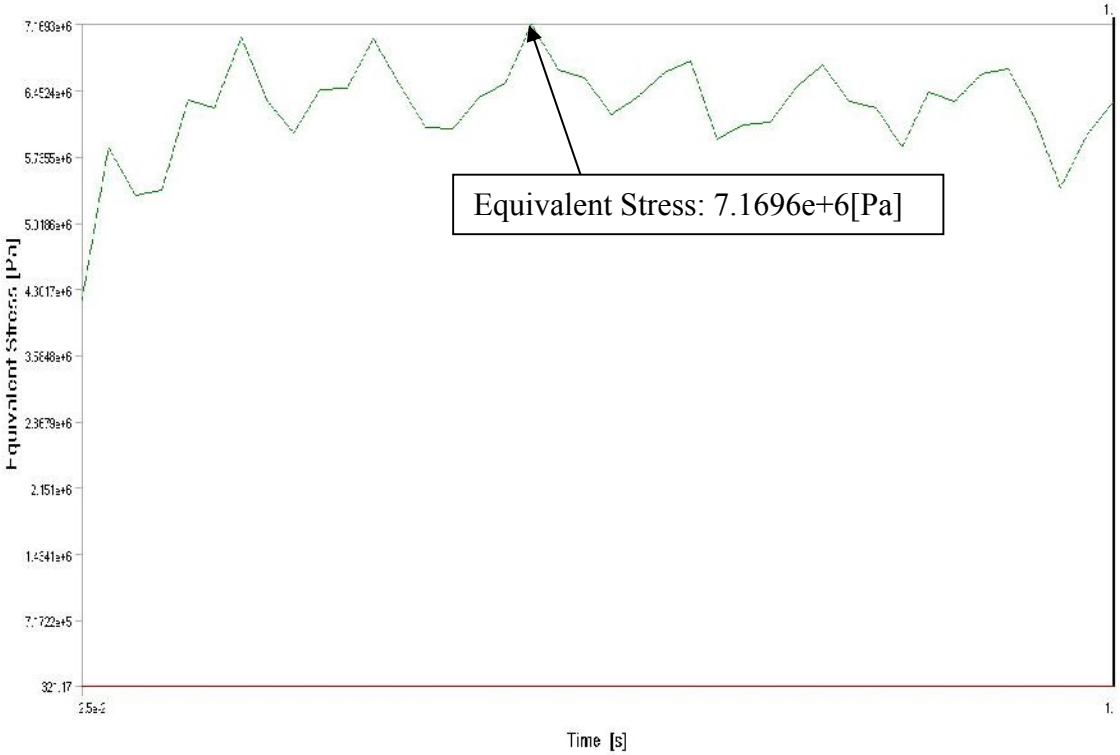

Figure 4.81 Equivalent Stress of EN44(V=102,F=20,A=0.25)

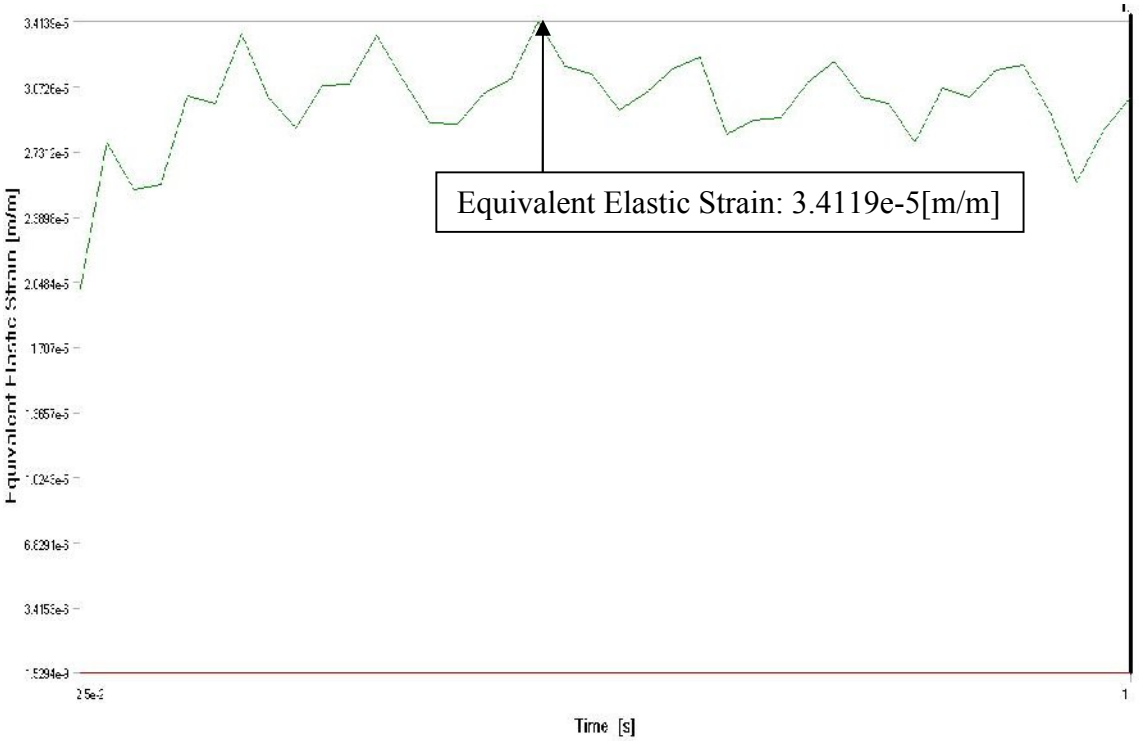

Figure 4.82 Equivalent Elastic Strain of EN44(V=102,F=20,A=0.25)

4.2.4.2

Table 4.37 Machining parameters of EN44

SPEED	102	r.p.m
FEED	35	mm/min
DOC	0.25	mm

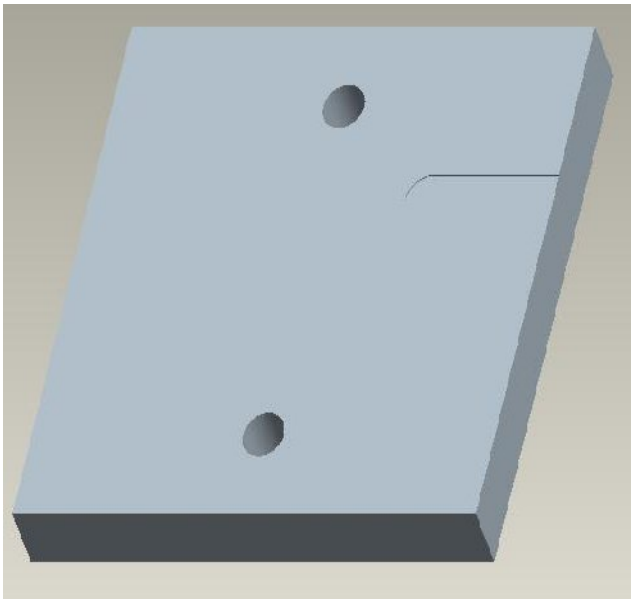

Figure 4.83 Pro-E Model of Specimen of EN44

Table 4.38 Force Value (Kistler\Dayno Ware)

File Type:			
Path:	C:\Kistler\DynoWare\Data\		
Filename:	millig2.dwd		
Config ID:	millig2.cfg		
Sampling rate [Hz]:	10		
Measuring time [s]:	40		
Delay time [s]:	0		
Cycle time [s]:	0		
Cycles:	1		
Samples per channel:	401		
Cycle interval:	0		
Channel enabled:	1	1	1
Cycle No:	1		
Time [s]	Fx	Fy	Fz
0	-0.18311	9.16E-02	-0.50049
1	-207.718	53.7262	-176.855
2	-197.128	89.8743	-134.802
3	-178.94	52.7039	-116.772
4	-97.229	58.136	-60.0098
5	-26.8555	25.8179	1.80664
6	-145.37	67.8101	-206.604
7	-199.6	59.0668	-164.551
8	-166.763	71.5637	-118.958
9	-109.1	57.8918	-45.4224
10	-146.072	34.8358	-105.945
11	-27.3438	31.8298	-52.1362
12	-201.874	67.5049	-250.195
13	-173.431	74.4019	-141.968
14	-160.263	53.3752	-126.66
15	-69.2596	54.9774	-26.2329
16	-48.5535	30.014	-17.5659
17	-21.9727	35.5682	-100.122
18	-186.31	58.0597	-212.964
19	-166.641	80.0171	-140.186
20	-119.4	40.8478	-71.5088
21	-100.51	45.7764	-90.2466
22	1.67847	2.5177	0.219727
23	-118.53	51.2085	-211.255
24	-133.057	64.0717	-128.76

25	-137.207	60.8368	-120.679
26	-79.8645	57.9681	-31.9458
27	-71.6858	31.9214	-38.5376
28	-16.1896	38.1775	-65.7227
29	-145.569	56.8237	-215.234
30	-131.348	66.864	-119.287
31	-127.579	44.4183	-108.911
32	-84.1217	50.0183	-87.2559
33	-7.85828	10.3455	2.91748
34	-56.4423	53.9703	-196.619
35	-108.597	50.5066	-142.102
36	-101.074	77.2858	-107.349
37	-76.5991	52.3529	-36.499
38	-90.0879	34.8816	-78.8818
39	-11.1084	26.5045	-68.103
40	-93.3533	59.7839	-221.069

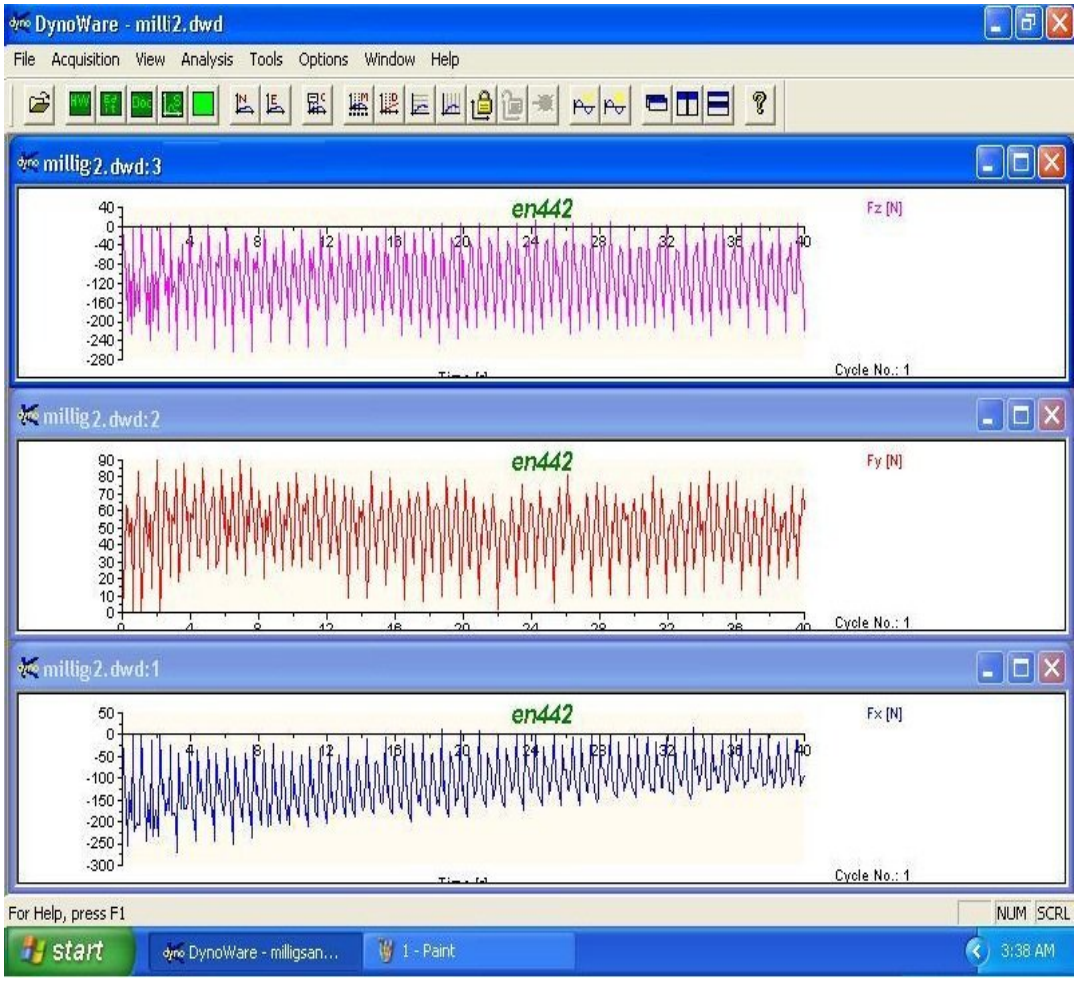

Figure 4.84 Graphical Representation of Force Variation of EN44

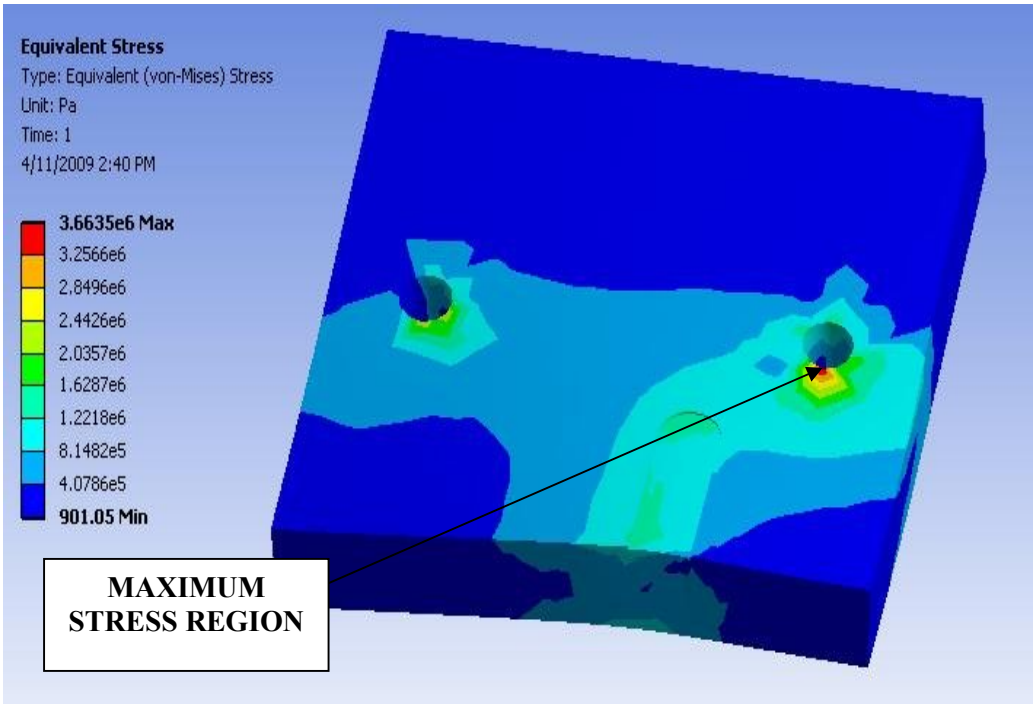

Figure 4.85 Analysis of EN44(V=102,F=35,A=0.25)

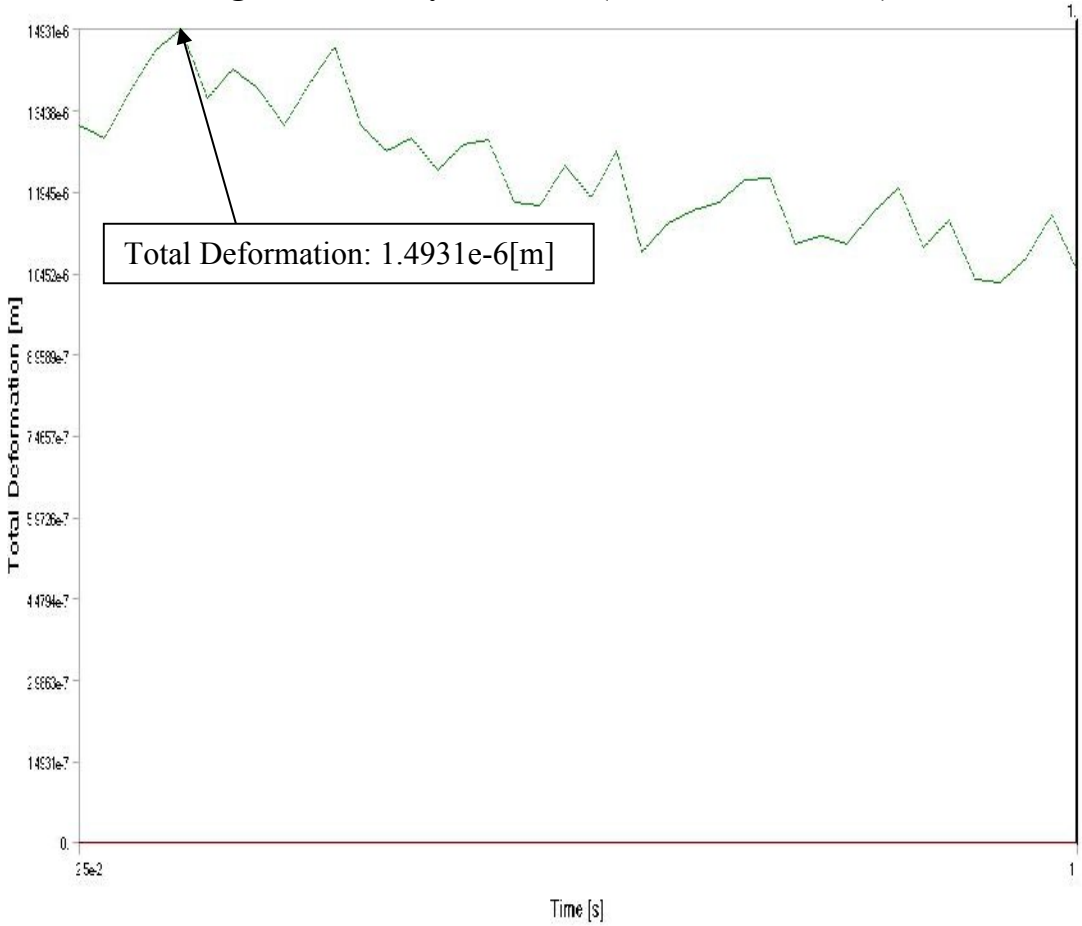

Figure 4.86 Total Deformation of EN44(V=102,F=35,A=0.25)

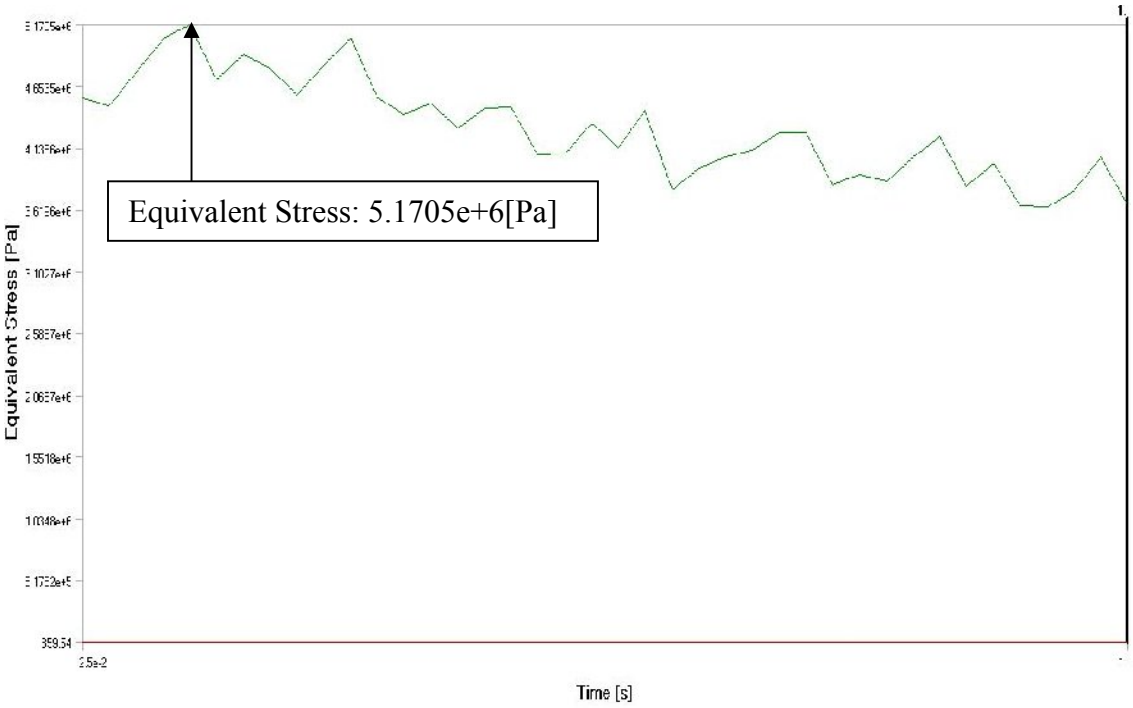

Figure 4.87 Equivalent Stress of EN44(V=102,F=35,A=0.25)

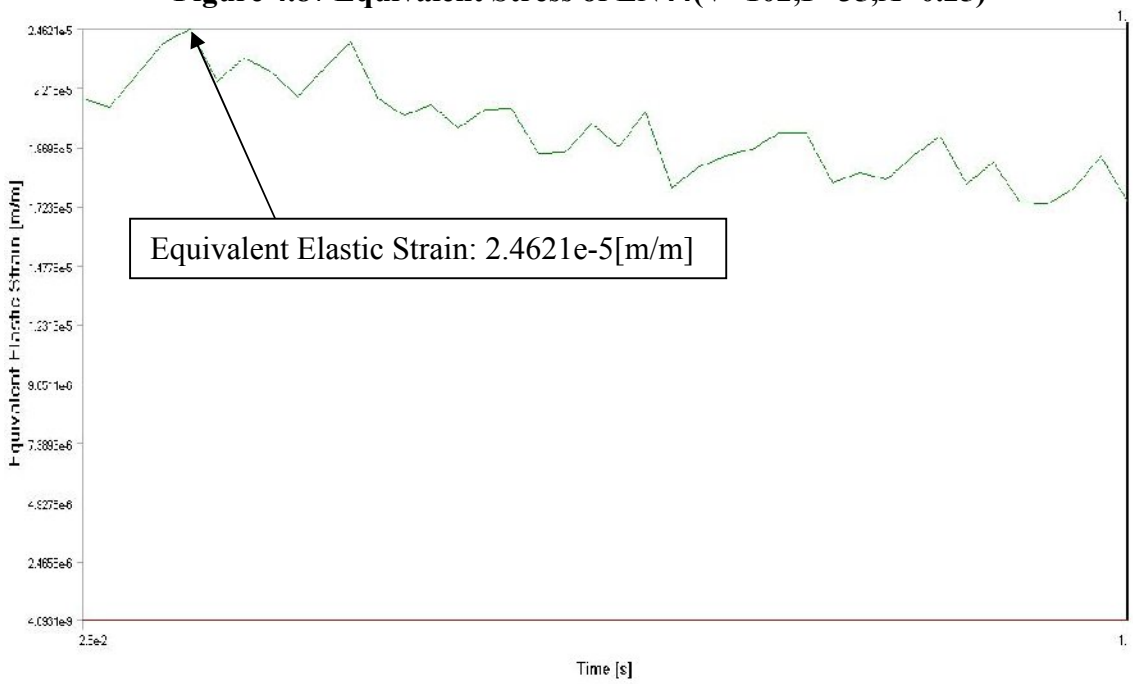

Figure 4.88 Equivalent Elastic Strain of EN44(V=102,F=35,A=0.25)

4.2.4.3

Table 4.39 Machining parameters of EN44

SPEED	102	r.p.m
FEED	65	mm/min
DOC	0.25	mm

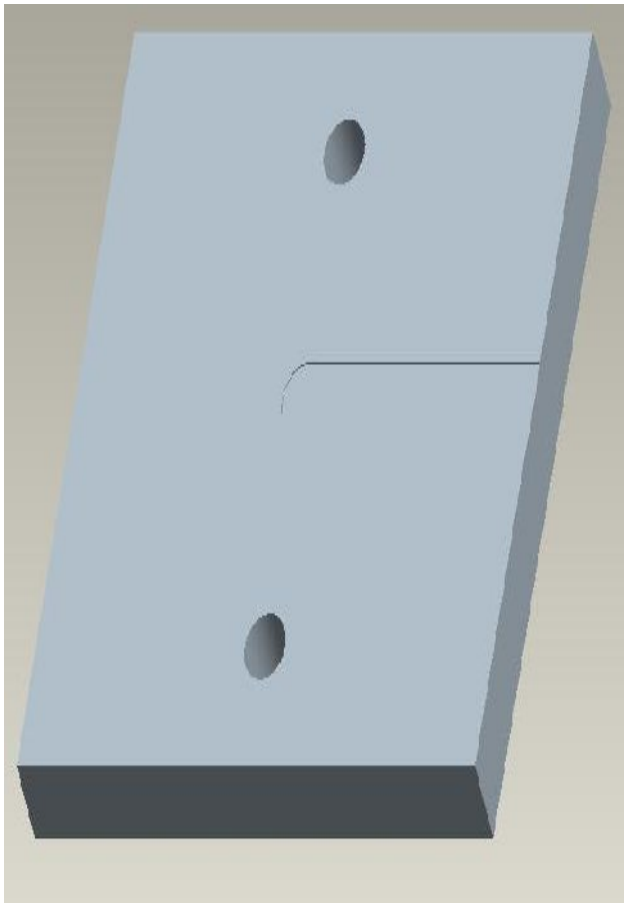

Figure 4.89 Pro-E Model of Specimen of EN44

Table 4.40 Force Values (Kistler\Dyno Ware)

File Type:			
Path:	C:\Kistler\DynoWare\Data\		
Filename:	milli2.dwd		
Config ID:	millig2.cfg		
Sampling rate [Hz]:	10		
Measuring time [s]:	40		
Delay time [s]:	0		
Cycle time [s]:	0		
Cycles:	1		
Samples per channel:	401		
Cycle interval:	0		
Channel enabled:	1	1	1
Cycle No:	1		
Time [s]	Fx	Fy	Fz
0	-105.606	39.2761	-111.475
1	-142.166	54.8096	-151.294

2	-182.617	61.0046	-207.202
3	-222.137	70.5566	-253.723
4	-140.076	86.0901	-180.762
5	-104.919	56.2744	-130.969
6	-123.047	51.6815	-153.259
7	-136.169	50.7202	-174.28
8	-154.48	74.0814	-212.5
9	-148.392	83.7402	-210.229
10	-124.359	76.4771	-190.271
11	-33.8898	44.7998	-59.2773
12	-85.7544	58.7616	-136.731
13	-116.165	60.5011	-184.717
14	-135.01	79.5593	-229.736
15	-124.664	97.3816	-236.194
16	-97.8699	63.2782	-185.938
17	-36.5143	44.4031	-82.2876
18	-82.4432	65.2466	-172.986
19	-98.526	90.4236	-222.913
20	-88.4705	64.1174	-198.486
21	-76.0803	86.8378	-205.225
22	-32.6996	52.3529	-102.869
23	-47.6227	53.36	-134.314
24	-57.4036	57.1899	-162.854
25	-68.2831	103.775	-236.133
26	-65.9485	93.1396	-247.217
27	-39.7949	84.5337	-188.684
28	-7.64465	57.2968	-68.0542
29	-30.6854	71.2585	-160.815
30	-37.2925	71.7926	-208.35
31	-38.0859	84.8541	-242.932
32	-20.1263	105.942	-231.384
33	-15.0299	67.6117	-163.062
34	-7.75146	64.4379	-122.009
35	-10.849	74.9664	-196.619
36	-1.78528	115.219	-266.76
37	-1.06812	79.7272	-229.749
38	15.7318	96.6034	-176.88
39	10.4218	60.6384	-83.9844
40	14.7095	74.3561	-161.523

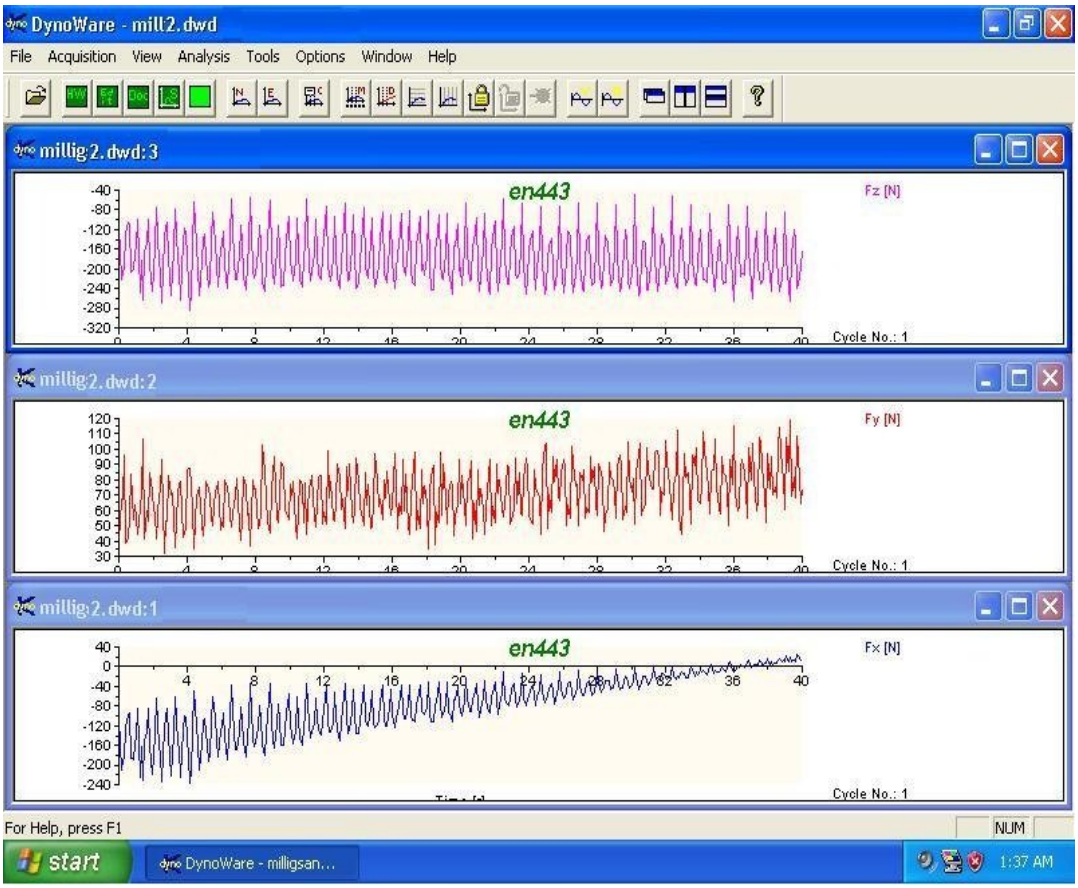

Figure 4.90 Graphical Representation of Force Variation of EN44

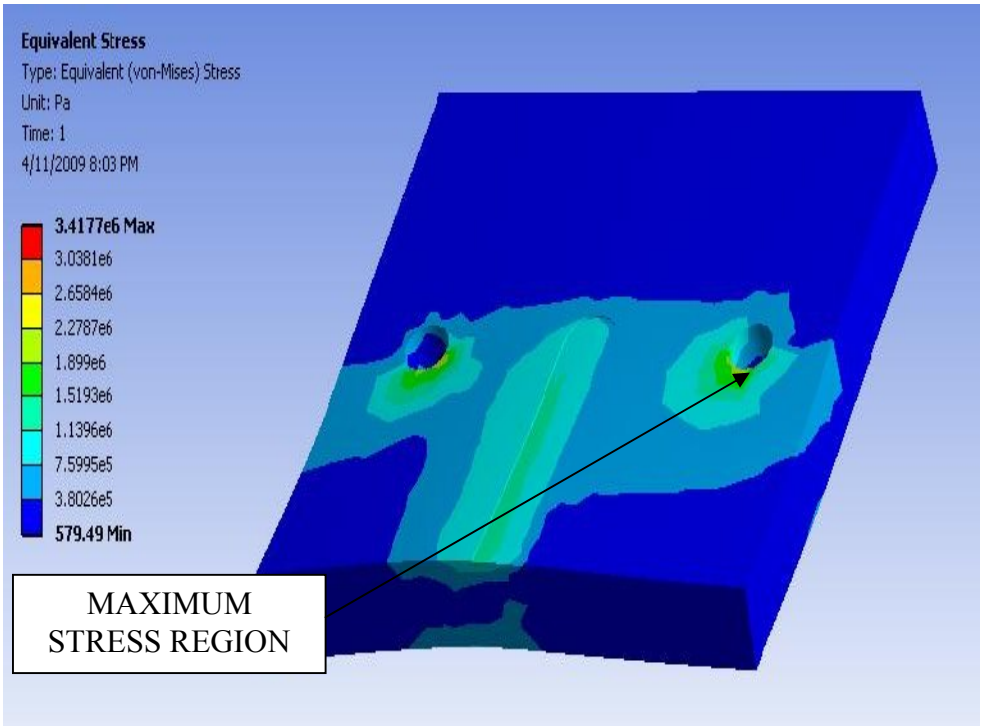

Figure 4.91 Analysis of EN19(V=102,F=65,A=0.25)

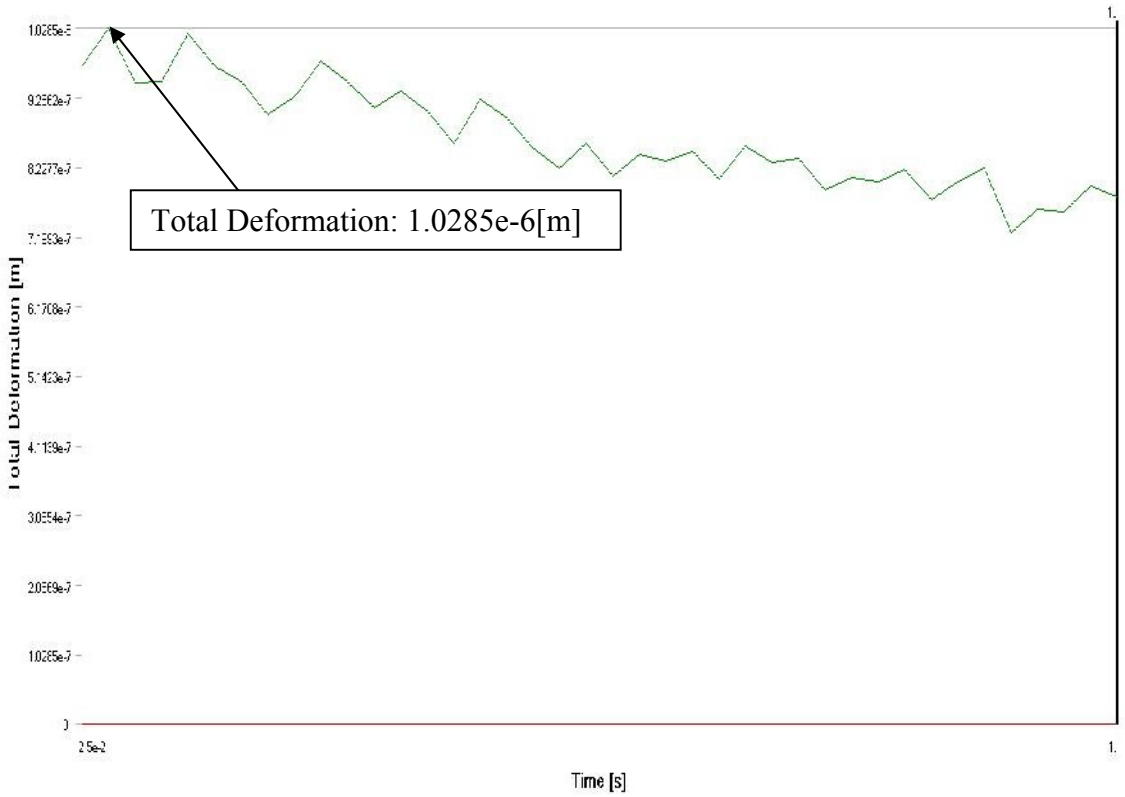

Figure 4.92 Total Deformation of EN44(V=102,F=65,A=0.25)

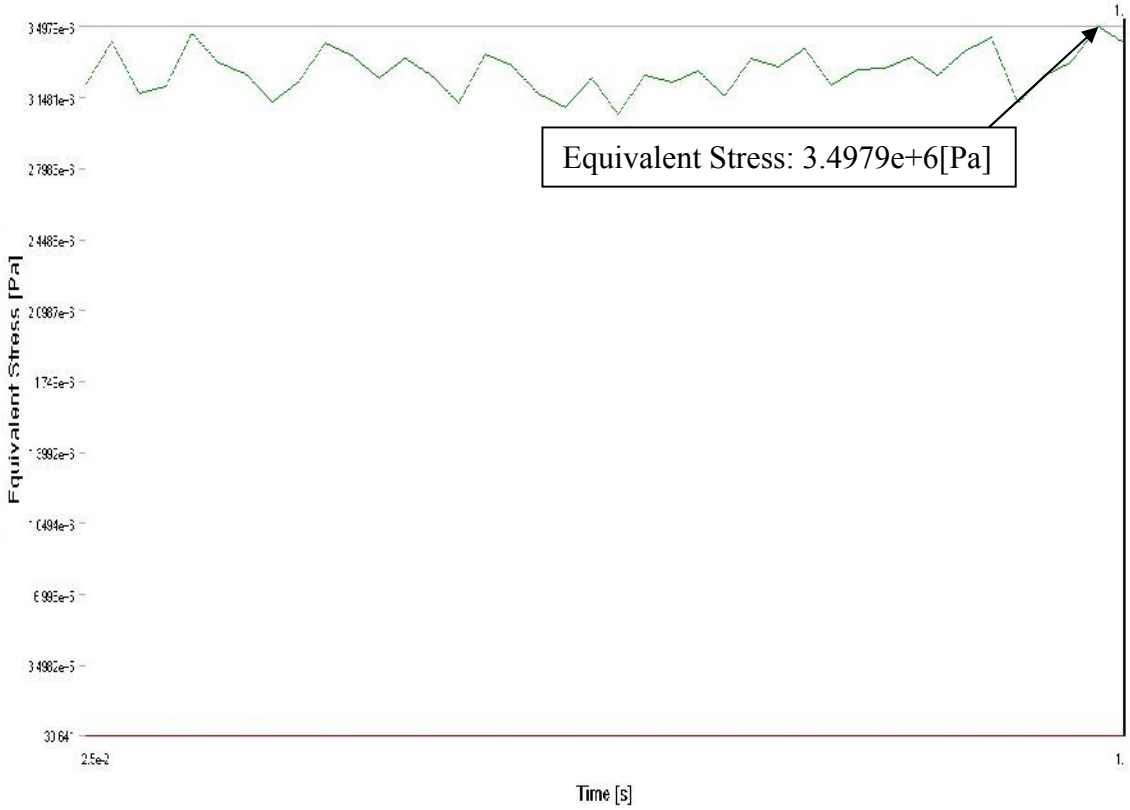

Figure 4.93 Equivalent Stress of EN44(V=102,F=65,A=0.25)

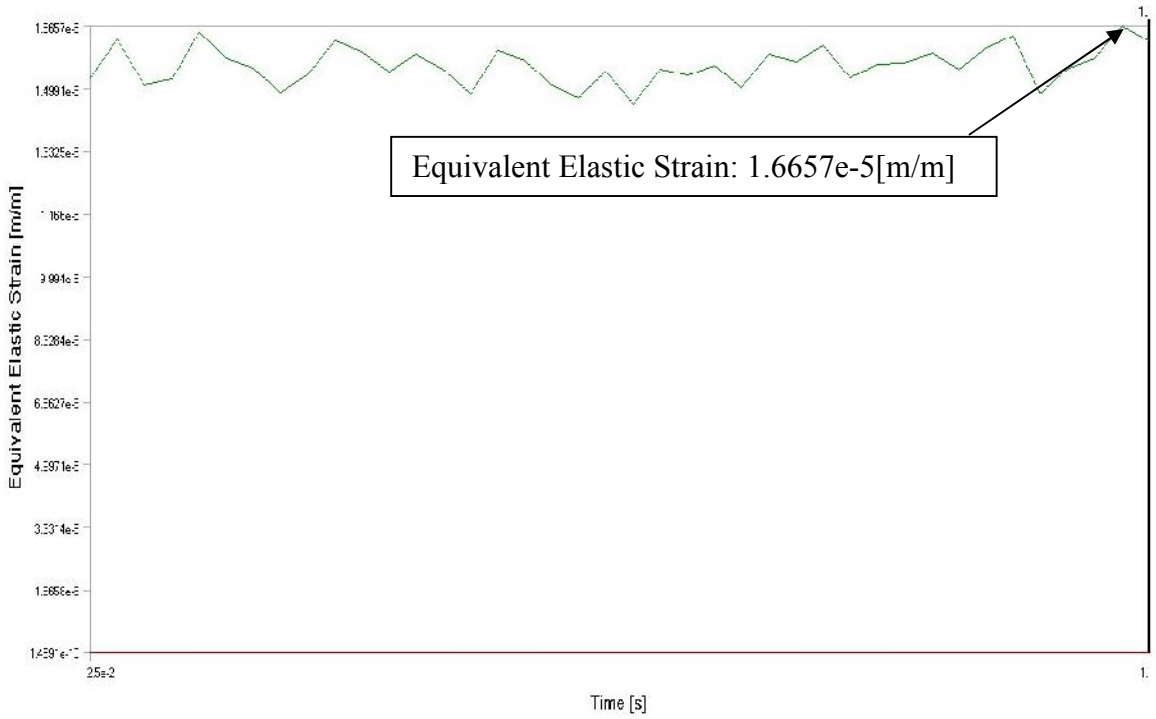

Figure 4.94 Equivalent Elastic Strain of EN44(V=102,F=65,A=0.25)

4.2.4.4

Table 4.41 Machining parameters of EN44

SPEED	204	r.p.m
FEED	20	mm/min
DOC	0.25	mm

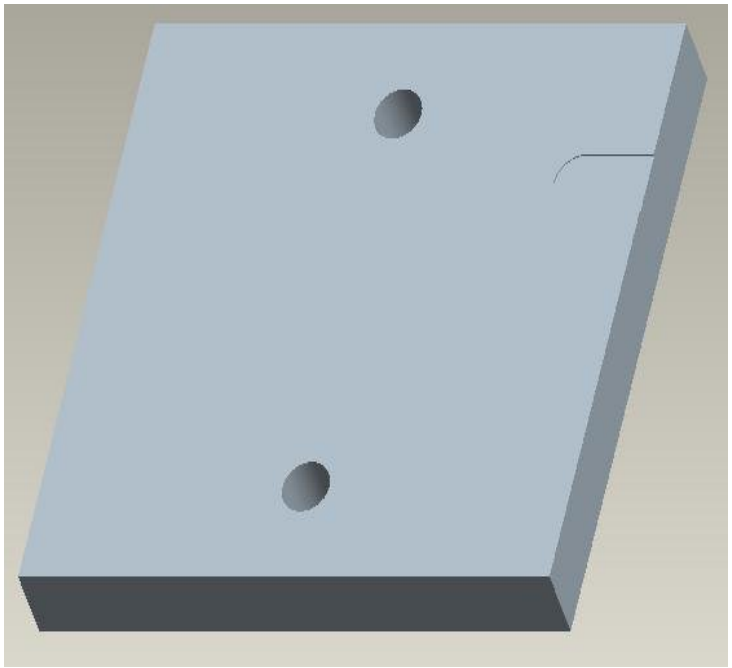

Figure 4.95 Pro-E Model of Specimen of EN44

Table 4.42 Force Values (Kistler\Dyno Ware)

File Type:			
Path:	C:\Kistler\DynoWare\Data\		
Filename:	millig2.dwd		
Config ID:	millig2.cfg		
Sampling rate [Hz]:	10		
Measuring time [s]:	40		
Delay time [s]:	0		
Cycle time [s]:	0		
Cycles:	1		
Samples per channel:	401		
Cycle interval:	0		
Channel enabled:	1	1	1
Cycle No:	1		
Time [s]	Fx	Fy	Fz
0	0	-0.22888	2.22168
1	-16.0217	10.3149	-6.72607
2	-62.7289	24.0479	-50.8667
3	-15.0757	3.31116	-6.56738
4	-78.2166	29.2053	-88.0615
5	-122.849	25.3906	-116.931
6	-24.9939	14.6637	-27.6245
7	-111.008	38.3453	-103.479
8	-107.803	34.6069	-75.8789
9	-61.7218	20.4315	-55.542
10	-109.1	33.4015	-88.0005
11	-39.978	14.9536	-21.3745
12	-22.1863	4.73022	-20.3369
13	-71.3043	32.8827	-49.8901
14	-8.22449	13.7024	-0.63477
15	-57.8461	25.7874	-68.8721
16	-48.3246	47.9889	-12.7075
17	-0.47302	0.549316	3.69873
18	-96.9238	49.4537	-101.587
19	-86.1511	44.9219	-69.2017
20	-33.9661	11.0474	-43.2007
21	-98.2361	57.6935	-87.915
22	-68.3594	30.0293	-48.1689
23	-29.9377	9.8114	-28.2104
24	-96.8781	32.3944	-92.2119

25	-31.1737	33.4625	0.708008
26	-45.578	17.0135	-33.4229
27	-63.3545	33.9203	-36.7065
28	-8.91113	17.4866	-0.50049
29	-82.0007	46.1731	-92.9321
30	-63.0493	59.2194	-30.5176
31	-35.7666	29.5563	-49.9268
32	-97.9614	53.0701	-112.39
33	-68.8782	45.5627	-43.6401
34	-79.2999	47.5769	-57.7881
35	-105.942	63.0646	-118.152
36	-74.6918	42.3737	-49.4995
37	-26.9623	11.5051	-33.2153
38	-108.154	41.3818	-103.247
39	-18.0511	41.3818	12.3047
40	-49.118	42.8925	-52.1484

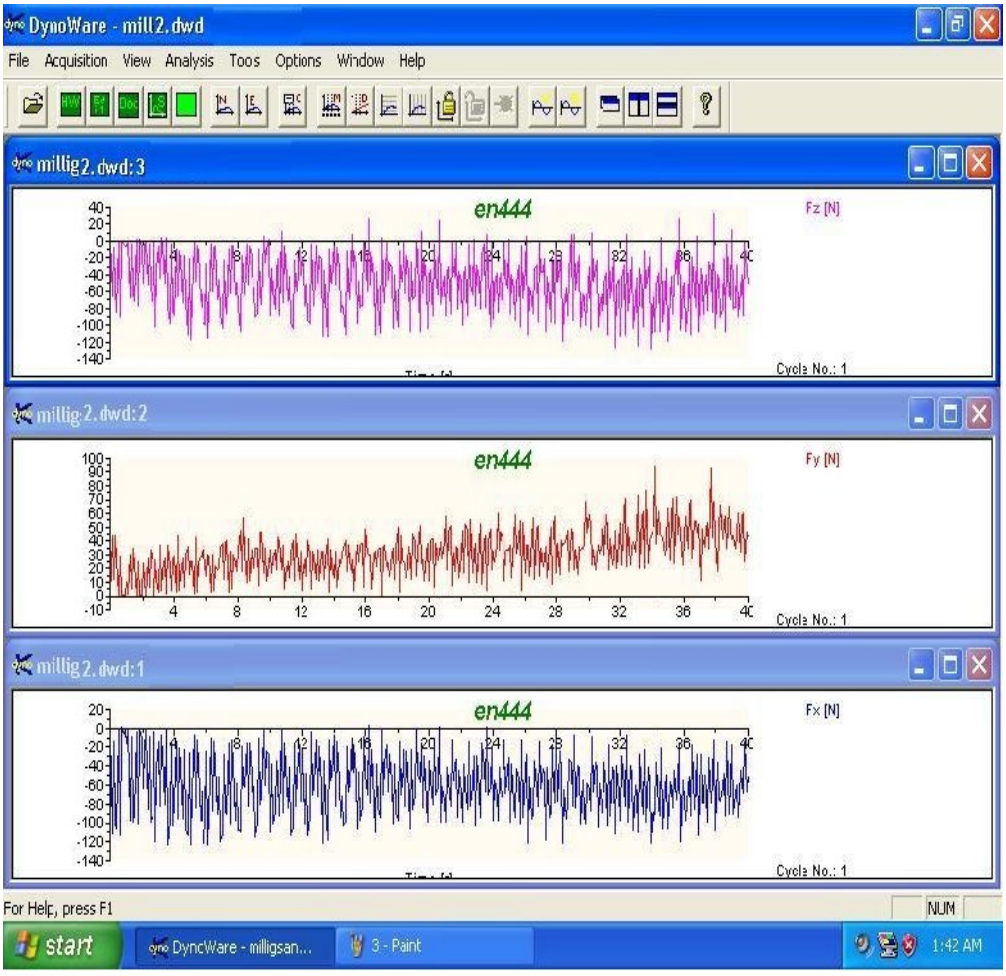

Figure 4.96 Graphical representation of Force Variation of EN44

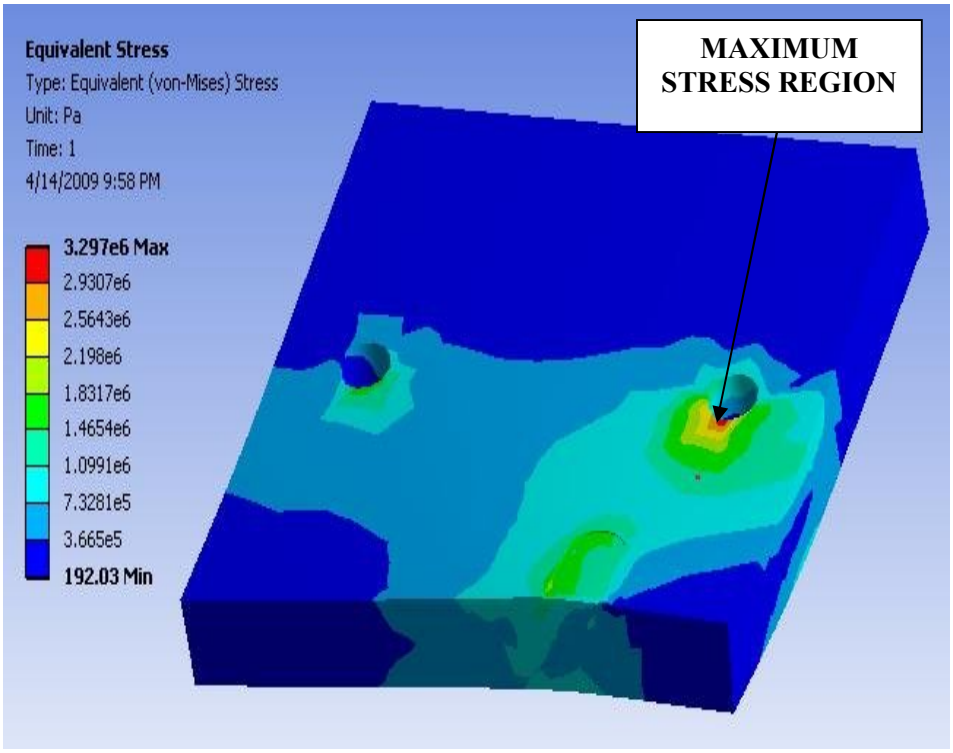

Figure 4.97 Analysis of EN19 of EN44(V=204,F=20,A=0.25)

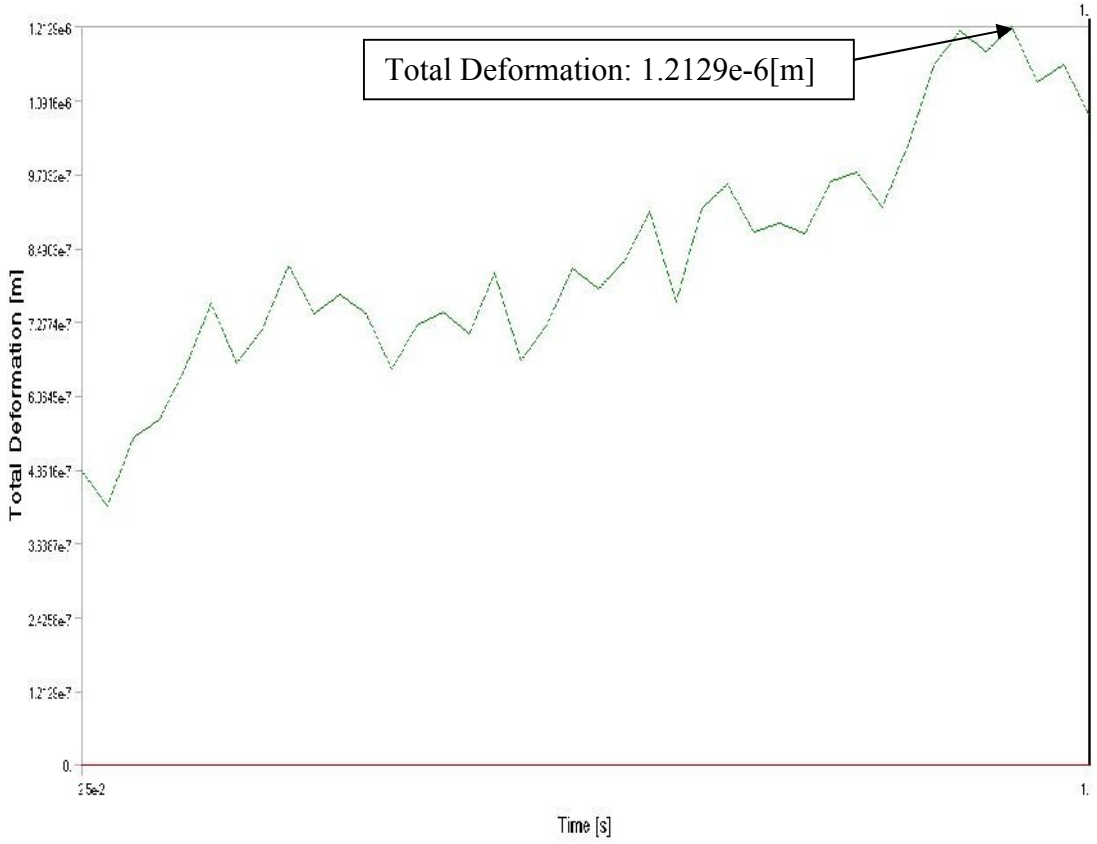

Figure 4.98 Total Deformation of EN44(V=204,F=20,A=0.25)

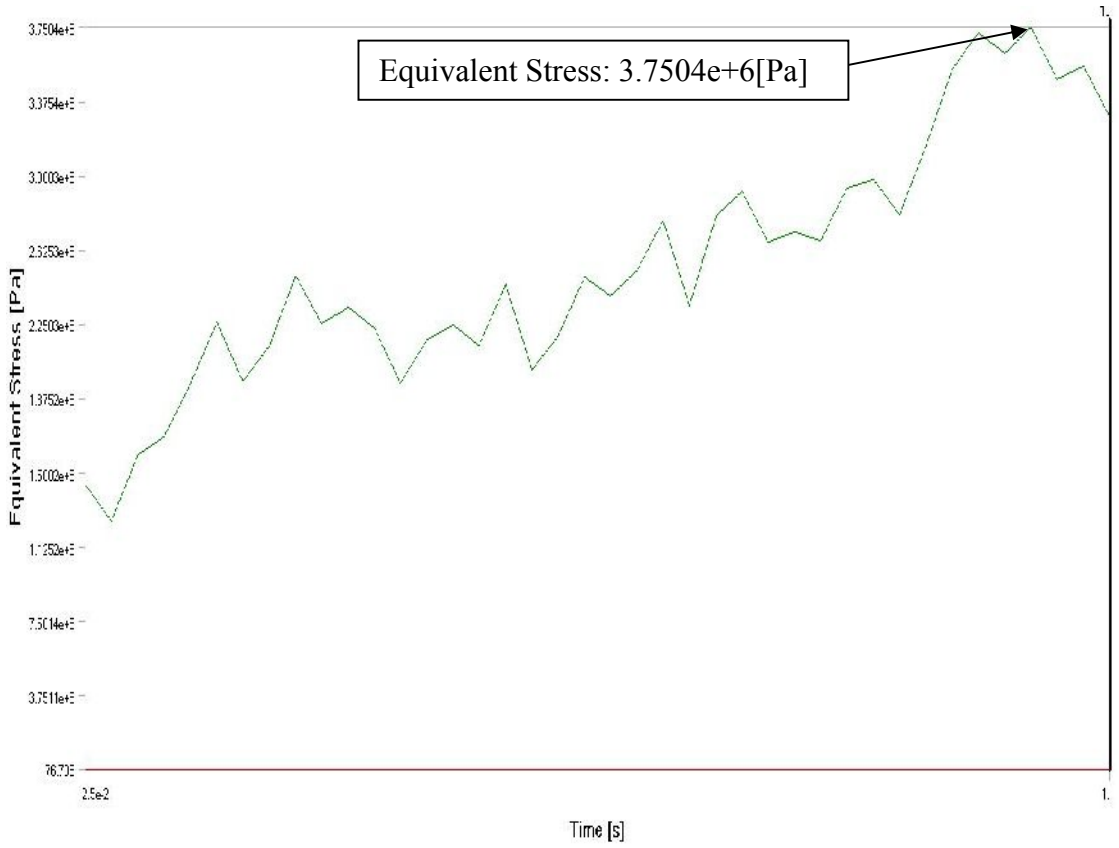

Figure 4.99 Equivalent Stress of EN44(V=204,F=20,A=0.25)

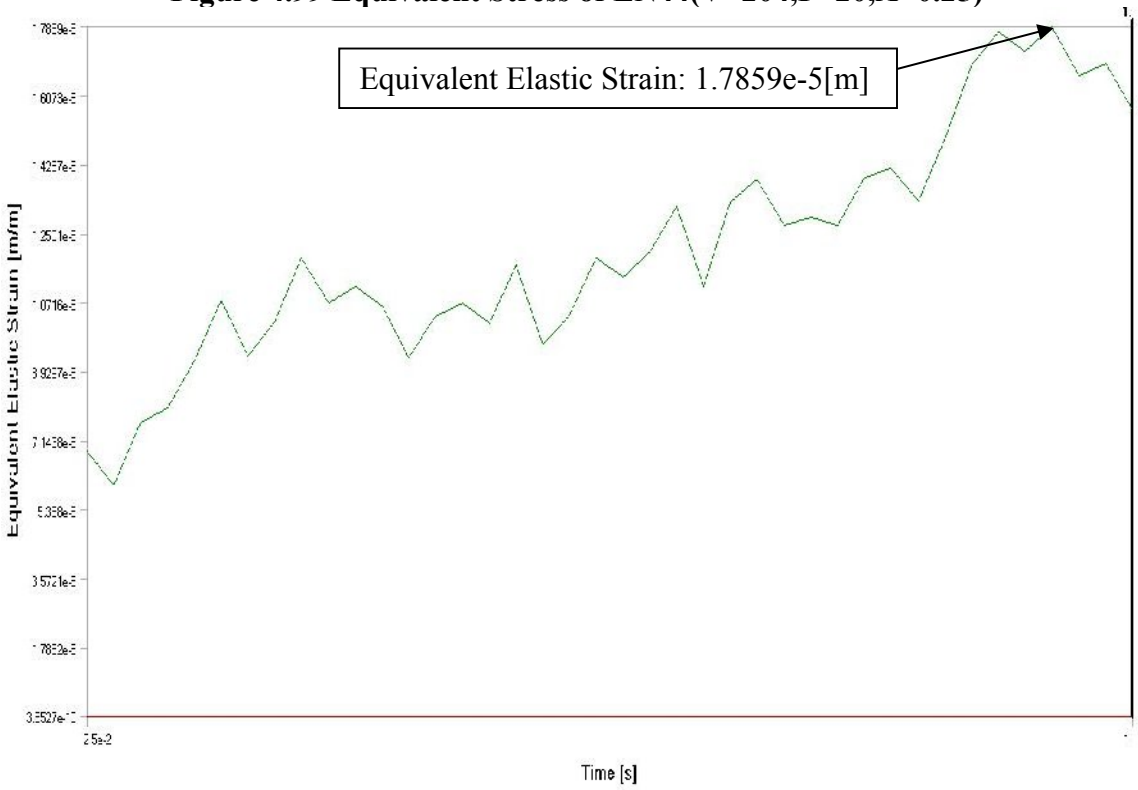

Figure 4.100 Equivalent Elastic Strain of EN44(V=204,F=20,A=0.25)

CHAPTER 5
MATHEMATICAL MODELING

The cutting forces exerted by the cutting tool on the work piece during a machining action to be identified in order to control the tool wear and occurrence of vibration, thus to improve tool-life. Modeling of cutting force in milling is often needed in machining automation. The objective of this study is to predict the effects of cutting parameters on the variations of cutting forces during end milling operation of EN Series Steel Alloy material. Cutting forces are measured for varies feed rates, cutting speed and depth of cut. In this study Response Surface Methodology is used by designing four factors, five level central composite rotatable design matrixes with full replication; for planning, conduction, execution and development of mathematical models. The average cutting forces are determined at different feed rates in tangential, radial, and axial directions per tooth period by keeping immersion and axial depth of cut as constant. A comparison between modeling and experiment is presented. This model and analysis are useful not only for predicting the tool wear but also for selecting optimum process parameters for achieving the stability of the end milling process

5.1 INTRODUCTION

The analysis of cutting forces generated during machining has been a main subject of research over the years and force measurements have since been shown to be an invaluable output for monitoring the cutting process. The primary objective of this modeling is to determine the model values of different parameters for milling process. This outcome facilitates the effective planning of the machining operations to achieve optimum productivity, quality and cost. A basic requirement for achieving this goal is a reliable method for predicting cutting forces for arbitrary process conditions. Many attempts were made in the past in analyzing force patterns as an indication of tool wear of the end milling process. In this study, also deals with the application of response surface methodology (RSM) in developing mathematical model and plotting graphs relating primary input variables namely the cutting speed (V), the feed rate(F), depth of cut (A) in the end milling process.. These developed models are very useful for the users to

predict the cutting force components in all the directions for the proposed values of input variables, to select an optimum combination of input variables for the optimum cutting force condition and to automate the milling process through the development of a computer program. When the cutting forces are used to predict the vibrations of the end mill or work piece, the numerical oscillations lead to faulty simulation of vibrations. Also, an accurate prediction of force distribution along the end mill and flexible thin webs is necessary to predict the dimensional form errors left on the finish surface. In this paper, a methodology for understanding relationship between the principal factors such as cutting speed (V), feed (F), depth of cut (A) and development of mathematical model for the cutting force components are presented. This new approach for milling force prediction is verified through comparison of the simulated and the experimental results, with good agreement.

5.2 EXPERIMENTAL PROCEDURE

The key factor in developing a mathematical model is to obtain sufficient experimental data simulating the working environment in the laboratory. Three independently controllable factors affecting the wear performance were identified as the Depth of cut (A), Feed rate (F), Cutting speed. The Experiment has been conducted by milling the EN Alloy material, using HSS end mill cutter with 9mm diameter and four tooth tool in a vertical Milling machine. The cutting force components in feed, tangential, and radial directions have been measured with a Piezo-electric three-component dynamometer (Kistler, Type 5070A), a multi channel charge amplifier (Kistler, Type 5070A) and a data acquisition system. Before starting each experiment the gauges have been used to set the tool height. Experiments were carried out under various cutting conditions. To reduce the total number of experiments and to obtain data uniformly from all the regions of the selected working area, a factorial design procedure has been adopted. The secondary parameters that have been kept constant during the machining process are tool geometry, the tool height and hardness of the material. The experiments are planned as per the outline RSM method.

5.3 EXPERIMENT SET UP

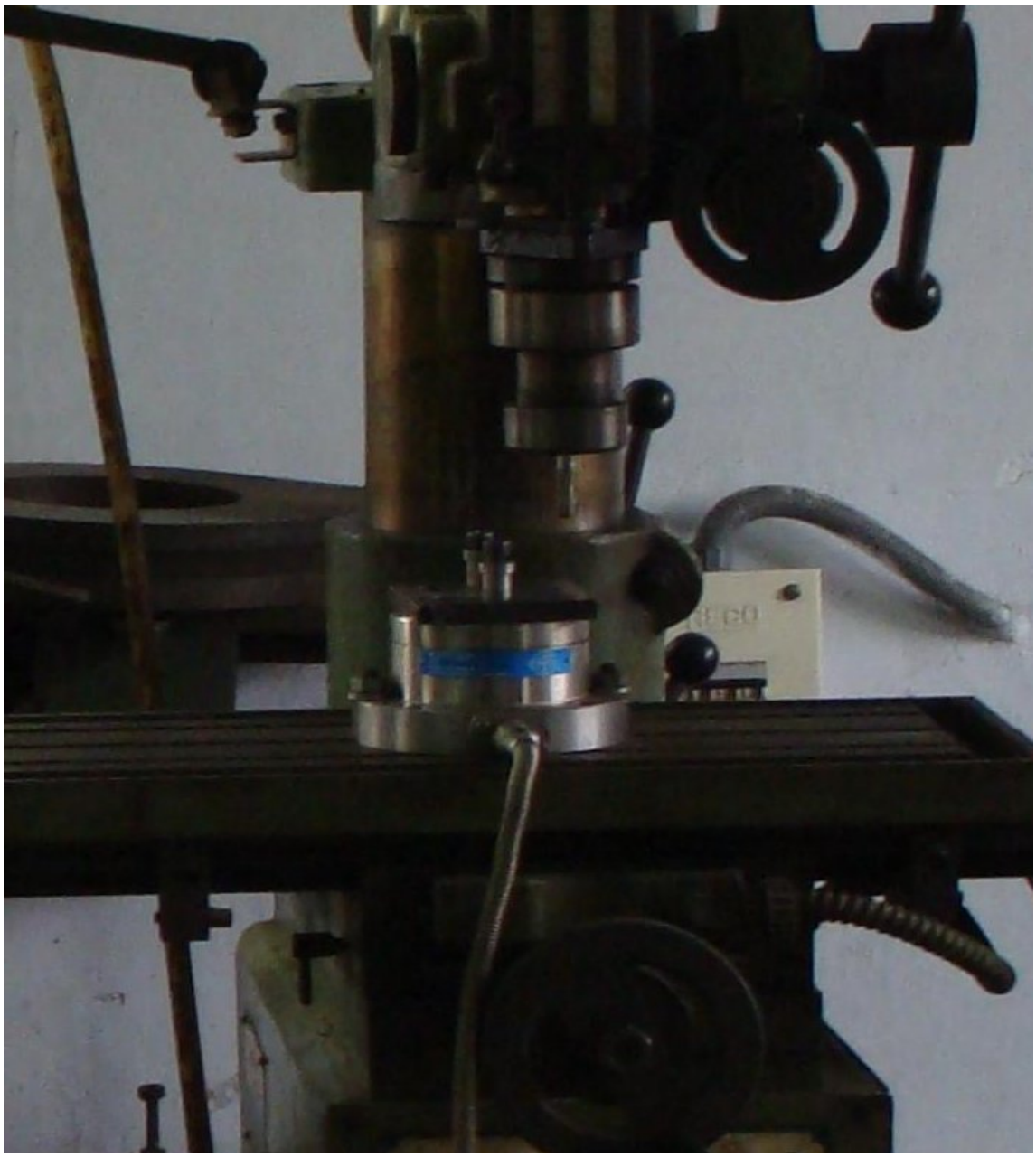

Figure 5.1 Piezo-electric three-component dynamometer(Kistler, Type 5070A)

5.4 DESIGN MATRIX

A Box-Behnken design matrix shown in Table 5.1 consisting of 15 sets of coded conditions was selected to conduct the experiments. Box-Behnken design uses a selection of corner, face and central points to span an experimental space with fewer points than a Complete Factorial Design (CFD).

Table 5.1 Box-Behnken design matrix

Run	Feed	Cutting speed	Depth of cut	Force Components		
				Fx(N)	Fy(N)	Fz(N)
1	-1	-1	0	-95.2086	-69.1444	13.24131
2	1	-1	0	10.00717	33.66358	-76.0589
3	-1	1	0	-24.1639	16.79169	26.77107
4	1	1	0	-47.0731	33.92486	8.608743
5	-1	0	-1	-75.8077	-32.3301	10.09028
6	1	0	-1	-47.0731	33.92486	8.608743
7	-1	0	1	-111.439	-24.0939	5.57563
8	1	0	1	-73.0574	71.2507	-178.048
9	0	-1	-1	-117.14	-65.7424	16.86728
10	0	1	-1	-61.1367	25.43489	-51.5726
11	0	-1	1	-44.1926	39.19606	-173.934
12	0	1	1	-86.556	12.61423	-78.9565
13	0	0	0	-38.8582	31.63642	67.30004
14	0	0	0	-37.2254	32.9453	66.223
15	0	0	0	-39.4353	30.3242	69.5654

5.5 CONDUCTING THE EXPERIMENT AND RECORDING OF RESPONSES

The process parameters such as cutting speed (V), feed (F) and depth of cut of EN Series Alloy Steel material were identified as the main factors influencing the responses cutting force component in feed, tangential, and radial directions. The working range of factors was set at five levels. The selected factors and their levels are shown in Table 5.2. A five level four factor full factorial design matrix shown in Table 5.1 has been selected to conduct the experiment. The Experiment has conducted by milling the EN Series Alloy Steel material on a vertical Milling machine.

Table 5.2 Factor and their levels

SI No.	Parameters	Unit	Notation	Factor Levels		
				-1	0	+1
1	Feed Rate	mm/min	F	20	35	65
2	Cutting Speed	m/min	V	102	204	340
3	Depth of cut	mm	A	0.25	0.50	0.75

5.6 DEVELOPMENT OF MATHEMATICAL MODELS

The response function representing the wear performance can be expressed as:

$$Y=f(A, F, V)$$

Where Y = the response or yield.

The second order polynomial (regression) equation used to represent the response surface for K factors is given by:

$$Y = b_0 + \sum_{i=1}^{k} b_i X_i \sum_{i,j=1}^{k} b_{ij} X_i X_j + \sum_{i\neq 1}^{k} b_{ii} Xi^2 \quad \text{..... (8)}$$

Where b_0 is the free term of the regression equation, the coefficients b_1, b_2... b_k are linear terms, b_{11}, b_{22}... b_{kk} are the quadratic terms, and b_{12}, b_{13}... $b_{k-1,\ k}$ are the interaction terms. For three factors, the selected polynomial could be expressed as:

$$Y = b_0 + b_1 a + b_2 f + b_3 V + b_{33} V^2 + b_{13} aV + b_{23} a + b_{12} a + b_{44} f^2 \text{.... (9)}$$

5.7 CALCULATION OF COEFFICIENTS OF MODELS

The values of the coefficients of the polynomial of Eq. 9 were calculated by regression method. The magnitude of the regression co-efficient is a good indication of the significance of the parameters. A statistical analysis software package SYSTAT was used to calculate the values of these coefficients and also to determine the significant direct and interaction effects precisely. For the required response, if all of the 31 observed values and the second order general mathematical model for the three factors are given to the software as input. These values were also checked with the values calculated using a commercial statistical package SYSTAT software. The significance of the coefficients was evaluated and insignificance coefficients are not included in the model.

5.8 FINAL DEVELOPED MODELS

The final mathematical models has been determined by above analysis is given below:

5.8.1 Tangential cutting force

Fx=-38.506+18.678*F+3.451*V-1.761*A-0.096*F*F-0.508*V*V-38.242*A*A-32.031*F*V-24.592*V*A+2.412*F*A ..... (10)

5.8.2 Radial cutting force

Fy=31.635+35.193*F+18.849*V+17.210*A-9.257*F*F-18.569*V*V-10.190*A*A-21.419*F*V-29.440*V*A+7.272*F*A ..... (11)

5.8.3 Axial cutting force

Fz=67.696-36.571*F+15.592*V-51.170*A-20.550*F*F-54.006*V*V-85.589*A*A+17.784*F*V+40.854*V*A-45.536*F*A ..... (12)

The adequacy of the model was tested using the analysis of variance technique. As per this technique, the calculated value of the F-ratio of the model developed does not exceed the standard tabulated value of F-Ratio for a desired level of confidence say 95 %.

Table 5.3 Coefficients of the models

Specimen Number	Coefficient	Tangential cutting force (Fx),N	Radial cutting force (Fy),N	Axial cutting force (Fz),N
1	b0	-38.506	31.635	67.696
2	b1	18.678	35.193	-36.571
3	b2	3.451	18.849	15.592
4	b3	-1.761	17.21	-51.17
5	b11	-0.096	-9.257	-20.55
6	b22	-0.508	-18.569	-54.006
7	b33	-38.242	-10.19	-85.589
8	b12	-32.031	-21.419	17.784
9	b13	-24.592	-29.44	40.854
10	b23	2.412	7.272	-45.536

5.9 RESULTS AND DISCUSSIONS

The results obtained through experiments have been presented in the graph is represented between tangential, radial, and axial cutting force and varies feed rate, speed and depth of cut.

5.9.1 Tangential cutting force (Fx)

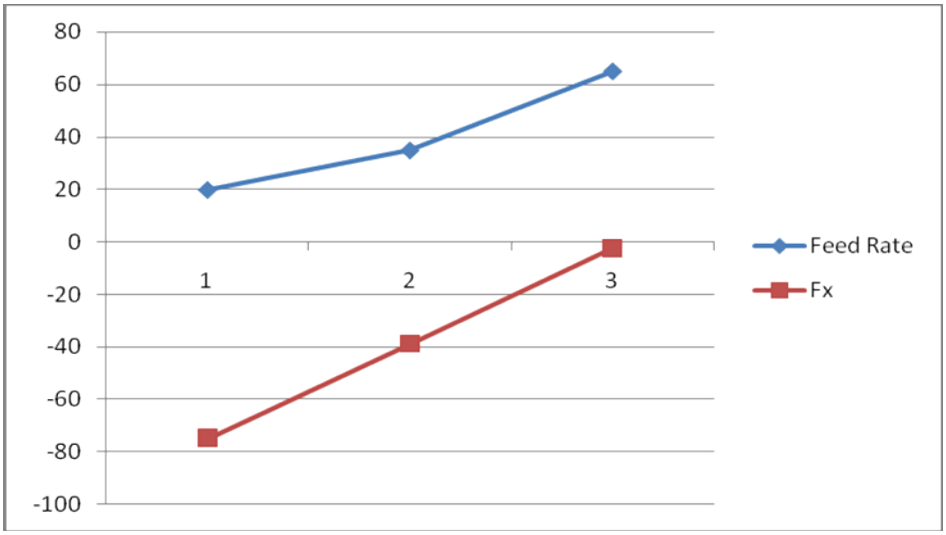

Graph 5.1 Tangential Force Vs Feed Rate

From the graph 5.1 it has been concluded that cutting force in X-direction is decreasing linearly with increasing feed rate. The values of feed rate taken as 20mm/min, 35mm/min and 65mm/min.

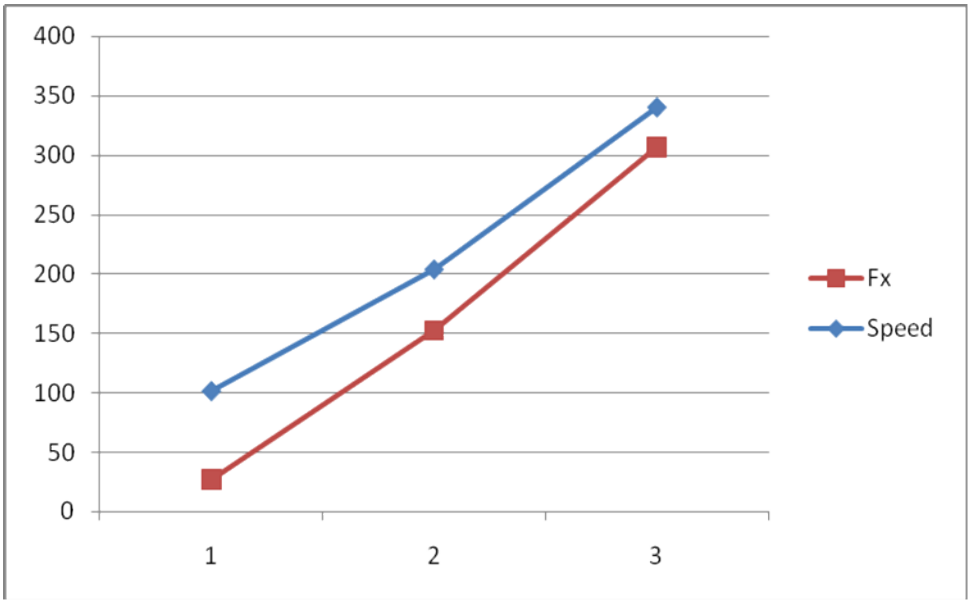

Graph 5.2 Tangential Force Vs Spindle Speed

From the graph 5.2 it has been concluded that cutting force in tangential direction is decreasing with increasing speed. The values of speed taken as 102 rpm, 204 rpm and 340 rpm respectively.

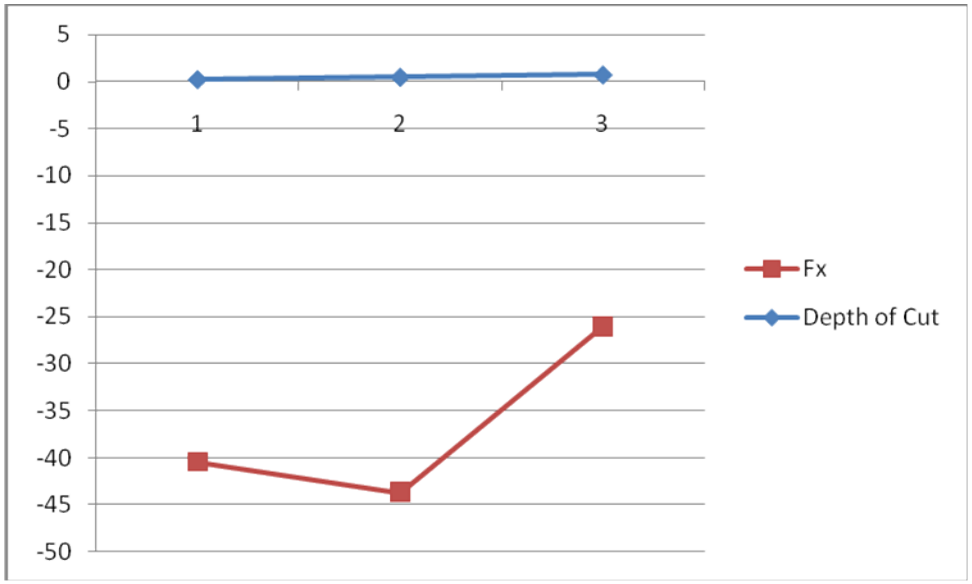

Graph 5.3 Tangential Force Vs Depth of cut

From the graph 5.3 it has been concluded that cutting force in X-direction is range of force is not high with the DOC. The depth of cut values taken as 0.25mm, 0.50mm and 0.75mm respectively.

5.9.2 Radial cutting force (Fy)

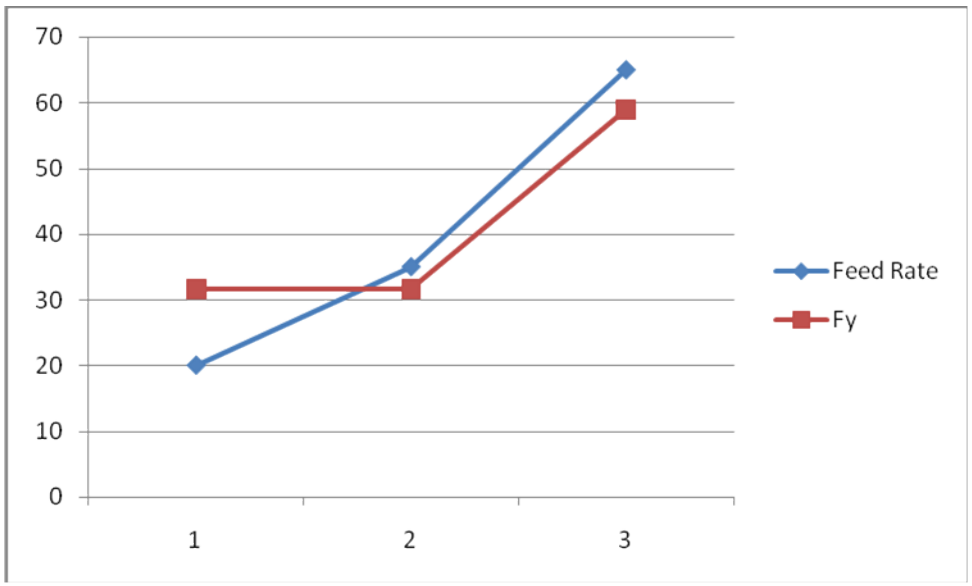

Graph 5.4 Radial cutting Force Vs Feed Rate

From the graph 5.4 it has been concluded that the effect of the feed rate on cutting force in radial direction is almost constant from first to second point but suddenly increasing after second point. The values of feed taken as 20mm/min, 35mm/min and 65mm/min.

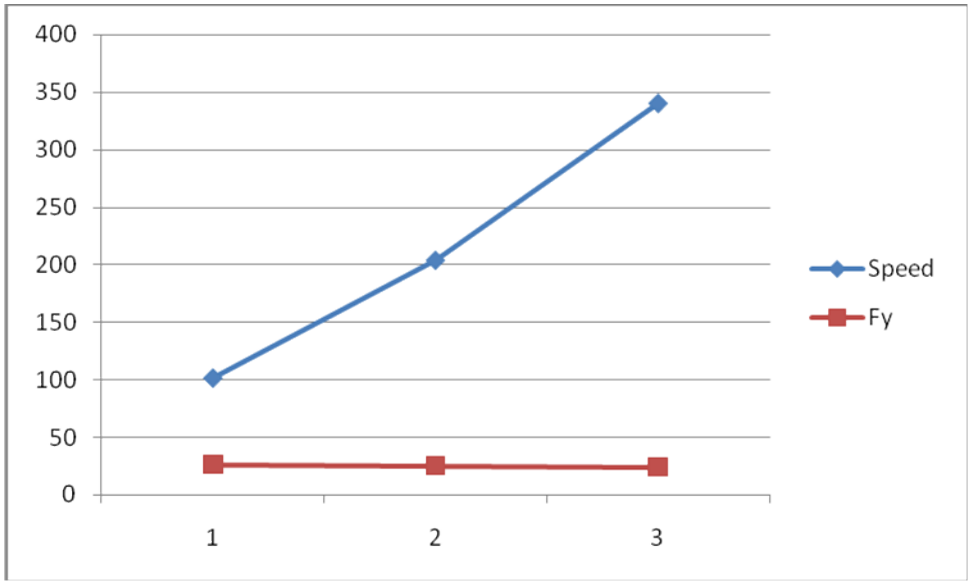

Graph 5.5 Radial cutting Force Vs Spindle Speed

From the graph 5.5 it has been concluded that cutting force in radial direction is almost constant with the all factor of spindle speed. It means no effect of cutting force due to varying in spindle speed. The values of speed taken as 102rpm, 204rpm and 340rpm respectively.

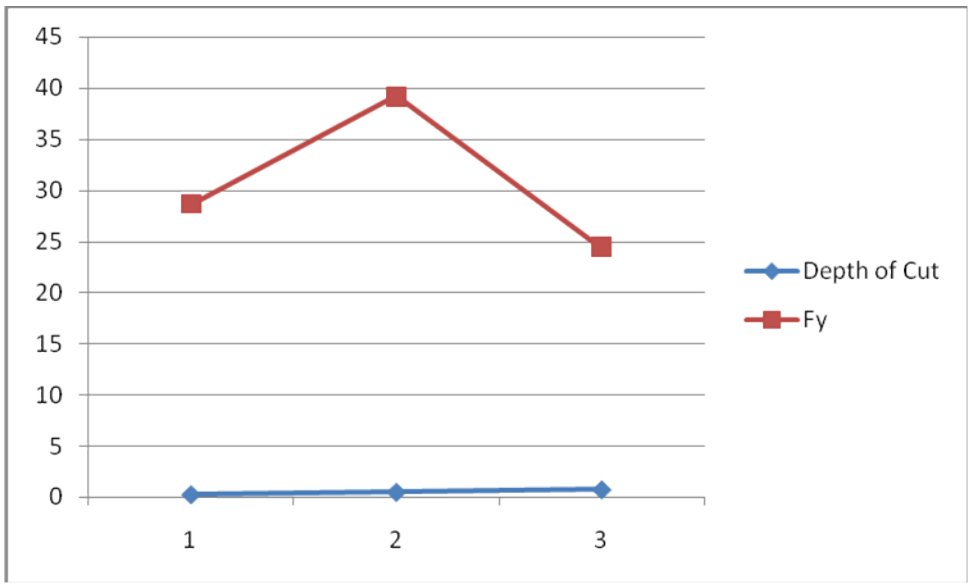

Graph 5.6 Radial cutting Force Vs Depth of cut

From the graph 5.6 it has been concluded that cutting force increasing with DOC at starting but decreasing after middle point with changing in to the DOC. The values of depth of cut taken as 0.25mm, 0.50mm and 0.75mm respectively.

5.9.3 Axial cutting force (Fz)

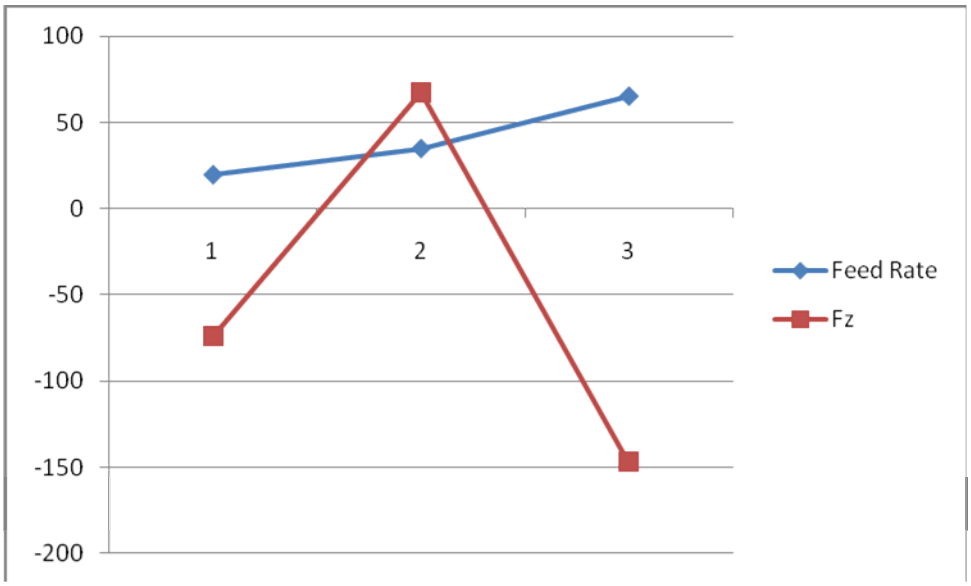

Graph 5.7 Axial cutting Force Vs Feed Rate

From the graph 5.7 it has been concluded that increasing in feed rate from 20 mm/min to 35 mm/min the force in axial direction change from negative to positive than from 35 mm/min to 65 mm/min force is again negative. Feed rate is 20mm/min, 35mm/min and 65mm/min.

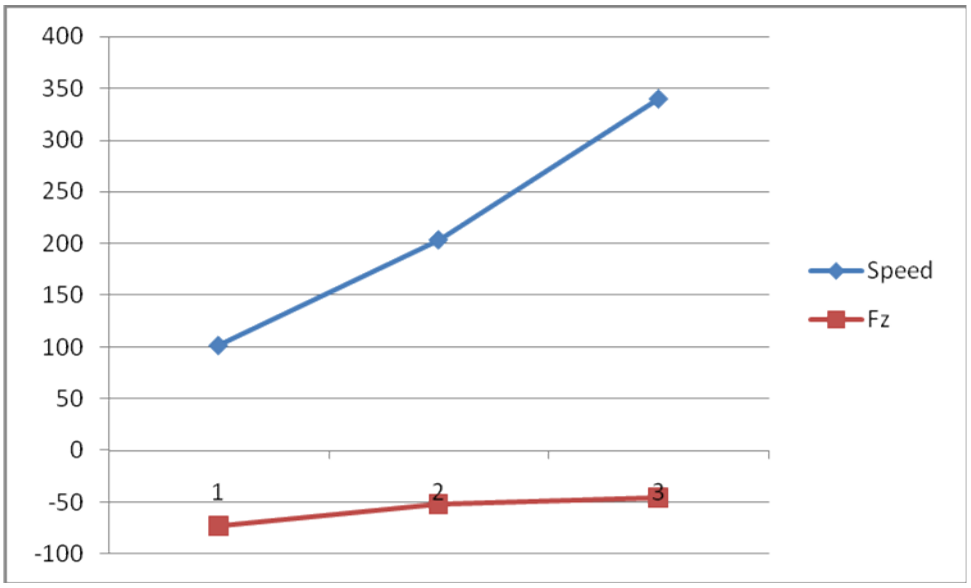

Graph 5.8 Axial cutting Force Vs Spindle Speed

From the graph 5.8 it has been concluded that increasing in spindle speed the cutting force in axial direction is not changing. The change in the cutting force due spindle speed is very small. The values of speed taken as 102 rpm, 204 rpm and 340 rpm.

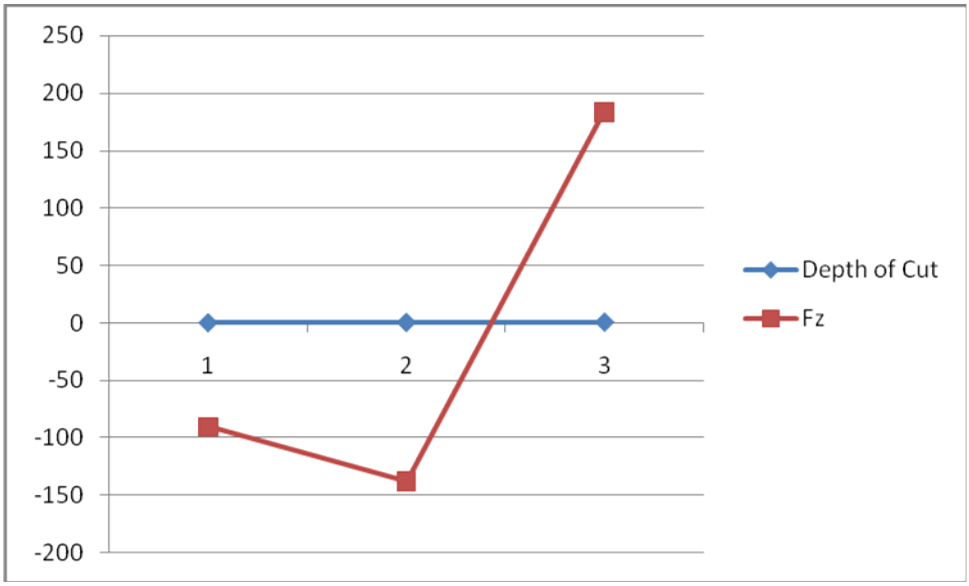

Graph 5.9 Axial cutting Force Vs Depth of cut

From the graph 5.9 it has been concluded that depth of cut is changing from 0.25mm to 0.75mm and because of DOC, cutting force in axial direction is gradually increasing with increasing in DOC. It means that deformation, equivalent stress and strain increasing with the DOC. The values of Depth of cut taken as 0.25mm, 0.50mm and 0.75mm.

CHAPTER-6
CONCLUSIONS

The cutting forces exerted by the cutting tool on the work piece during a machining has been identified in order to control the tool wear and occurrence of vibration, thus to improve tool-life. Modeling of cutting force in milling is often needed in machining automation. The aim of study is to predict the effects of cutting parameters on the variations of cutting forces during end milling operation of EN series steel alloy materials.

The experiment has been performed on various EN series specimens under varying parameters according to the design of experiments. The critical analysis of results shows that when depth of cut varies by keeping others parameter constant, the stress values seemed to be more sensitive to it. The specimen which are used of different in shapes and sizes. The maximum stress occurs near tool tip and holding position for the disc type specimen whereas rectangular shape specimen shows a greater variation near its extreme edges. When speed was varied the stress magnitude changes and it has adverse effect on the surface finish of work piece.

It has been calculated when feed rate is varied the variation in stress is not much but the displacement variation occurring is considerable.

Finally the mathematical result shows the same variation according to the parameter dealt during experimentations. From the results it was concluded that a stress value varies throughout the work piece during machining. It is maximum at tool tip and holding position and reduces to zero at neutral surfaces. From the experiment it has been concluded that when cutting force on the tool is high then surface finish is very less.

- Cutting force in tangential direction increases when the depth of cut increases.
- The rate of increase in force components with the increase in higher speed is predominant.
- The cutting forces are found to be low in radial and axial directions, when all the four factor values are in between levels 1 and 2.
- The cutting force components are more sensitive in the high speed and full immersion condition.

Case 1: Feed rate varying (Speed and DOC constant)

Table 6.1 Feed rate 20 m/min

Total deformation	2.3205e-7	m
Equivalent stress	2.0795e+6	Pa
Equivalent elastic strain	1.0398e-5	m/m

Table 6.2 Feed rate 35 m/min

Total deformation	7.5892e-8	m
Equivalent stress	1.3919e+6	Pa
Equivalent elastic strain	6.9597e-6	m/m

Table 6.3 Feed rate 65m/min

Total deformation	1.5565e-7	m
Equivalent stress	1.748e+6	Pa
Equivalent elastic strain	8.7399e-6	m/m

From above results it is being evaluated that when feed rate is increased deformation decreases but equivalent stress and strain increases. Feed rate is changed with values 20m/min, 35 m/min, 65 m/min according to machine specification.

Case 2: Speed varying (Feed rate and DOC constant)

Table 6.4 Speed 204 rpm

Total deformation	1.6273e-7	m
Equivalent stress	1.9921e+6	Pa
Equivalent elastic strain	9.9607e-6	m/m

Table 6.5 Speed 340 rpm

Total deformation	1.3628e-7	m
Equivalent stress	1.6541e+6	Pa
Equivalent elastic strain	8.2706e-5	m/m

Table 6.6 Speed 680 rpm

Total deformation	8.7904e-8	m
Equivalent stress	1.0848e+6	Pa
Equivalent elastic strain	5.4242e-6	m/m

From above results it is being evaluated that when speed is increased deformation decreases but equivalent stress and strain decreases. Speed is changed with values 102rpm, 204rpm and 340rpm according to machine specification.

Case 3: Depth of cut varying (Speed and Feed rate constant)

Table 6.7 Depth of cut 0.25mm

Total deformation	1.2898e-7	m
Equivalent stress	1.645e+6	Pa
Equivalent elastic strain	8.2251e-6	m/m

Table 6.8 Depth of cut 0.50mm

Total deformation	1.7215e-7	m
Equivalent stress	1.967e+6	Pa
Equivalent elastic strain	9.8351e-6	m/m

Table 6.9 Depth of cut 0.75mm

Total deformation	2.1056e-7	m
Equivalent stress	2.4474e+6	Pa
Equivalent elastic strain	1.2237e-5	m/m

From above results it is being evaluated that when depth of cut is increased deformation increases but equivalent stress and strain increases. Depth of cut is changed with values 0.25mm, 0.50mm, 0.75mm according to machine specification.

References

[1] C. Betegon Biempica , J.J. del Coz Diaz, P.J. Garcia Nieto ,I. Penuelas Sanchez, "Nonlinear analysis of residual stresses in a rail manufacturing process by FEM, Applied Mathematical Modeling" Applied Mathematical Modeling, Volume 33, Issue 1, pp 34-53, January 2009.

[2] G. Amit, "Thermal modeling & analysis of carbide tool using finite element method, Thermal Engineering", ME Thesis, Mechanical Department, Thapar University, June 2005.

[3] A. Narimanyan, "Unilateral conditions modeling the cut front during plasma cutting: FEM solution, Applied Mathematical Modeling", Applied Mathematical Modeling Volume 33, Issue 1, pp 176-197, January 2009.

[4] E. Correa, A. Blazquez, A. Estefani, F. Paris, J. Canas, "Effects of the stress state generated during the manufacturing process of copper anodes on the moulds: Warping and cracking", Engineering Failure Analysis, Volume 16, Issue 1, pp 309-320, January 2009.

[5] Z. Barsoum, I. Barsoum, "Residual stress effects on fatigue life of welded structures using LEFM, Engineering Failure Analysis", Engineering Failure Analysis, Volume 16, Issue 1, pp 449-467, January 2009.

[6] W.L. Chan, M.W. Fu, J. Lu, "An integrated FEM and ANN methodology for metal-formed product design, Engineering Applications of Artificial Intelligence", Engineering Applications of Artificial Intelligence, Volume 21 , Issue 8, pp 1170-1181, December 2008.

[7] S. Parveen, "Numerical analysis of stereo lithography process using the finite element method, Numerical analysis", ME Thesis, Mechanical Department, Thapar University, June 2008

[8] Z. Li, "Modeling, Analysis, and Experimental investigations of grinding processes, Industrial and Manufacturing Systems engineering", Available online on: http://krex.k-state.edu/dspace/bitstream/2097/198/1/ZhichaoLi2006.pdf.

[9] S. Vinod, "Modeling and analysis of tool wear rate in EDM using FEM", ME Thesis, Mechanical Department, Thapar University, June 2008.

[10] H. singh, “Process analysis and monitoring in WDM using FEM approach”, ME Thesis, Mechanical Department, Thapar University, june-2008.

[11] M. Koç , Mehmet A. Arslan, “Design and finite element analysis of innovative tooling elements (stress pins) to prolong die life and improve dimensional tolerances in precision forming processes, Journal of Materials Processing Technology, Volume 142, Issue 3, 10, pp 773-785, December 2003.

[12] C. Simion, Corneliu Manu, Saleh Baset, Julian Millard, “Distortions Generated by Welding Process Using ANSYS-FEA”, Available online on: http://www.ansys.com/ events/proceedings/2006/PAPERS/335.pdf

[13] S.D. Madnaik , R.C. Chaturvedi, “F.E.M. analysis of the effect of aspect ratio in plane strain compression of a preshaped strain hardening material between inclined tools”, Materials and Manufacturing Processes, Volume 2, Issue 1, pp 169 – 188, 1987.

[14] K Choi,W Kim, K Kim, S Im, C-M Kim and J-B Lee, “Large-scale finite element analysis of arc-welding processes”, J. Phys. D: Appl. Phys. pp2869–2875, 2006.

[15] J.C. Outeiro, J.C. Pina , R. M’Saoubi , F. Pusavec , I.S. Jawahir, “Analysis of residual stresses induced by dry turning of difficult-to-machine Materials”, Manufacturing Technology pp 77–80, 2008

[16] X. Lai, Hongtao Li, Chengfeng Li, Zhongqin Lin, Jun Ni, “Modeling and analysis of micro scale milling considering size effect, Micro cutter edge radius and minimum chip thickness, Machine Tools & Manufacture”, International Journal of Machine Tools and Manufacture, Volume 48, Issue 1,Pages 1-14, , January 2008.

[17] B. Ganesh babu, V. Selladurai and R. Shanmugam, “Analytical modeling of cutting forces of end milling operation on aluminum silicon carbide particulate metal matrix composite material using response surface methodology”, Available online on: http://www.arpnjournals.com/jeas/research_papers/rp_2008/jeas_0408_89.pdf

[18] W. Hsiang Lai, “Modeling of Cutting Forces in End Milling Operations”, Tamkang Journal of Science and Engineering, Volume 3, pp. 15-22, 2000.

[19] Yawei Li, Steven Y. Liang, "Cutting Force Analysis in Transient State Milling Processes",http://www.springerlink.com/content/w1a6v7wr2j8rdeg6/fulltext.pdf.

[20] Kuang-Hua Fuh, Ren-Ming Hwang, "A predicted milling force model for high-speed end milling operation", J. Manuf. Sci. Eng, Volume 127, Issue 2, pp11-23, May 2005

[21] S. G. Kapoor, R. E. DeVor, I. Lazoglu, "Machining Process Modeling", Available online on: http://www.malinc.com/pdf/course_schedule.pdf

[22] B. Li, S. N. Melkote and S. Y. Liang, "Analysis of Reactions and Minimum Clamping Force for Machining Fixtures with Large Contact Areas", Available online on: http://www.springerlink.com/content/hjur2je25je7h9ly/fulltext.pdf

[23] K Kandirgama, K A Abou-El-Hossein, B Mohammad, Habeeb A L-Ani and M M Noor, "Cutting force prediction model by FEA and RSM when machining Hastelloy C-22HS with 90^0 holder", Journal of Scientific & Industrial Research, Volume 67, pp. 421-427, June 2008

[24] David Burton, G. Scott Duncan, John C. Ziegert, Tony L. Schmitz, "High Frequency, Low Force Dynamometer for Micro-Milling Force Measurement", Available online on: http://highspeedmachining.mae.ufl.edu/htmlsite/publications/dr_schmitz/ASPE%20Dynamometer.pdf

[25] Turnad L. Ginta, "Improved Tool Life in End Milling Ti-6Al-4V through Work piece Preheating", European Journal of Scientific Research ISSN 1450-216X, Volume 27, pp.384-391 2009.

[26] Smaoui, Bouaziz, Zghal, "Simulation of cutting forces for complex surface in Ball-end milling", Int j simul model, pp93-105, 2008.

[27] J.P. Wulfsberg, G. Brudek, "Detection of Cutting Forces in Micro Machining Operations", Available online on: http://www.mikromaschinenbau.com/brudek/Brudek_cutting_forces_micro_machining.pdf

[28] A. Chukwujekwu Okafor and S. Aramalla, "Modeling Cutting Forces in High Speed End-Milling of Titanium Alloys using Finite Element Analysis and Mechanistic Model", Available online on: http://www.fs.uni-lj.si/lasin/cirp9ws06/abstracts/Okafor.pdf

[29] F. Cus, M. Milfelner, J. Balic, “An overview of data acquisition system for cutting force measuring and optimization in milling”, Journal of Materials Processing Technology, Volumes 164-165, pp 1281-1288, 15 May 2005.

[30] A. Otieno and Clifford Mirman, “Finite Element Analysis of Cutting Forces and Temperatures on Microtools in the Micromachining of Aluminum Alloys”, Available online on: http://www.ijme.us/cd_08/PDF/191ENG103.pdf

[31] Süleyman Yaldız, Faruk Ünsaçar, “Design, Development and Testing of a turning dynamometer for cutting force measurement”, Available online on: http://alaeddin.cc.selcuk.edu.tr/~tekbil/makformat.pdf